REVISTA PORTUGUESA DE QUÍMICA

RPTQAT 25(1) 1-62 (1983)
ISSN 0035-0419

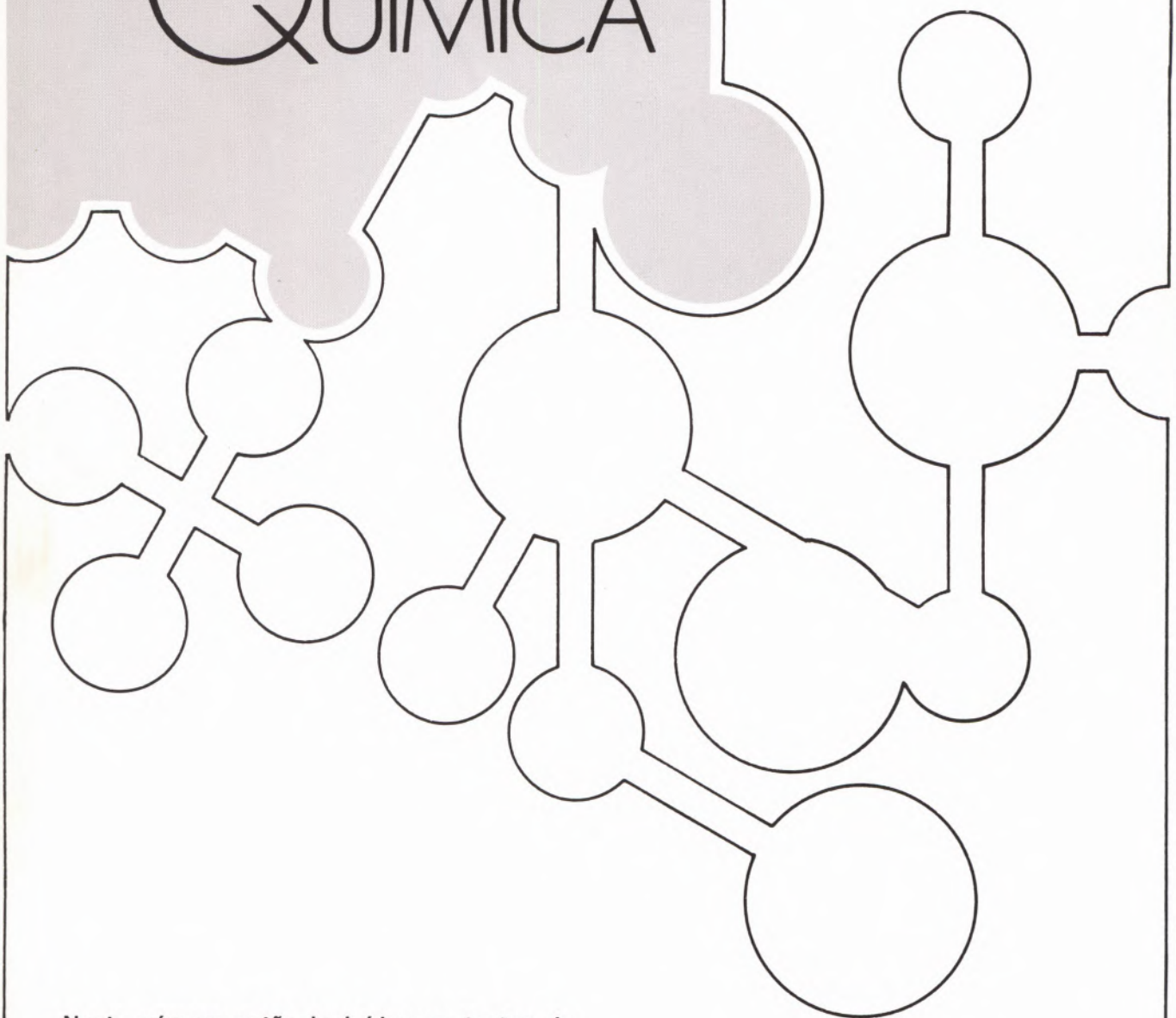

Neste número estão incluídos os textos de conferências proferidas durante o Simpósio sobre Propriedades de Transporte de Fluidos realizado em Março de 1982 em Lisboa.

Rev. Port. Quím., Vol. 25, N.° 1
Pp. 1-62 — Lisboa, 1983

REVISTA PORTUGUESA DE QUÍMICA

Propriedade e edição da
SOCIEDADE PORTUGUESA DE QUÍMICA
em continuação da
REVISTA DE QUÍMICA PURA E APLICADA
fundada em 1905 por
Ferreira da Silva.
Subsidiada pelo
INSTITUTO NACIONAL DE INVESTIGAÇÃO CIENTÍFICA

Redacção e administração	Instituto Superior Técnico — 1096 Lisboa Codex
Fotocomp., montagem, impressão e acabamento	PROENÇA — Coop. Op. Artes Gráfica, CRL, Rua D. Carlos Mascarenhas, 39-51 B — 1000 Lisboa
Capa	Luís Filipe de Abreu

Publicação trimestral. Número avulso: 150$00. Assinatura (quatro números): Portugal, Brasil e Espanha: 500$00
outros países: U.S. $18.00

índice

E. A. MASON
Huygens Laboratorium
Rijksuniversiteit Leiden
Nederland

on leave from
Brown University
Providence
Rhode Island
U.S.A.

EXTENDED PRINCIPLE OF CORRESPONDING STATES AND INTERMOLECULAR FORCES

Although the classical principle of corresponding states dates back to 1880, and its statistical-mechanical basis was firmly established in the period 1939-1950, it is only in the past ten years that its remarkable scope and accuracy have begun to be fully appreciated. Improvements in experimental accuracy and in knowledge about intermolecular forces have both contributed to these recent advances. In 1972 Kestin, Ro, and Wakeham gave a remarkably accurate correlation, involving only two adjustable parameters, for nearly all the low-density thermodynamic and transport properties of the noble gases and their multicomponent mixtures. They carefully avoided models of the intermolecular forces on the grounds that the latter were inadequate to do justice to the experimental data. Subsequently, they were also able to correlate some properties of polyatomic gases, but not all. These advances were due almost entirely to improvements in the accuracy and range of experimental data. Since then, important advances have also occurred in our knowledge of intermolecular forces, and these can be used as the basis for extensions and improvements to the two-parameter correlation.

This paper briefly reviews the two-parameter correlation, and then summarizes the improvements in the range and accuracy of the correlation that have been achieved for the noble gases. Finally, a short summary in given of one of the most interesting crucial advances in knowledge of intermolecular forces, namely direct numerical inversion of transport coefficients.

This paper is an edited version of the lecture delivered at the Symposium on Transport Properties of Fluids, Lisbon (23-26 March 1982).

CONTENTS

INTRODUCTION

The principle of corresponding states goes back over 100 years, to J.D. van der Waals in 1880, in connection with the equation of state and the critical constants of gases. It played an important role around the turn of the century in the liquefaction of the last of the so-called permanent gases, hydrogen and helium, by Dewar and by Kamerlingh Onnes, respectively, who used it to predict boiling points and other properties. Thereafter it was widely applied to many other substances. In the period of about 1939-1950, the molecular basis of the principle was firmly established through statistical mechanics, and it was extended to include quantum effects and transport properties.

Unfortunately, the quantitative aspects of the principle were often considered a bit dubious — it was considered to furnish a useful correlation scheme, but to have only moderate accuracy. Perhaps this was at first caused by its association with the approximate van der Waals equation of state, and then by its over-enthusiastic application to so many different substances. At any rate, it was essentially abandoned by chemists and physicists as a subject of serious study, although of course it was much used by engineers.

Why do we now bother with a 100-year old theory of only modest accuracy? In the first place, it turns out that the accuracy and the range of properties covered are much better than had been thought. Secondly, there have been important advances in our knowledge of intermolecular forces in the last ten years or so. Together, these two developments have completely revitalized the subject. The purpose here is to give a brief survey of these developments.

In 1972, KESTIN, RO, and WAKEHAM [1,2] assembled a large body of consistent, accurate results, especially on the low-density gas viscosity, and decided to try taking the principle of corresponding states very seriously, at least for the noble gases. To the surprise of nearly everyone, they achieved a remarkable accuracy, an improvement of nearly one order of magnitude. Moreover, they were able to correlate nearly all the low-density thermodynamic and transport properties of the noble gases and their multicomponent mixtures. They needed to assign only two parameters to each of the fifteen possible pair interactions between two noble gas atoms. For concreteness, the parameters can be thought of as an energy parameter ϵ representing the depth of the potential energy well, and a range or distance parameter σ representing the interatomic separation for which the potential is zero. However, they carefully avoided using models of the potentials on the excellent grounds that the latter — such as the LENNARD-JONES (6,12) model — were inadequate to do justice to the experimental data, and they based their results exclusively on general statistical-mechanical theory and accurate experimental measurements. The numerical values of ϵ and σ were thus found by fitting (primarily) viscosity data. Subsequently [3-5], they were also able to correlate some properties of diatomic and polyatomic gases, but not all.

These advances were due almost entirely to improvements in the accuracy and range of experimental data. But at about the same time there were important advances occurring in our knowledge of intermolecular forces. Certainly for the noble gases it is now safe to refer to the potential itself without undue fear of degrading the accuracy of the correlations, and there is hope that the same will soon be true for some of the simpler polyatomic gases. A number of extensions and improvements to the two-parameter correlation thereby become possible, which are now largely worked out. Although the details are rather voluminous [6,7], it is possible to summarize the essential results succinctly.

This report is organized as follows. A brief review of the basis of the two-parameter correlation is first given, together with indications of where failure is likely to start. Second, the most important new developments on intermolecular forces are summarized, and it is shown how they can be used to extend the range and accuracy of the two-parameter correlation for the noble gases and their mixtures. Finally, a short summary is given of one of the most interesting recent advances in knowledge of intermolecular forces, namely the direct numerical inversion of transport coefficients. Until recently, this was thought to be impossible, both in principle and in practice. The literature connected with all these topics is understandably extensive, and only a few of the key references are given here.

REVIEW OF TWO-PARAMETER CORRELATION

The molecular theory underlying the principle of corresponding states involves only very general results from statistical mechanics, plus relatively straightforward dimensional analysis. The pair potential V(r) can always be written in a dimensionless form as

$$V(r) = \epsilon\, f(r/\sigma, \alpha_1, \alpha_2, \ldots)\,, \qquad (1)$$

where ϵ and σ are the energy and range parameters already mentioned, and α_1, α_2, ... are additional dimensionless parameters characterizing the shape (rather than the scale) of the potential. The fundamental assumption used by Kestin, Ro, and Wakeham can be divided into two parts:

(1) The function $f(r/\sigma, \alpha_i)$ is the same for all noble gas pairs.

(2) the parameters α_i have the same values for all noble gas pairs.

The first part is required in order to have any corresponding states at all, and the second part allows a correlation involving only the two parameters ϵ and σ. Improved knowledge of V(r) enables us to relax this second condition and thus to make extensions of the correlation.

We can illustrate the success of the two-parameter correlation with a few samples [1,3,4]. The top part of fig. 1 shows a universal reduced collision integral for viscosity, Ω_{22}, as a function of reduced temperature, T^*, for noble gases. These quantities are defined as

$$\frac{5}{16}(mkT/\pi)^{\frac{1}{2}}\eta^{-1} \equiv \sigma^2\,\Omega_{22} \equiv \sigma^2\,\Omega^{(2,2)^*}/f_\eta\,, \qquad (2)$$

$$T^* \equiv kT/\epsilon\,, \qquad (3)$$

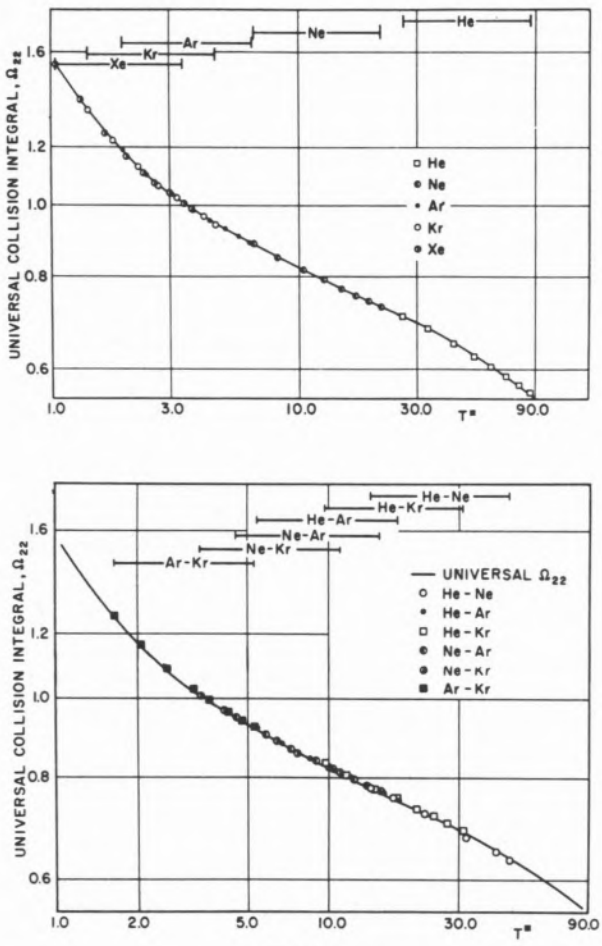

Fig. 1

Two-parameter correlation for the viscosity collision integral as a function of reduced temperature, $T^* = kT/\epsilon$, for noble gases (upper) and noble gas mixtures (lower). The horizontal lines show the temperature ranges covered by the experimental data

where m is the molecular mass, k is Boltzmann's constant, η is the viscosity, and f_η is a higher-order kinetic-theory correction [8] that deviates only slightly from unity. The curve shown is arranged to fit the points, which are seen to all lie on a single curve with remarkable precision (about 0.4% deviation, on the average). The bottom part of fig. 1 shows a similar plot for noble gas mixtures. Here the viscosity is not the total mixture viscosity, but only the interaction viscosity, η_{12}, which is equivalent to the viscosity of a hypothetical pure gas having the given V(r) and a mass $m = 2m_1m_2/(m_1 + m_2)$ [8]. The curve here is the *same* as the one for the single gases, with no tinkering. Fig. 2 shows a similar result for some polyatomic gases and gas mixtures. Again the curve is the same as in fig. 1, with no adjustment.

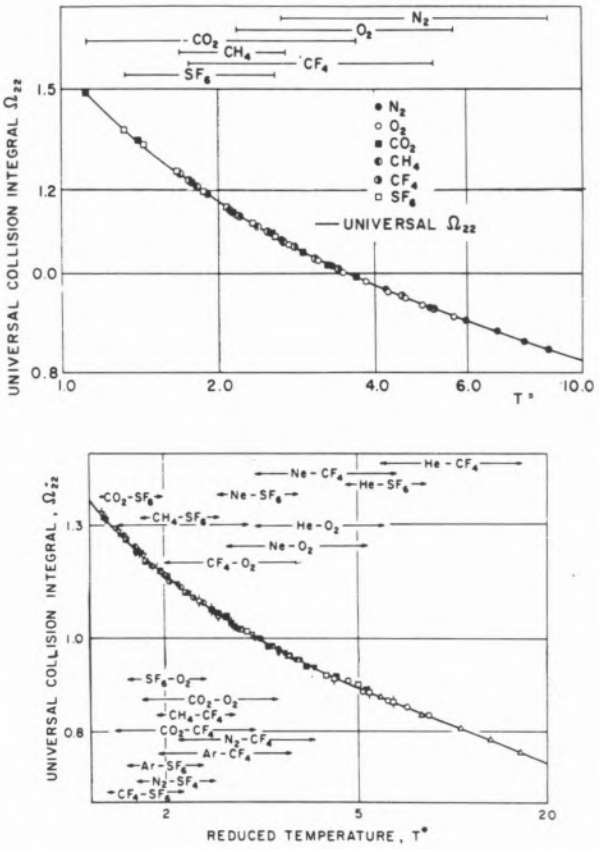

Fig. 2

Same as fig. 1, for polyatomic gases and gas mixtures

Fig. 3 shows the reduced second virial coefficient,

$$B^* \equiv B(T)/(\frac{2}{3}\pi N_o \sigma^3)\,, \qquad (4)$$

where N_o is Avogadro's number, as a function of T^* for noble gases. The correlation is quite good.

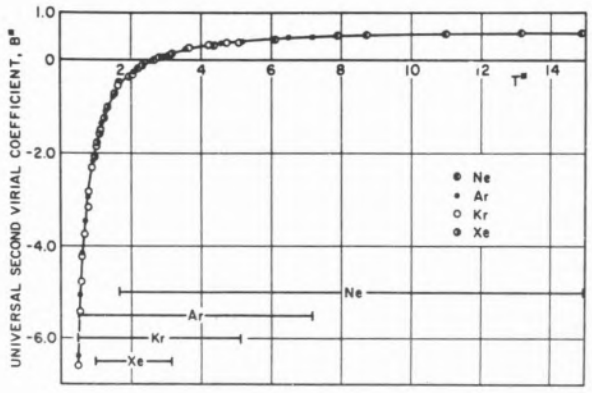

Fig. 3

Two-parameter correlation for the reduced second virial coefficient as a function of T^* for noble gases. A similar correlation for polyatomic gases fails

No comparison is shown for noble gas mixtures because of the scarcity of accurate measurements. The lack of a comparison for single plyatomic gases is more significant — here the correlation fails. This was no surprise at the time, because it was known that the second virial coefficient is much more sensitive to the non-spherical parts of the potential than is the viscosity [9]. What was somewhat surprising was the fact that the viscosities of polyatomic gases were so well correlated with only two parameters. We shall see the reason for this is the next section. If accurate data were available at lower and higher temperatures, we might expect to see some deviations from the excellent correlations illustrated in figs. 1-3, but as far as direct experimental results can tell us, a two-parameter correlation is adequate. To do better we must know something about V(r), either from theory or from some entirely different type of measurement whose only link to thermodynamic and transport properties is indirectly through V(r).

A qualification must be added at this point. Deviations *are* seen for some noble gas pairs at lower temperatures [1], but these are quantum deviations, not deviations from a two-parameter correspondence of V(r). That is, even if the potentials scaled strictly according to the assumptions of Kestin, Ro, and Wakeham, there would be deviations at low temperatures because the collisions do not follow classical mechanics. A third parameter is then needed, but it is so obviously available that it is not even regarded as a parameter — it is the atomic mass. It usually is introduced through the so-called de Boer parameter, Λ^*, which is a reduced de Broglie wavelength [10],

$$\Lambda^* \equiv h/\sigma(m\epsilon)^{\frac{1}{2}}, \qquad (5)$$

where h is Planck's constant. These quantum deviations are virually impossible to isolate by the methods of Kestin, Ro, and Wakeham, and reference to V(r) is necessary.

EXTENSIONS BASED ON INTERMOLECULAR FORCES

A — *ADVANCES IN DETERMINATION OF V(r)*

Fifteen years ago, a review [11] of intermolecular forces closed with the following remark: "We seem to be on the verge of accurate determinations of 'true' potential energy curves for simple atoms". This prospect seems now to have been realized, at least for many of the noble-gas interactions. The specific advances in our knowledge of V(r) that have been crucial for extending and improving the principle of corresponding states are as follows:

(1) Development, by SMITH, MAITLAND, and coworkers [12], of numerical methods for direct inversion of measured transport coefficients to find the potential, without any explicit assumption about the functional form of the potential.

(2) Collection of a body of experimental data, largely by Y.T. LEE and his coworkers [13], on the scattering of beams of noble gases by noble gases in the thermal energy range.

(3) Accurate values of the coefficients of the long-range dispersion energy are now available through a combination of quantum theory plus dielectric and optical data [14].

(4) Accurate information on the repulsive wall of the potential is now available from a synthesis [15] of theoretical calculations [16,17] and high-energy beam scattering [18].

In addition, two other advances have been helpful but not crucial:

(5) Determination of vibrational levels in noble-gas dimers from their vacuum ultraviolet absorption spectrum [19]. The data can be inverted by the RYDBERG-KLEIN-REES method [11] to find the width of the potential well as a function of its depth.

(6) Direct inversion of second virial coefficients [20], similar to the inversion of transport coefficients in (1) above.

As a result of these advances, we can now see directly that V(r) does not scale perfectly with only two parameters, even for the noble gases. This is illustrated in fig. 4, which shows V/ϵ *vs.* r/r_m, where r_m is the position of the potential minimum, for several noble gas systems for which the potentials have been rather accurately determined [21-24]. Although the correspondence is rather close around the bottom of the potential well, deviations are apparent at both smaller and larger r. This result suggests two questions:

(1) How do the deviations shown in fig. 4 affect the gas properties?

(2) What new parameters are needed to characterize these deviations?

Before answers to these questions are attempted, it is interesting to make a short digression to

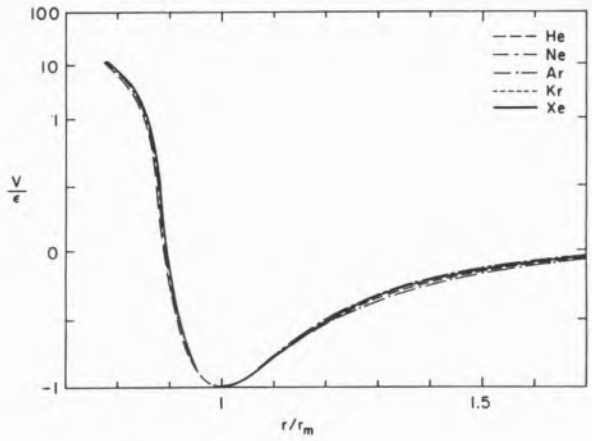

Fig. 4
Reduced plot of noble-gas potentials, showing deviations from correspondence at large and small separations

illustrate some of the insight that can be obtained through consideration of V(r). It was mentioned previously that it was a bit puzzling why the two--parameter correlation worked so well for viscosities of polyatomic gases. A direct inversion [25] of the viscosity correlation curve of figs. 1 and 2 showed that only the repulsive wall of V(r) was involved (i.e., $r<r_m$) in the temperature range covered by the correlation. It is not surprising that this rather featureless section of V(r) can be fitted with only two parameters, but reference to fig. 4 shows that an adjustment that makes the repulsive walls agree will spoil the agreement of the wells. The correlation based on viscosities will therefore fail for other properties — such as second virial coefficients — that depend on the well region of the potential.

B — *NEW PARAMETERS NEEDED*

The long-range part of V(r) has the form

$$V(r) = -C_6/r^6 - C_8/r^8 - C_{10}/r^{10} - \dots , \qquad (6)$$

and the coefficients C_6, C_8, ... have been determined from quantum theory plus dielectric and optical data [14]. This part of the potential is dominant in determining the transport coefficients at low temperatures, but not the second virial coefficients. If a two-parameter principle of corresponding states held to very low temperatures, we would find that the reduced parameters $C_6^* \equiv C_6/\epsilon\sigma^6$, $C_8^* \equiv C_8\epsilon\sigma^8$, ... were the same for all the noble gas pairs. Table 1

Table 1
The low-temperature scaling parameter, $C_6^* = C_6/\epsilon\sigma^6$

	He	Ne	Ar	Kr	Xe
He	3.09	2.940	2.681	2.498	2.346
Ne		2.594	2.429	2.424	2.204
Ar			2.210	2.426	2.053
Kr				2.164	2.051
Xe					2.162

shows that the C_6^* have systematic variations. A low-temperature correlation of transport coefficients thus requires the introduction of C_6^* as a new parameter, in addition to ϵ and σ. KESTIN, RO, and WAKEHAM [1] were of course well aware of all this, but the accuracy of the C_6 coefficients available to them was still too low to justify anything beyond the assumption of a universal value for C_6^*. The values of C_8^* (not shown) also vary, but their effect on the transport properties is small enough that the variations can be neglected for most purposes.

The second virial coefficients at low temperatures are determined by the region of the potential around the minimum (dimer formation) [9], and fig. 4 shows that the two-parameter correlation holds in this region. Hence there is no need to introduce another new parameter representing, for instance, the reduced curvature of the potential at the minimum.

Both the transport and equilibrium properties at high temperatures depend on the short-range repulsive portion of V(r), which can be conveniently represented by an exponential function,

$$V(r) = V_o \exp(-r/\varrho) , \qquad (7)$$

where V_o and ϱ are energy and range parameters. Since there are only two parameters, it is obvious that a two-parameter correlation must hold at high temperatures. Unfortunately, this turns out to be a different correlation than that given by the parameters ϵ and σ, as shown by the fact that $V_o^* \equiv V_o/\epsilon$ and $\varrho^* \equiv \varrho/\sigma$ are not the same for all noble gas pairs, as recorded in Table 2. The values of V_o and ϱ in Table 2 were obtained from various theoretical calculations and scattering results [15,16]. The high-temperature correlation of transport and equilibrium properties therefore requires the introduction of V_o^* and ϱ^* as additional parameters. To summarize, the present extension of the principle of corresponding states requires five para-

Table 2
The high-temperature scaling parameters, $V_o^* = V_o/\epsilon$ and $\varrho^* = \varrho/\sigma$

$V_o^* \times 10^{-5}$

	He	Ne	Ar	Kr	Xe
He	8.50	10.60	9.740	10.89	13.37
Ne		11.09	9.235	9.929	11.20
Ar			5.117	4.849	4.878
Kr				4.491	4.337
Xe					3.898

ϱ^*

	He	Ne	Ar	Kr	Xe
He	0.0797	0.0788	0.0791	0.0772	0.0764
Ne		0.0784	0.0795	0.0786	0.0785
Ar			0.0836	0.0833	0.0835
Kr				0.0831	0.0837
Xe					0.0854

meters arising from the potential — ϵ, σ, C_6^*, V_o^*, and ϱ^* — plus the quantum parameter Λ^*. As an example of how such an extension appears, fig. 5 shows the correlation curves for the viscosity

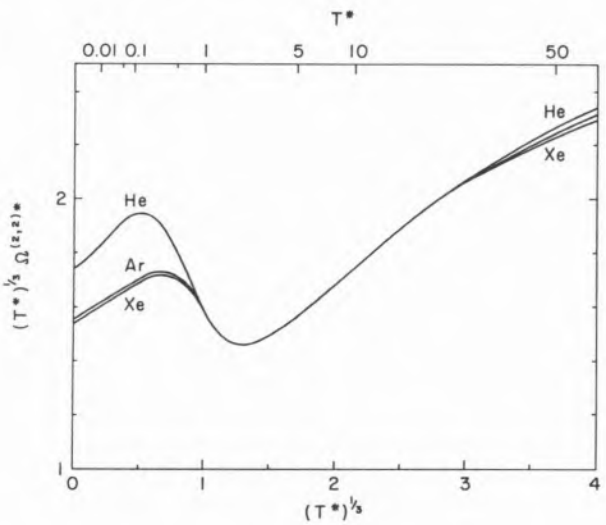

Fig. 5
Correlation curves for $\Omega^{(2,2)*}$, the reduced collision integral for viscosity. The single curve at intermediate T^* is the region of the two parameter (ϵ, σ) correlation. At low temperatures the additional parameter C_6^* is needed, and at high temperatures the repulsion parameters (V_o, ϱ^*) are needed

reduced collision integral, $\Omega^{(2,2)*}$, defined in Eq. (2). The region where only one curve appears is the same as represented by the original two-parameter correlation curves in figs. 1 and 2, but the result is plotted in a different way to take advantage of the theoretically known asymptotic behavior of $\Omega^{(2,2)*}$ at low T^*. The splitting of the single curve into families appears at both low and high temperatures. This splitting is indexed by C_6^* at low temperatures and by (V_o^*, ϱ^*) at high temperatures.

C — *EXTENSION OF CORRESPONDING STATES PRINCIPLE*

Here we set out explicitly what advantages can be obtained in a corresponding-states correlation by knowledge of V(r), but can give only a brief selection of actual results.

(1) The range of validity of the two-parameter (ϵ, σ) correlation can be specified more precisely. Outside of this range, deviations gradually set in and more than two parameters are needed. As an example, notice that the correlation for Ω_{22} in fig. 1 appears to be universal up to $T^* = 90$, whereas in fig. 5 it does not extend beyond $T^* = 30$. A closer look at fig. 1 shows that the high-temperature end of the correlation is based entirely on He, and is thus not demonstrated to be universal.

(2) Values of one property that is known accurately can be used to refine or predict other properties that are known less accurately from experiment. As an example, viscosity is usually measured with substantially greater accuracy than are diffusion coefficients and thermal diffision factors. By proceeding through V(r) we can use the accuracy of viscosity to improve that of diffusion coefficients.

(3) Joint analysis of two properties through the potential can improve the accuracy and range of validity of both, because different properties give information on different regions of the potential. For example, the second virial coefficient at very low temperatures is determined by the region near the potential minimum, whereas the viscosity at very low temperatures is determined by the long-range tail of the potential. Thus, viscosity data at only moderately low temperatures could be used to specify the second virial coefficient at very low temperatures, or *vice versa*.

(4) Data not directly related to the thermodynamic and transport properties of the gases can be used to extend the temperature range of the correlations to both lower and higher temperatures, as well as to improve accuracy in the original temperature range. Such data include scattering measurements, theoretical calculations, dielectric and optical data, and spectroscopic measurements that locate the

bound states in the potential well. This has allowed the temperature range of the correlation to be extended from virtually 0 K to the onset of first ionization.

(5) Statistical-mechanical theory can be used with knowledge of V(r) to find useful asymptotic forms for the temperature dependence of gas properties, and to include new properties. An example of the first is shown in fig. 5. An example of the second are the quantum corrections for the second virial coefficient, which can be isolated through V(r) but which are virtually impossible to extract accurately from experimental data alone.

Space permits only a few selected examples of the correlations obtained. A deviation plot for the viscosity of krypton is shown in fig. 6, including the

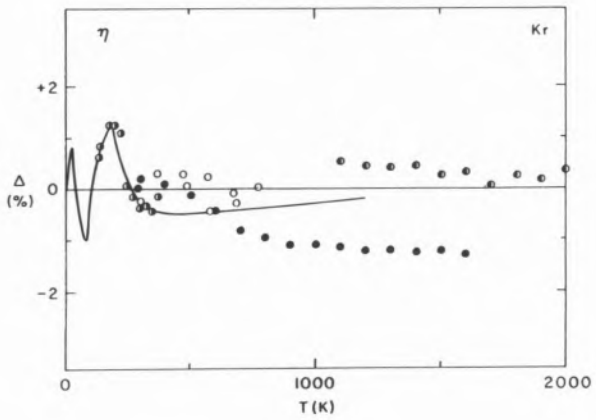

Fig. 6

Deviation plot for the viscosity η of Kr as a function of temperature. Δ(%) ≡ 100(expt − calc)/calc.

○ Ref. [26]; ● Ref. [27]; ◐ Ref. [28]; ◑ Ref. [29]; ——— Ref. [24]

experimental data considered best [26-29] and the results calculated from an accurate potential [24]. A similar deviation plot for the second virial coefficient of krypton is shown in fig. 7, together with experimental data [30-34]. The agreement shown in these two figures is typical. It should be remembered that the parameters ϵ and σ have been adjusted to optimize the fit, but the parameters C_6^*, V_o^*, and ϱ^* are specified independently.

The deviation plot for the self-diffusion coefficients of the noble gases, shown in fig. 8, supplies an independent test of the correlations, since these data were not used in any parameter adjustment.

Comparable results are obtained for other properties, and for mixtures of any number of components.

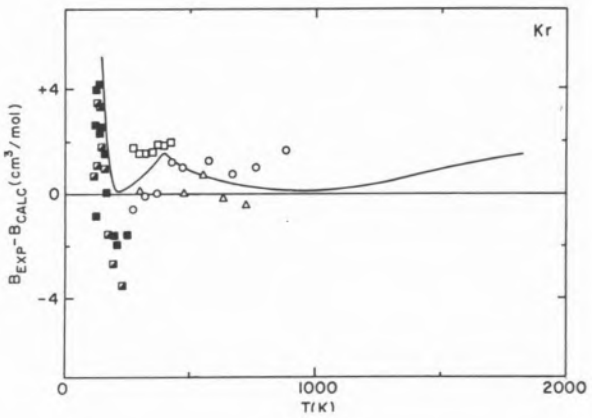

Fig. 7

Deviation plot for the second virial coefficient B of Kr as a function of temperature

○ Ref. [30]; □ Ref. [31]; ◪ Ref. [32]; ■ Ref. [33]; △ Ref. [34]; ——— Ref. [24]

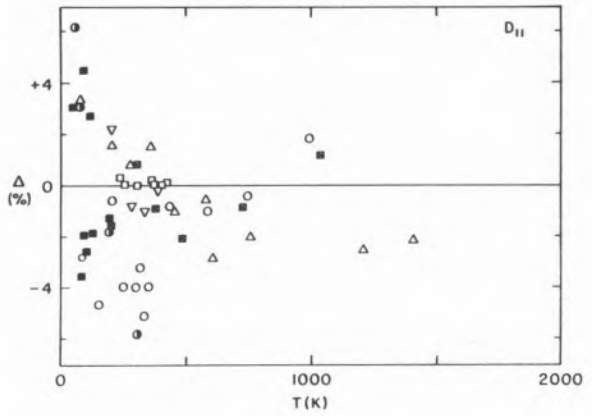

Fig. 8

Deviation plot for the self-diffusion coefficients, D_{11}, of the noble gases as a function of temperature. Δ(%) ≡ 100(expt − − calc)/calc.

○ , ◑ He; △ Ne; □ , ■ Ar; ⊠ Kr; ▽ Xe

AN EXAMPLE: DIRECT INVERSION OF GAS VISCOSITY

Historically, the earliest estimates of intermolecular potentials were based on macroscopic properties, such as second virial coefficients or low-density transport coefficients, and proceeded through parameterized models. Until fairly recently, computing limitations restricted the number of adjustable parameters to two or three, so that the models used were always a bit too crude. The direct inversion problem, proceeding from data to potential without explicit assumption of a mathematical model, was considered hopeless both in

principle and in practice, since there were direct demonstrations that such inversions cannot be unique [3]. Thus one of the surprising results of the past decade has been the development of direct inversion methods for both transport and second virial coefficients. The unexpected success of these methods is, in fact, still somewhat puzzling, although some progress has been made in understanding their success [12]. Here we give a brief account of direct inversion, using viscosity as an example.

From Eq. (2) we see that V(r) is entirely contained in the quantity $\sigma^2\Omega_{22}$, or in $\sigma^2\Omega^{(2,2)*}$, which is a thermally averaged cross section [8],

$$\pi\sigma^2\Omega^{(2,2)*} = \\ = [6(kT)^4]^{-1}{}_0\int^\infty Q^{(2)}(E)\exp(-E/kT)E^3dE\,, \qquad (8)$$

where E is the relative energy of collision. Two further layers of integration still shield V(r):

$$Q^{(2)}(E) = 3\pi_0\int^\infty [1-\cos^2\theta(E, b)]b\,db\,, \qquad (9)$$

$$\theta(E, b) = \pi - 2b_{r_0}\int^\infty \left[1-\frac{b^2}{r^2}-\frac{V(r)}{E}\right]^{-\frac{1}{2}} r^{-2}dr\,, \qquad (10)$$

where θ is the angle of deflection in a collision of energy E with impact parameter b.

The key idea is that η at a given T is determined by the interaction of two atoms over only a small range of separations. This is surely not obvious from Eqs. (8)-(10), but we return to the point later. This range is centered around some distance $\bar{r}$, such that $V(\bar{r})$ is of the order of kT, and $\sigma^2\Omega^{(2,2)*}$ is about equal to $\bar{r}^2$. This result is known to be roughly true, and we can make it exact by defining a suitable function G such that

$$G\,kT = V(\bar{r})\,, \qquad (11)$$

$$\bar{r}^2 = \sigma^2\Omega^{(2,2)*}. \qquad (12)$$

These quantities are illustrated in the upper part of fig. 9. In general, G depends in a complicated way on V(r) and T, but a remarkable feature emerges for potentials with the simple shape shown in fig. 9-G depends almost entirely on the single variable T^*, and is relatively insensitive to details of the shape of V(r). A typical function $G(T^*)$ is shown in the

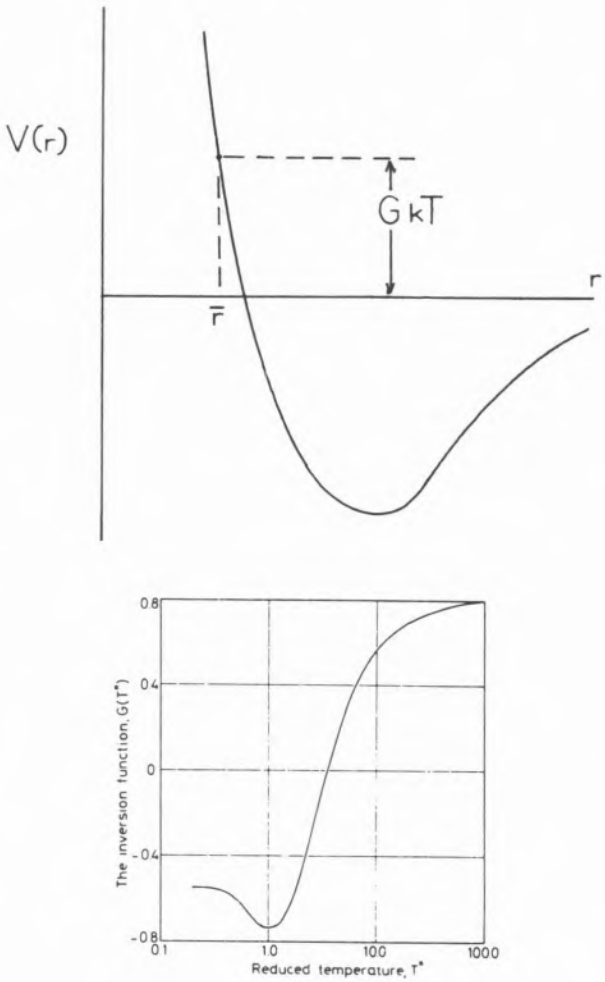

Fig. 9
Upper; Significance of G and $\bar{r}$. Lower: Typical inversion function $G(T^*)$

lower part of fig. 9. This almost miraculous behavior of G makes a direct inversion possible.

First a rough model of V(r) is used to calculate a first approximation to $G(T^*)$. The values of $\bar{r}$ are known from the measured $\eta(T)$ according to Eqs. (2) and (12). The corresponding values of $V(\bar{r})$ are then found from Eq. (11), using the first approximation to $G(T^*)$. This step requires the assumption of a provisional value of ϵ. From the series of measured points constituting $\eta(T)$, a corresponding series of points $V(\bar{r})$ is thus obtained. (Actually $\bar{r}(V)$ is obtained). This $V(\bar{r})$ is then used to calculate an improved approximation to $G(T^*)$, and the process is repeated until $V(\bar{r})$ becomes stable. Then this $V(\bar{r})$ is used to calculate $\eta(T)$ for comparison with experiment. The value of ϵ is found by numerical search to be the one that produces the best fit

of the data. The results are remarkably good when V(r) has a reasonably simple shape (e.g., as in fig. 9). How is this possible?

The first question to consider is how V(r) manages to survive three layers of integration. We can see how this happens from a closer examination of Eqs. (8)-(10). From Eq. (10) we find that the dominant contribution to θ for given b and E comes from the region of r near r_o, the distance of closest approach — the integrand is infinite at r_o. From Eq. (9) we notice two things: the factor $(1-\cos^2\theta)$ suppresses small-angle scattering, and the factor b db emphasizes collisions at large impact parameters. The appearance of b db is a result of the three--dimensional nature of the problem. The result is that $Q^{(2)}$ at a given E is dominated by a very small range of b (or, equivalently, of r_o) in which both θ and b are simultaneously large. Thus V(r) survives the second integration. The third integration of Eq. (8) has a peaked weighting factor of $E^3 \exp(-E/kT)$, which only smears the results a bit without washing them out entirely.

The second question to consider is how the inversion manages to work, despite demonstrations that it cannot be unique for the general case. Here our best hope is to make a connection with other inversion problems in physics that have already been worked out, of which there are quite a number [35]. Suppose we consider the surface of $|\theta|$ as a function of E and b, as shown in fig. 10. If we slice the surface at fixed b (or at fixed angular momentum), the resultant projection of $\theta_b(E)$ can be inverted. So can the projection $\theta_E(b)$ resulting from a slice at fixed E. If we examine in more detail the calculation of $Q^{(2)}(E)$, we find that the crucial small range of b or r_o that determines $Q^{(2)}$ always corresponds to a nearly constant value of the deflection angle, approximately $|\theta| = 1/\pi$. Thus the information contained in $\eta(T)$ is roughly equivalent to knowing b as a function of E at constant $|\theta| \approx 1/\pi$, which is the third orthogonal slice of the ($|\theta|$, b, E) surface (lower half of fig. 10). It is at least plausible that an inversion is possible for $b_\theta(E)$ if it is possible for $\theta_b(E)$ and $\theta_E(b)$, and more detailed considerations show that this is so [12].

The problem of uniqueness still remains. It is clear that some extra information has to be included for uniqueness, and that this occurs through implicit assumptions about the "shape" of V(r). This has been somewhat clarified by the use of simulated experimental data generated from a known V(r),

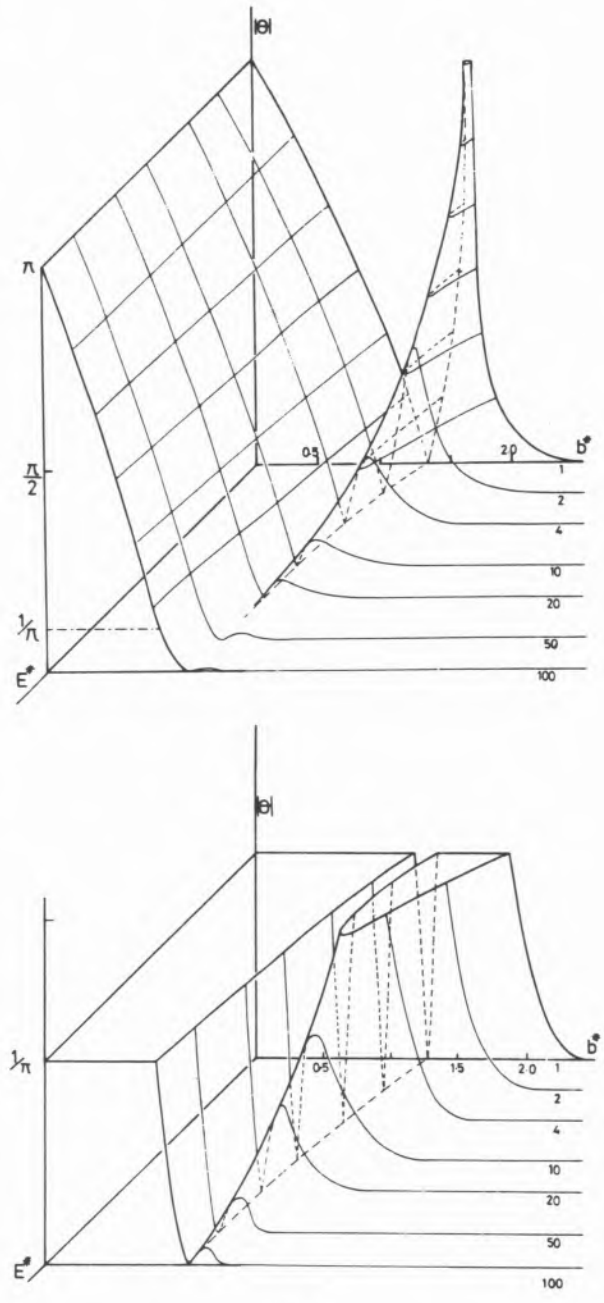

Fig. 10
Upper: Three-dimensional ($|\theta|$, b, E) surface. Lower: A slice through this surface at constant $|\theta| = 1/\pi$

into which various pathological feactures are introduced one by one. But many fascinating questions, both fundamental and practical, remain to be answered.

CONCLUDING REMARKS

I hope that this short review has given some insight into one small aspect of recent work on

transport properties. Even with a subject as old as the principle of corresponding states, there is much to be learned. Indeed, like all good scientific problems, recent work has raised at least as many questions as it has answered. Here are two. First, why is the extended principle of corresponding states so remarkably accurate for noble gas pairs? There must be an amazing similarity among the potentials involved, which persists to a very subtle degree on the energy scale at which quantum chemists currently make their calculations. It seems too much to believe that all this is merely fortuitous, but there is so far no inkling of a fundamental explanation. Second, why is the direct inversion of transport coefficients so successful? All the known mathematical theorems seem to argue against it, and it is easy enough to produce pathological cases that fail, but the method goes right on being practical. One is reminded of the old parable of the bee and the aeronautical engineers.

ACKNOWLEDGMENTS

Much of the work reported here has benefitted from the persistence and insight of Professor J. Kestin. A great debt is also owed for the contributions of A. Boushehri, K.D. Knierim, G.C. Maitland, B. Najafi, S.T. Ro, L.A. Viehland, W.A. Wakeham, and M. Waldman. This work was supported in part by U.S. National Bureau of Standards Grant NB 81 NADA 2013, and by the Stichting voor Fundamenteel Onderzoek der Materie (FOM) of the Nederlandse Organisatie voor Zuiver-Wetenschappelijk Onderzoek (ZWO).

REFERENCES

[1] J. KESTIN, S.T. RO, W.A. WAKEHAM, *Physica* **58**, 165 (1972).

[2] J. KESTIN, S.T. RO, W.A. WAKEHAM, *J. Chem. Phys.* **56**, 4119 (1972).

[3] J. KESTIN, E.A. MASON, *AIP Conf. Proc.* **11**, 137 (1973).

[4] J. KESTIN, H.E. KHALIFA, S.T. RO, W.A. WAKEHAM, *Physica* **88A**, 242 (1977).

[5] J. KESTIN, H.E. KHALIFA, W.A. WAKEHAM, *Physica* **90A**, 215 (1978).

[6] B. NAJAFI, Ph. D. Thesis, Brown University (1981).

[7] B. NAJAFI, E.A. MASON, J. KESTIN, Proc. 8th Int. Conf. Thermophys. Prop., ASME, New York, 1982.

[8] J.O. HIRSCHFELDER, C.F. CURTISS, R.B. BIRD, *Molecular Theory of Gases and Liquids*, Wiley, New York, 1964, Chap. 8.

[9] E.A. MASON, T.H. SPURLING, *The Virial Equation of State*, Pergamon, Oxford, 1969.

[10] J. DE BOER, *Repts. Prog. Phys.* **12**, 305 (1949).

[11] E.A. MASON, L. MONCHICK, *Adv. Chem. Phys.* **12**, 329 (1967).

[12] G.C. MAITLAND, E.A. MASON, L.A. VIEHLAND, W.A. WAKEHAM, *Mol. Phys.* **36**, 797 (1978). This is a review and theoretical justification for direct inversion procedures, from which full references can be obtained.

[13] J.M. FARRAR, T.P. SCHAFER, Y.T. LEE, *AIP Conf. Proc.* **11**, 279 (1973). This paper reviews much of the thermal-beam scattering work.

[14] K.T. TANG, J.M. NORBECK, P.R. CERTAIN, *J. Chem. Phys.* **64**, 3063 (1976), give a survey and compilation of reliable results.

[15] N.A. SONDERGAARD, E.A. MASON, *J. Chem. Phys.* **62**, 1299 (1975). This paper includes a survey and correlation of the scattering data of Amdur and coworkers, and of the electron-gas model calculations of Gordon and Kim.

[16] D.R. MCLAUGHLIN, H.F. SCHAEFER III, *Chem. Phys. Lett.* **12**, 244 (1971). *Ab initio* quantal calculations of the He-He repulsion.

[17] R.G. GORDON, Y.S. KIM, *J. Chem. Phys.* **56**, 3122 (1972). Electron-gas model calculations of the noble gas repulsive potentials.

[18] I. AMDUR, J.E. JORDAN, *Adv. Chem. Phys.* **10**, 29 (1966). A review of much of the experimental work.

[19] D.E. FREEMAN, K. YOSHINO, Y. TANAKA, *J. Chem. Phys.* **61**, 4880 (1974). References to most of the earlier work can be otained from this paper on the Xe_2 molecule.

[20] H.E. COX, F.W. CRAWFORD, E.B. SMITH, A.R. TINDELL, *Mol. Phys.* **40**, 705 (1980).

[21] R.A. AZIZ, V.P.S. NAIN, J.S. CARLEY, W.L. TAYLOR, G.T. MCCONVILLE, *J. Chem. Phys.* **70**, 4330 (1979). He-He potential.

[22] B. BRUNETTI, R. CAMBI, F. PIRANI, F. VECCHIOCATTIVI, M. TOMASSINI, *Chem. Phys.* **42**, 397 (1979), Ne-Ne potential.

[23] R.A. AZIZ, H.H. CHEN, *J. Chem. Phys.* **67**, 5719 (1977). Ar-Ar potential.

[24] J.A. BARKER, R.O.WATTS, J.K. LEE, T.P. SCHAFER, Y.T. LEE, *J. Chem. Phys.* **61**, 3081 (1974). Kr-Kr and Xe-Xe potentials.

[25] A. BOUSHEHRI, L.A. VIEHLAND, E.A. MASON, *Physica* **91A**, 424 (1978).

[26] J. KESTIN, H.E. KHALIFA, W.A. WAKEHAM, *Physica* **90**, 215 (1978).

[27] R.A. DAWE, E.B. SMITH, *J. Chem. Phys.* **52**, 693 (1970).

[28] M. GOLDBLATT, F.A. GUEVARA, B.B. MCINTEER, *Phys. Fluids* **13**, 2873 (1970).

[29] A.G.CLARKE, E.B. SMITH, *J. Chem. Phys.* **48**, 3988 (1968).

[30] E. WHALLEY, W.G. SCHNEIDER, *Trans. Am. Soc. Mech. Engrs.* **76**, 1001 (1954).

[31] N.J. TRAPPENIERS, T. WASSENAAR, G.J. WOLKERS, *Physica* **32**, 1503 (1966).

[32] R.D. WEIR, I.W. JONES, J.S. ROWLINSON, G. SAVILLE, *Trans. Faraday Soc.* **63**, 1320 (1967).

[33] M.A.BYRNE, M.R. JONES, L.A.K. STAVELEY, *Trans. Faraday Soc.* **64**, 1747 (1968).

[34] H.P. RENTSCHLER, B. SCHRAMM, *Ber. Bunsenges. Phys. Chem.* **81**, 319 (1977).

[35] J.A. WHEELER, in *Studies in Mathematical Physics*, E.H. Lieb, B. Simon, and A.S. Wightman, eds., Princeton Univ. Press, Princeton, New Jersey, 1976, pp. 351-422.

NOTE ADDED IN PROOF

Many details have now been published by B. NAJAFI, E.A. MASON, J. KESTIN, *Physica* **119A**, 387 (1983) and by J. KESTIN, K. KNIERIM, E.A. MASON, B. NAJAFI, S.T. RO, M. WALDMAN, *J. Phys. Chem. Ref. Data* **13** (1984).

JOSÉ AGUILAR PERIS
Catedratico de Termologia
Facultad de Fisica
Universidad Complutense
MADRID

FENOMENOS DE TRANSPORTE A TRAVES DE MEMBRANAS

1 — INTRODUCCION

Uno de los problemas fundamentales de la industria química es la separación, concentración y purificación de las sustancias presentes en una mezcla. En los últimos años las técnicas convencionales de separación como son la destilación, la cristalización, la extracción de disolventes, etc. se han visto suplementadas por un nuevo tipo de procesos que utilizan las membranas semipermeables como barreras de separación.

Realmente estos procesos son conocidos desde la Antiguedad. El poeta latino Lucrecio en su famoso poema *De natura rerum* (60 años A.C.) cuenta como el hombre aprendió primero a purificar el agua filtrándola a través de la tierra o la arena. Después y durante muchos siglos para separar las sustancias en suspensión de un líquido se utilizaron arcillas, gelatinas, resinas, pergaminos y membranas intestinales como la vejiga de cerdo. En 1688 La Hire escribía que esta vejiga era más permeable al agua que al alcohol y en 1774 el Abate Nollet, utilizando membranas inorgánicas como barreras semipermeables, descubría los fenómenos osmóticos que condujeron mucho más tarde a la formulación de las leyes coligativas (leyes de Van't Hoff) y culminó con la termodinámica de las soluciones de Gibbs.

Graham en 1861 demonstró que existían membranas permeables a las sustancias disueltas de bajo peso molecular, pero prácticamente impermeables a las partículas coloidales. Si se sitúa una de estas membranas en el fondo de una vasija donde se introduce la dispersión coloidal y se introduce el conjunto en un recipiente que contiene el disolvente, las moléculas y los iones disueltos pasan a través de la membrana y se separan de la disolución coloidal (fig. 1).

La diálisis tuvo en la historia de la química-física coloidal un papel capital. Se aplica todavía como procedimiento de separación y purificación en partículas, para eliminar de una solución coloidal las moléculas o iones que contiene. Así se purifican las macromoléculas de origen biológico: proteínas, enzimas, hormonas, etc. Se utiliza igualmente para recuperar la sosa en las industrias celulósicas, en la industria azucarera para separar las melazas de las sales minerales que perjudican la cristalización, para la purificación de los jabones, hidrocarburos, etc. Es un procedimiento que presenta la ventaja de no

This paper is an edited version of the lecture delivered at the Symposium on Transport Properties of Fluids, Lisbon (23-26 March 1982).

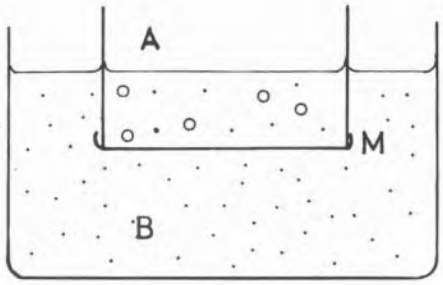

Fig. 1

Dializador de Graham. *En A se situa la solución que encierra macromoléculas o partículas coloidales (○) y pequeñas moléculas o iones (·); en B el disolvente; entre los dos la membrana M. Las partículas de débil peso molecular pasan de A a B por difusión*

necesitar más que un dispositivo muy simple y poco costoso. Su principal inconveniente es la duración del proceso, que puede durar varios días.

Durante la segunda guerra mundial los científicos que prepararon la bomba atómica de Hiroshima consiguieron separar los átomos de uranio-235 y uranio-238 (sólo los primeros eran aptos para la fisión nuclear) convirtiéndolos en compuestos gaseosos y la mezcla se difundía lentamente a través de una delgada pared porosa. A pesar de la pequeña diferencia de masa entre ambos tipos de uranio, el gas compuesto de partículas más ligeras se difundía a través de la pared a una velocidad algo más rápida que el formado por partículas más pesadas.

Recientemente el interés científico de los procesos de membranas ha sido estimulado por la purificación en gran escala de los productos químicos, utilizando nuevas técnicas como la cromatografía, la electroforesis, el refino por zonas, etc., en lugar de las técnicas tradicionales, como eran la sedimentación, la destilación o la cristalización. A ello contribuyó también el descubrimiento de la difusión del hidrógeno a través del paladio hace ahora unos 100 años. El paladio es atravesado por el hidrógeno con preferencia a los demás gases en virtud de un efecto catalítico (fig. 2). La red metálica disocia el hidrógeno en protones y electrones que pueden pasar a través de la lámina matálica y se recombinan al otro lado. Por esta razón las membranas de Pd son tan útiles en la purificación del hidrógeno.

Otra razón del énfasis actual en la investigación de membranas es biológica. Los especialistas en citología, patología y farmacología estudian intensamente los límites de las células — las membranas — donde se encuentran los centros activos que controlan el transporte químico a través de las mismas.

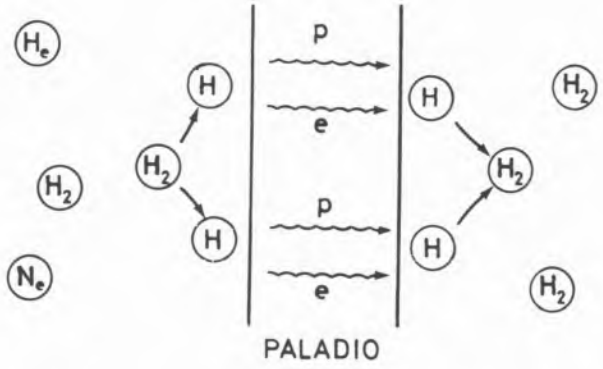

Fig. 2

El hidrógeno gaseoso atraviesa el paladio en virtud de un efecto catalítico

El estudio de los fenómenos de transporte a través de las membranas puede ayudar a entender la estructura de las membranas biológicas. El lado práctico de tal estudio puede verse en las *unidades de hemodiálisis* utilizadas para purificar la sangre, los denominados *riñones artificiales* y en las unidades de oxigenación utilizadas en operaciones de corazón extracorpóreas mediante el llamado *pulmón artificial*.

Los geólogos utilizan membranas como modelos para la unión entre esquistos impermeables y areniscas portadoras de agua y petróleo.

Los físicos utilizan membranas de intercambio iónico para hacer rectificadores y amplificadores electrolíticos (no electrónicos).

Los ingenieros especiales, en un tipo de célula combustible hidrógeno-oxígeno utilizada por vez primera en el vehículo Geminis-5, utilizaron una membrana de intercambio iónico como electrolito sólido hermético. Otras dos razones han espoleado el resurgir actual de las membranas. Una, el interés masivo por parte de muchos gobiernos para encontrar procedimientos económicos para desalinizar el agua del mar y aguas subterráneas salobres. La otra razón es la habilidad siempre creciente de los químicos de polímeros para obtener membranas orgánicas ajustadas ("tailor-made") a una tarea definida, como desalinizar el agua del mar, purificar la sangre, concentrar o fraccionar soluciones macromoleculares, limpiar efluentes industriales, etc.

En muchos casos los procesos de separación mediante membranas son más rápidos, más eficaces y más económicos que las técnicas convencionales. A veces la ventaja es sustancial, como ocurre en las industrias de alimentos y de medicamentos, pues la separación con membranas puede verificarse

a la temperatura ambiente evitando que los constituyentes sean dañados o químicamente alterados. Hoy la investigación en el campo de las membranas incluye varias disciplinas científicas:
(1) Los químicos de polímeros desarrollan nuevos materiales.

(2) Los termodinámicos describen las propiedades de transporte según la teoría de los procesos irreversibles y definen modelos que predicen las características de separación de una membrana.

(3) Los ingenieros químicos utilizan los modelos desarrollados para diseñar procesos de separación en la industria química.

Nuestros trabajos en el Departamento de Termología de la Universidad Complutense de Madrid se incluyen en el Apartado [2] y en esta charla pretendemos exponer los principios fundamentales de los procesos de transporte a través de las membranas y nuestra modesta contribución a los mismos.

2 — DEFINICION Y TIPOS DE MEMBRANAS

No es fácil dar una definición completa y precisa de una membrana que cubra todos sus aspectos. La definición se simplifica si nos limitamos a las membranas artificiales o sintéticas, y prescindimos de fenómenos como el transporte activo que se presenta en las membranas de las células vivas.
En sentido general, una membrana sintética es un sistema que separa dos medios distintos y restringe el transporte a su través de las especies químicas de un modo específico, Una membrana puede ser, según su estructura homogénea o heterogénea. Sin embargo, puede ser desconcertante comprobar que lo que llamamos membrana homogénea puede estar formada por tres fases separadas (por ejemplo, una parte hidrófoba, otra parte hidrofílica y una tercera de agua). El término homogéneo se usa aquí para expresar que la membrana posee algún grado de transparencia a la luz y que ha sido formada a partir de un sólo componente polimérico. En cambio, una membrana heterogénea puede estar construída con un solo material activo (usualmente una sustancia cristalina o cuasicristalina y no necesariamente un polímero) disperso en un soporte elastomérico como caucho o en un soporte plástico amorfo.

Según su carga una membrana puede ser neutra o transportar cargas positivas, negativas o ambas. Su espesor puede variar entre 0,1 μm y 1 cm. Su resistencia eléctrica puede oscilar entre miles de megohms y fracciones de 1 ohm. La transferencia de masa a través de una membrana puede ser causada por difusión de partículas individuales o por flujo convectivo inducido por un campo eléctrico o por un gradiente de concentración, presión o temperatura, es decir, por una fuerza termodinámica generalizada.
El requisito fundamental de una membrana es el siguiente: cuando se interpone entre dos fases, ejerce un control selectivo del transporte de materia y de energía entre ellas. Así una membrana se define por su función y no por su composición o forma. Todas las membranas poseen una propriedad en común: *restringen el paso de diversas especies químicas de un modo muy específico*. El mecanismo de transporte a través de la membrana depende de su estructura y ésta puede controlarse por el método de preparación.
Así, ya hemos visto que existen membranas cuyo efecto selectivo depende de procesos catalíticos (como ocurre con el paladio y otros metales nobles). Otras discriminan las moléculas en función del tamanõ del poro. Cuando éste posee un diámetro superior a 50 Å el mecanismo de transporte es fundamentalmente de tipo convectivo; las membranas se llaman *macroporosas* y actuan como auténticas barreras o filtros moleculares (fig. 3). Son muy importantes en la diálisis, ultrafiltración y presión osmótica.

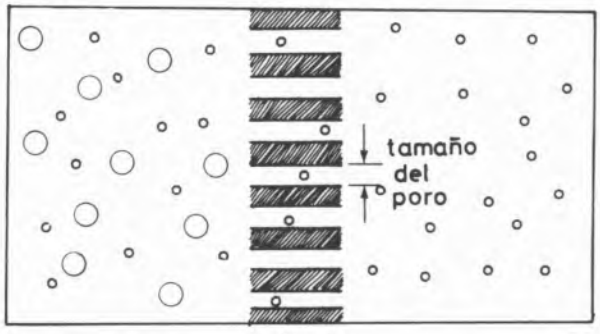

Fig. 3
Membrana de barrera molecular que discrimina las moléculas en función del tamaño del poro

En cambio, las *membranas microporosas* poseen unos huecos tan estrechos (inferiores a 50 Å) que el transporte sólo puede explicarse por intercambio de posiciones de las moléculas o iones móviles dentro

de la membrana. El acoplamiento de flujos puede despreciarse y el transporte por convección no es posible. A este tipo de membranas corresponde la hiperfiltración.

Las *membranas hidrofílicas* verifican su función selectiva gracias a su capacidad de romper la estructura de "clusters" o racimos de moléculas de agua no coordinadas con iones salinos. Las moléculas disgregadas atraviesan la membrana mientras que los "clusters" salinos permanecen al otro lado y se produce la separación. Otras membranas tienen una avidez semejante por disolventes no acuosos (fig. 4).

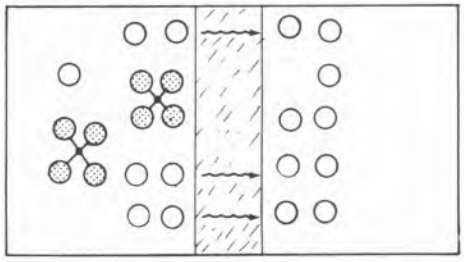

Fig. 4
Membrana hidrofílica

Desde hace pocos años la sofistificación ha llegado al extremo de construir *membranas asimétricas*, es decir láminas cuya composición del polímero cambia a través del espesor. Este avance es importante, pues "el gradiente de composición" da a la membrana propriedades direccionales muy valiosas: las moléculas pasan en una dirección y no en la otra (fig. 5). Es la propia membrana la que ocasiona la direccionalidad y no los gradientes de presión, concentración, temperatura, etc. Este es un paso importante para la comprensión de los fenómenos de transporte unidireccionales que con tanta frecuencia se encuentran en los sistemas biológicos, si bien todavía queda un largo camino para la polimerización de membranas con una propagación controlada estereoespecífica.

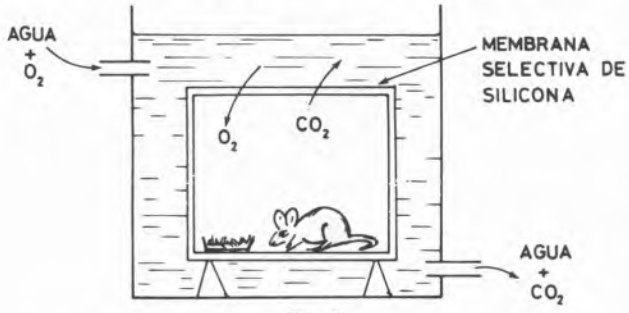

Fig. 5
Una membrana de caucho de silicona incolora cierra parcialmente el tanque situado bajo el agua en donde vive el hamster. Bajo condiciones apropiadas de presión y de flujo de agua la membrana extrae selectivamente el O_2 del agua en una dirección y el CO_2 en dirección opuesta permitiendo la función respiratoria del animal

Una forma de conseguir la discriminación de los iones a través de una barrera es aprovechar su carga eléctrica mediante las *membranas de intercambio iónico*. Estas membranas son electrolíticamente conductoras en el seno de electrolitos. Pueden ser de varios tipos:

a) Intercambio catiónico (polímeros cargados negativamente). Dejan pasar solamente a los cationes (Na^+, K^+, Ca^{++}, etc.).

b) Intercambio aniónico (polímeros cargados positivamente). Dejan pasar solamente a los aniones (Cl^-, $SO_3^=$...).

c) Anfóteras (mezcla de las dos anteriores).

d) Bipolares (laminado de a) y b)).

e) Mosaico (mezcla por regiones de a) y b)).

En la estructura química (polímeros orgánicos de tipo poliestireno-divinil-benceno) estas membranas contienen posiciones en donde los iones cargados de un determinado signo (SO_3^-, $-NR_3^+$...) están fijos. Cada una de las cargas fijas (por enlaces covalentes) está equilibrada eléctricamente por un contra-ión de carga opuesta. Los contraiones son móviles (enlaces iónicos) y cambian fácilmente de lugar con otros iones móviles de igual carga, de modo que la solución atraviesa la membrana: diálisis permiónica, electrodiálisis y piezodiálisis. Cuando las cargas fijas son negativas y los contraiones positivos, la membrana deja pasar preferentemente los iones positivos y viceversa (fig. 6).

Una medida de la selectividad que proporcionan las membranas de intercambio iónico viene dada por la siguiente comparación. El "poro" más ancho en una membrana no cargada que es suficientemente pequeño para evitar el flujo convectivo de pequeñas moléculas o iones, pero todavía suficientemente grande para permitir su difusión es de 15 Å. En cambio, las membranas de intercambio iónico pueden rechazar iones de tamaño idéntico de la misma carga con poros de 40 Å de anchura.

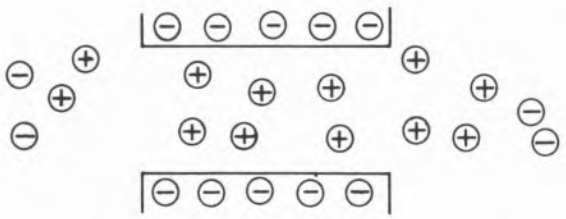

Fig. 6

Membrana catiónica. Los aniones son repelidos y los cationes toman parte preferente en el proceso de transporte a través de la membrana

Cuando una membrana de intercambio iónico se introduce en una solución salina acuosa, sus paredes se hinchan y se establece un equilibrio, "el equilibrio de Donnan", según el cual el producto de las actividades de los iones de signo contrario en la fase acuosa dentro de un cambiador iónico es igual al producto de las actividades de los mismos en la solución externa; por ejemplo:

$$[(a_{Na^+})\ (a_{Cl^-})]_{membrana} = [(a_{Na^+})\ (a_{Cl^-})]_{solución}$$

es decir, los iones móviles se distribuyen entre las dos fases de modo que cada una de ellas sea eléctricamente neutra y los potenciales químicos de las especies que se difunden sean iguales. Estas condiciones implican que los cationes penetran más fácilmente que los aniones en el seno de una red polianiónica y a la inversa. Por ello, una membrana formada a partir de un poliácido es más permeable a los cationes que a los aniones (fig. 7).

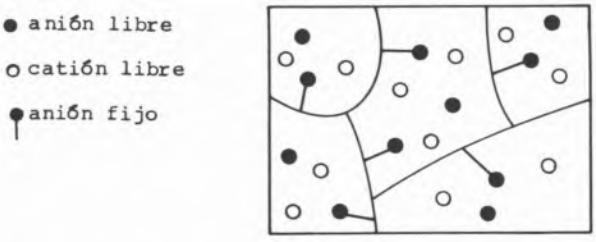

Fig. 7

Introducción de un electrolito en una red polianiónica. La electroneutralidad de la fase hinchada implica una penetración más fácil, es decir, una filtración más rápida de los iones libres cuyo signo es opuesto al de los lugares ionizados de la red macromolecular

Las *membranas bipolares* consisten en una combinación de capa doble de regiones aniónicas y catiónicas, cuyo conjunto actúa como el análogo electrolítico de una unión electrónica p—n (fig. 8).

Una *membrana mosaico* (fig. 9) es simplemente una membrana de intercambio iónico dentro de la

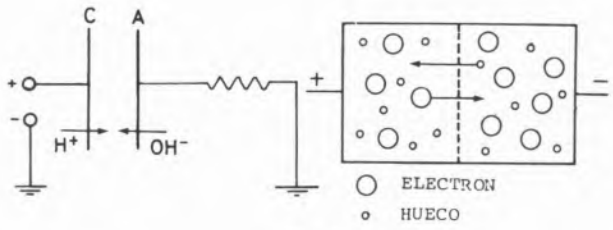

Fig. 8

Membrana bipolar y su analogía electrónica

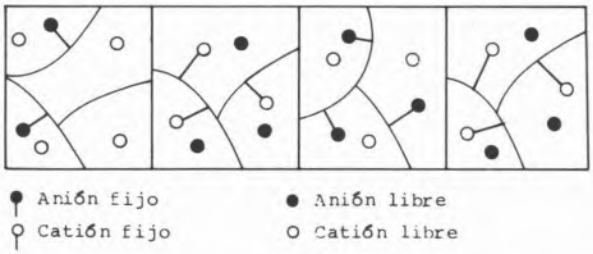

Fig. 9

Membrana mosaico

cual las áreas aniónicas y catiónicas se distribuyen en capas paralelas. Artificialmente se han construído membranas de este tipo asimétricas (mediante un gradiente en la composición) con lo cual se consigue discriminar entre iones del mismo signo, pero con carga diferente.

Las *membranas anfóteras* difieren de las membranas mosaico en el hecho de que sus regiones aniónicas y catiónicas están tan intermezcladas que son físicamente indistinguibles.

3 — FENOMENOS DE TRANSPORTE EN MEMBRANAS

La separación en los procesos de membrana es el resultado de las diferencias en las velocidades de transporte de las especies químicas a través de la interfase. La velocidad de transporte y por tanto, la magnitud del flujo, viene determinada por la fuerza o fuerzas que actúan sobre los componentes individuales y de su movilidad y concentración en la interfase. La movilidad depende del tamaño molecular del soluto y de la estructura física de la membrana (dureza, cristalinidad, flexibilidad de la cadena del polímero, tamaño del poro, etc.) y la concentración del soluto en la interfase depende fundamentalmente de la compatibilidad química del soluto y del material de la interfase.

El proceso de transporte en sí mismo es un proceso no equilibrado y convencionalmente se describe por una ecuación fenomenológica que relaciona el flujo con la fuerza conjugada en forma proporcional.

Tabla 1
Relaciones fenomenológicas entre diversos flujos y las correspondientes fuerzas conjugadas

Relación fenomenológica	Flujo	Fuerza conjugada	Constante de probabilidad
Ley de Fick $J = -D\Delta C$	Masa J	Diferencia de concentración, ΔC (o potencial químico, $\Delta\mu$	Coeficiente de difusión D
Ley de Ohm $I = \frac{\Delta\epsilon}{R}$	Intensidad de corriente I	Diferencia de potencial $\Delta\epsilon$	Conductancia eléctrica 1/R
Ley de Fourier $Q = K\Delta T$	Calor Q	Diferencia de temperatura ΔT	Conductividad térmica k
Ley de Hagen-Poiseuille $V = h_d \Delta P$	Volumen V	Diferencia de presión ΔP	Permeabilidad hidrodinámica h_d

En la Tabla 1 se exponen algunas de estas ecuaciones fenomenológicas más familiares:

Las fuerzas impulsoras en algunos procesos de membrana pueden ser interdependientes dando lugar a nuevos efectos. Así, un flujo de calor J_q puede ser impulsado por un gradiente de temperaturas Δt (conducción térmica ordinária) o por un gradiente de presiones, Δp (efecto mecánico-calórico). Igualmente un flujo de volumen J_v puede estar impulsionado por un gradiente de presiones Δp (permeabilidad hidráulica) o por un gradiente de temperaturas Δ (termoósmosis). Si el Δt permanece constante la variación de presión necesaria para que el flujo J_v se anule se denomina *diferencia de presión termoosmótica* (fig. 10).

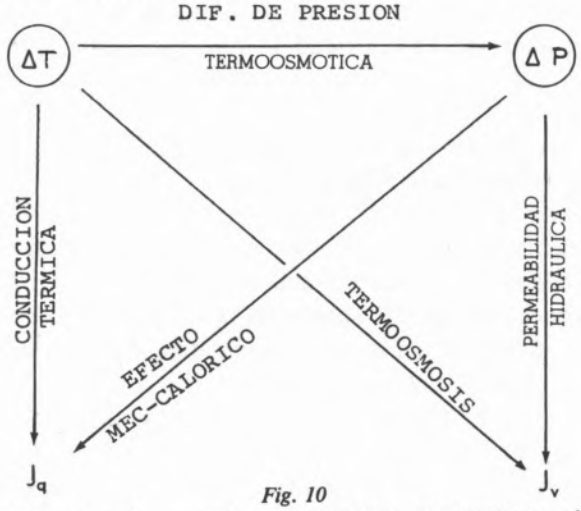

Fig. 10
Flujos de calor y volumen impulsados por gradientes de temperatura y presión

Si acoplamos además el gradiente de concentración o potencial químico se produce un flujo de volumen, J_v (ósmosis) y un flujo iónico J_i (diálisis). Este último puede producirse también por causa de un gradiente de presión Δp (piezodiálisis). Si la presión hidrostática es superior a la osmótica se produce un flujo de volumen en sentido inverso, J_v (ósmosis inversa). El flujo de calor dirigido por el gradiente de potencial se denomina *efecto Dufour* y el flujo de materia producido por el gradiente de temperaturas se llama *efecto Soret*, (fig. 11).

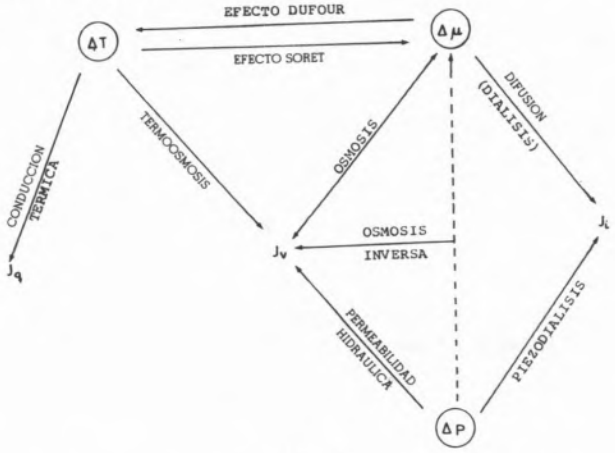

Fig. 11
Flujos acoplados a los gradientes de temperatura, presión y potencial químico

Del mismo modo, la introducción de la diferencia de potencial eléctrico, $\Delta\epsilon$ hace aparecer nuevos efectos que vienen especificados en las figs. 12 y 13.

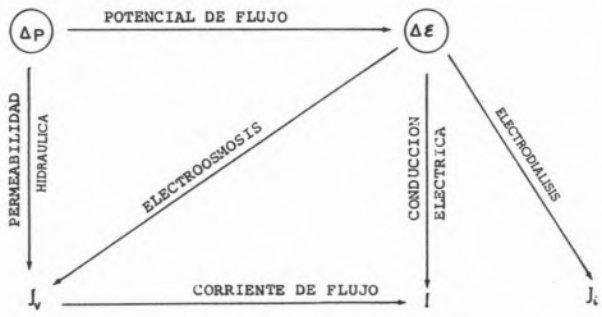

Fig. 12

Flujos acoplados a los gradientes de presión y potencial eléctrico (efectos electrocinéticos)

Fig. 13

Flujos acoplados a los gradientes de temperatura potencial eléctrico y concentración

La fig. 14 es un resumen de estas interacciones.

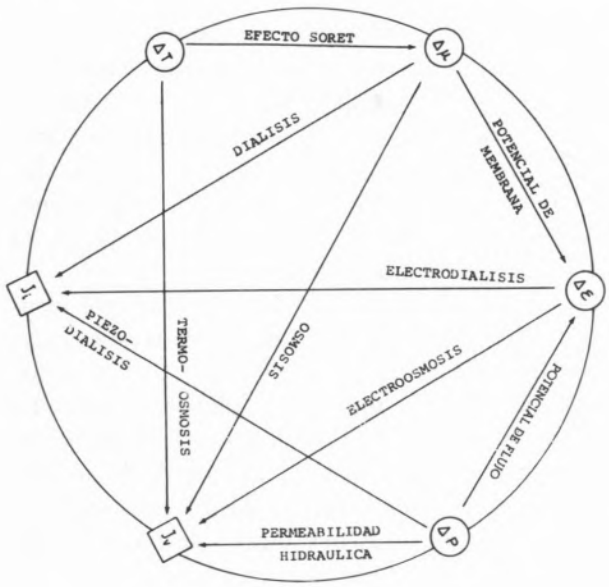

Fig. 14

Ciclo de los fenómenos de transporte em membranas. [Adaptado de H.Z. FRIEDLANDER y R.N. RICKLES, Chem. Eng., *73, 111 (1966)]*

Por último, en la fig. 15 se indican las interacciones que tienen lugar a través de una membrana que separa dos recintos gaseosos sometidos a gradientes de temperatura y presión. J_m es el flujo isotermo gaseoso producido por una diferencia de presión. Si inicialmente las presiones a los dos lados de la membrana son iguales pero se establece una diferencia de temperaturas, ΔT, el gas fluye del recinto más frío al más caliente, fenómeno llamado *transpiración térmica*.

Fig. 15

Flujos acoplados a los gradientes de temperatura y presión sistemas gaseosos

Para describir los fenómenos de transporte a través de membranas se han elaborado diversas teorías que se distinguen por la ecuación del flujo que utilizan. Todas ellas pueden englobarse en cuatro grupos fundamentales.

(1) *Ecuación de Nernst-Planck*

Expresa el flujo en iones gramo como consecuencia de la existencia de un gradiente de concentración y un gradiente de potencial.

$$J_i = -Di\left(\frac{dc_i}{dx} + ac\frac{d\ln\gamma_i}{dx} + \frac{z_l c_i F}{RT}\frac{d\epsilon}{dx}\right)$$

en donde γ_i es el coeficiente de actividad $\gamma_i = c_i/a_i$ y los demás simbolos tienen el significado habitual. Si la disolución es ideal $\gamma = 1$ y se anula el segundo término. Si además la solución no es iónica y $d\epsilon = 0$, resulta la ley de Fick:

$$J_i = -D_i\frac{dc_i}{dx}$$

(2) *Termodinámica de los procesos irreversibles*

Es una teoría fenomenológica que no suministra información sobre los mecanismos internos de transporte. Sin embargo proporciona un marco teórico muy útil respecto a los factores que intervienen en el transporte.
Las ecuaciones fenomenológicas correspondientes se expresan en la forma

$$J_i = L_{i1}X_1 + L_{i2}X_2 + \ldots + L_{in}X_n = \sum_1^n L_{ik}X_k$$

cumpliéndose el teorema de Onsager

$$L_{ik} = L_{ki}$$

Para cualquier valor de i y k ($i \neq k$).
La ley de la producción de entropía exige además que

$$\dot{S} = \sum_1^n J_i X_i > 0$$

Existen dos caminos en la aplicación de la TPI a los procesos de transporte en membranas:
a) *Tratamiento discontinuo.* No tiene en cuenta los fenómenos ocurridos en el interior de la membrana. Las ecuaciones de transporte se describen a partir de las variables observables de las fases a ambos lados de la membrana. También se llama tratamiento de "caja negra" y su análisis es análogo al de un circuito eléctrico donde sólo interesa el "input" y el "output".
b) *Tratamiento continuo.* Pretende dar una información sobre los procesos que ocurren en el interior de la membrana. Esta se considera como un continuo y el tratamiento pretende expresar los flujos y las fuerzas como funciones de las coordenadas espaciales.

(3) *Teoría de los procesos de velocidad (rate processes)*

Consideran la membrana como una barrera de potencial, que debe ser superada por la especie transportada. En condiciones estacionarias e isotermicas y con $\Delta p = 0$ se cumple

$$M = A(T)\, e^{-E_a/Rt}$$

en donde M es el coeficiente de difusión, A(T) es un factor de frecuencia y E_d la energía de activación. En intervalos pequeños de T se puede considerar que $A(T) = Cte$ y $E_a = Cte$. Por tanto, representando ln M en función de 1/T se puede calcular la energía de activación o altura de la barrera.

(4) *Teorías de transporte microscópicas.* Están basadas en las ecuaciones cinéticas del transporte de Boltzmann. Son las teorías más generales e interesantes, pues nos dan un conocimiento microscópico de los fenómenos. Sin embargo tienen el inconveniente de su gran complejidad y a veces su difícil aplicación a la interpretación de los datos experimentales.

4 — PROCESOS DE SEPARACION POR MEMBRANAS

En los procesos de separación por membranas sólo son de interés aquellas fuerzas impulsoras que dan lugar a un flujo de materia significativo. Tales son la presión hidrostática y las diferencias de potencial eléctrico y de concentración.

a) *FUERZA IMPULSORA: DIFERENCIA DE PRESION HIDROSTATICA*

Una diferencia de presión hidrostática entre dos fases separadas por una membrana puede dar lugar a un flujo de volumen y a una separación de especies químicas cuando la permeabilidad hidrodinámica de la membrana es diferente para los distintos componentes. Los procesos mejor conocidos son la *microfiltración*, la *ultrafiltración*, la *ósmosis inversa* y la *piezodiálisis.*
Los tres primeros procesos son básicamente idénticos y sólo difieren en el tamaño de las partículas a separar y las membranas utilizadas. En todos ellos una mezcla de componentes químicos se pone en contacto con la superficie de una membrana semipermeable y bajo la fuerza impulsora de un gradiente de presión, unas especies atraviesan la membrana, mientras que otras son más o menos retenidas.
El término *microfiltración* se utiliza cuando se separan de un disolvente partículas de diámetros comprendidos en el intervalo 0,1-10 μm. Las membranas utilizadas son estructuras microporosas

simétricas de tamaño de poro en el intervalo 0,1-10 μm y las diferencias de presión hidrostáticas de 0,1 a 2 bars.

El proceso se llama *ultrafiltración* cuando los componentes son moléculas reales o partículas de diámetro inferior a 0,3 μm, que corresponde al límite de resolución del microscopio óptico. Se utilizan presiones hidrostáticas de 1 a 5 bars. En la fig. 16 se muestran los principios básicos de la microfiltración y la ultrafiltración. Bajo la presión hidrostática el disolvente y las partículas pequeñas del soluto atraviesan la membrana, mientras son retenidas y concentradas las partículas de mayor diámetro.

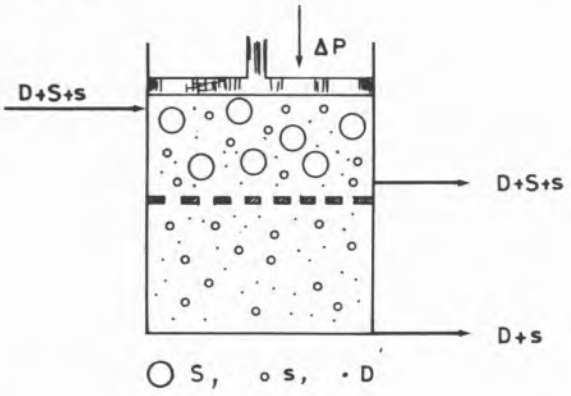

Fig. 16
Principios básicos de la microfiltración y la ultrafiltración

Si las moléculas que deben separarse son de bajo peso molecular, como sales, azúcares, etc., sus soluciones poseen presiones osmóticas elevadas que deben vencerse mediante una adecuada presión hidrostática. El fenómeno se llama *ósmosis inversa* y las presiones utilizadas pueden variar de 20 a 100 bars.

La piezodiálisis es un proceso que consiste en enriquecer una disolución salina acuosa haciéndola pasar bajo presión a través de una membrana cambiadora de iones del tipo mosaico (fig. 17).

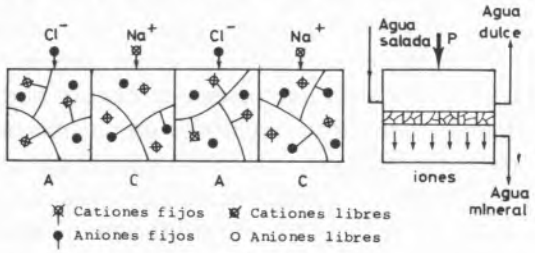

Fig. 17
Piezodiálisis

La piezodiálisis, como la ósmosis inversa, hace uso de la presión y de una membrana selectiva. Pero en lugar de ser el agua la que atraviesa la membrana reteniendo los iones, en la piezodiálisis las membranas iónicas que constituyen el mosaico absorben los iones de Cl^-, Na^+ y Mg^{2+} selectivamente y en virtud de la electroneutralidad que exige la relación de Donnan la penetración se hace con rapidez, mientras el agua permanece sin atravesar la membrana. Como las aguas del mar más cargadas contienen menos de un 4% de sal, la disposición de estas membranas produce una desmineralización rápida y eficaz con una menor transferencia de materia.

Sin embargo, el desarrollo de este dominio depende aún de la puesta a punto de películas satisfactorias. Las regiones de la membrana mosaico alternativamente aniónicas y catiónicas deben tener dimensiones del orden de algunas micras. Para ello se efectuan dos injertos radioquímicos sobre una película inerte. El primero con un monómero ácido y el segundo con un reactivo básico, orientándoles hacia regiones adyacentes de la película mediante una pantalla perforada que es opaca a la radiación. Se calcula que el gasto será 6 veces menor que con una unidad de ósmosis inversa.

b) *FUERZA IMPULSORA: DIFERENCIA DE CONCENTRACION*

La ósmosis ordinaria aparece cuando dos disoluciones de diferente concentración están separadas por una membrana semipermeable. En la fig. 18 se muestra el fenómeno osmótico. La membrana separa dos disoluciones (1 y 2) cada una de ellas formada por un disolvente y un solo soluto. Según los valores relativos de las concentraciones c, las presiones hidrostáticas p, las presiones osmóticas π y los potenciales químicos μ a ambos lados de la membrana, se presentarán los casos (a) equilibrio total, (b) ósmosis directa, (c) equilibrio osmótico y (d) ósmosis inversa.

La relación entre el flujo de volumen a través de una membrana semipermeable que separa dos disolluciones de diferentes concentraciones y la diferencia de presión hidrostática se indica en la fig. 19. La velocidad de filtración o flujo en la ósmosis inversa J_v es proporcional a la diferencia entre la

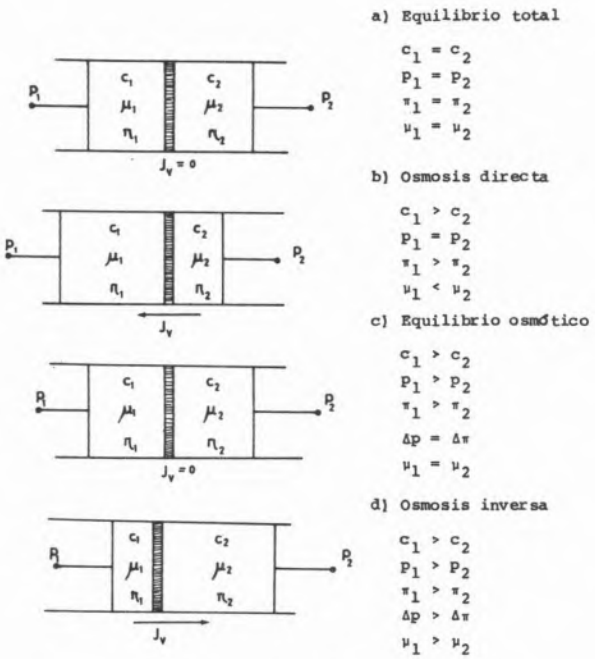

Fig. 18

Fenómenos osmóticos. [Adaptado de H. STRATHMANN, Jour. of Memb. Sc., *9, 121 (1981)]*

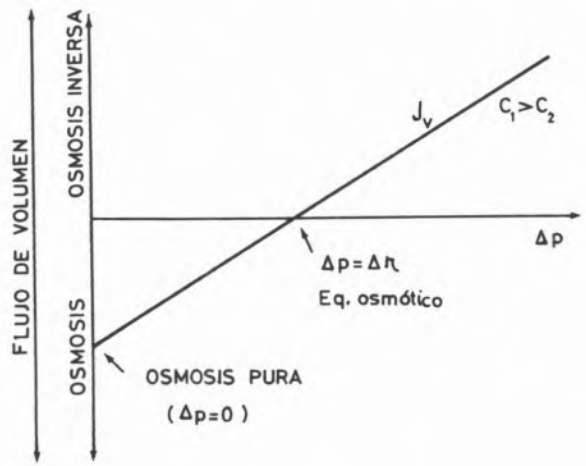

Fig. 19

Relación entre la ósmosis directa y la ósmosis inversa

presión hidrostática aplicada y la presión osmótica de la solución considerada. Se expresa generalmente por la relación.

$$J_v = L_p (\Delta p - \sigma \Delta \pi)$$

en donde L_p es el cociente de permeabilidad y σ el coeficiente de reflexión que es un factor de corrección que tiene en cuenta el hecho de que la mayor parte de las membranas prácticas no son estrictamente semipermeables, sino que dejan pasar algo de soluto. En una membrana perfectamente semipermeable, $\sigma = 1$.

La ecuación anterior suele escribirse también en la forma

$$J_v = L_{11} \Delta_p + L_{12} \Delta \pi$$

en donde L_{11} es el coeficiente que hemos llamado de permeabilidad y L_{12} es el coeficiente de flujo osmótico.

La presión osmótica de una solución con solutos de bajo peso molecular, tales como una solución de sal o azúcar es bastante elevada incluso a concentraciones relativamente bajas. La presión osmótica del agua del mar, por ejemplo, oscila entre 20 y 25 bars. La presión osmótica del jugo de naranja varía entre 25 y 30 bars. Una concentración tres o cuatro veces mayor de jugo de naranja supone una presión osmótica en exceso de 100 bars. Esta presión osmótica debe vencerse con una presión hidrostática para que se produzca la ósmosis inversa. Debido a las propiedades mecánicas del material de las membranas y por razones económicas esta presión hidróstatica no puede superar los 100 bars.

Por otra parte, si consideramos sólo el flujo de soluto J_D relativo al disolvente se verificará igualmente

$$J_D = L_{21} \Delta p + L_{22} \Delta \pi$$

Evidentemente para que exista un flujo difusivo es necesaria una diferencia de concentración expresada aqui como la diferencia de presión osmótica $\Delta \pi$. Pero como indica la expresión anterior, incluso cuando $\Delta \pi = 0$, puede desarrollarse un flujo difusivo bajo la acción de una presión mecánica. El fenómeno es la ***ultrafiltración***, ya definida y bien conocida por los antiguos químicos coloidales.

Una interesante aplicación clínica de la ultrafiltración se ha propuesto recientemente. Los pacientes con edemas deben someterse a un proceso de extracción del agua que poseen en exceso, para lo cual se le suministran diuréticos que incrementan la excreción renal del agua. Pero algunos pacientes no responden a este tratamiento y en estos casos se ha utilizado con éxito la ultrafiltración del plasma sanguíneo que extrae el agua y el sodio dejando intactos los otros constituyentes.

En algunos procesos de separación se utilizan sucesivamente la ósmosis inversa y la ultrafiltración. Así, la concentración del jugo de naranja se suele realizar en dos etapas. En una primera fase el jugo se trata en una célula equipada de *una membrana de ósmosis inversa*, pero se limita la concentración del producto tratado de modo que su presión osmótica no exceda las 50 atm. A continuación el jugo se traslada a una segunda célula donde es *ultrafiltrado* por una membrana que no sólo es permeable al agua, sino también a los azúcares y a las moléculas orgánicas de pequeño tamaño. Esta "fuga controlada" permite mantener un flujo de transparencia satisfactorio pues sólo debe vencerse una contra-presión osmótica artificialmente reducida (fig. 20).

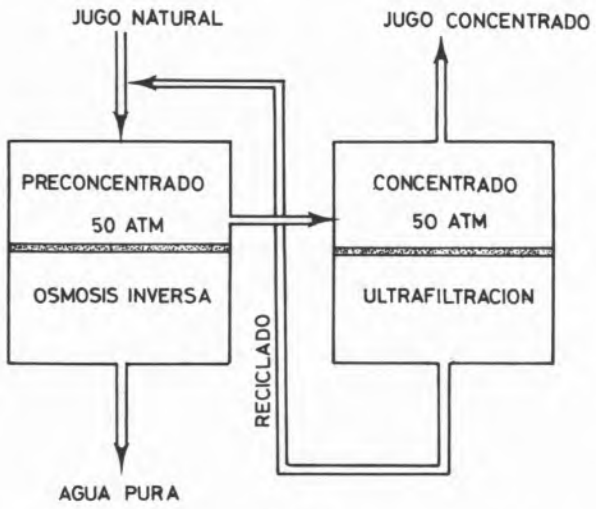

Fig. 20

La concentración de los jugos de frutas (naranja) se puede efectuar por ósmosis inversa en la célula de pre-concentración, seguida de ultrafiltración en la célula de concentración. De este modo se limita la presión osmótica del primer concentrado. [*J. NÉEL*, La Recherche, *5, 33 (1974)*]

Con membranas de intercambio iónico se produce también la llamada *diálisis permiónica* (fig. 21). Así, por ejemplo, una solución de SO_4H_2 contenida en el compartimiento del centro limitado por membranas catiónicas *c* constituye un auténtico intercambiador líquido de iones. Los iones Cu^{++} se concentran en el recinto 2 procedentes de 1 y 3, fig. 21 a)).

Igualmente con una membrana aniónica (A) se puede extraer SO_4H_2. Los aniones $SO_4^{=}$ se difunden a través de las membranas A y el proceso se verifica sin desequilibrio de las cargas eléctricas

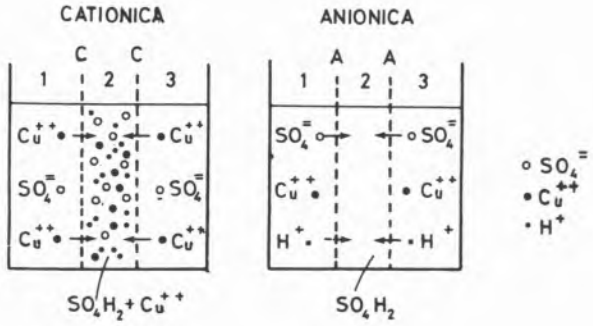

Fig. 21
Diálisis permiónica

porque los protones H^+ debido a su pequeño tamaño (6×10^{-5} Å) son capaces excepcionalmente de franquear las membranas aniónicas, (fig. 21 b)).

Una mención especial merece el proceso llamado *hemodiálisis*, mediante el cual es posible separar de la sangre la urea y otras toxinas. Ya a principios de este siglo se había tratado de remediar las insuficiencias renales dializando la urea acumulada en la sangre a través de una membrana. Sin embargo, la sangre es un fluido muy particular por su tendencia a coagular y las películas artificiales fueron rechazadas en operaciones clínicas. Las tentativas se limitaron a experiencias hechas con animales con paredes de nitrocelulosa.

Posteriormente se realizaron hemodiálisis a través de la membrana peritoneal del propio paciente con una estadística que llegó al centenar de casos. La primera operación realizada con una membrana artificial tuvo lugar en Holanda durante la II Guerra Mundial. La película utilizada por el Dr. Kolff era un cilindro de celofán montado sobre un tambor en rotación y desde entonces los riñones artificiales (diálisis extracorpórea de la sangre) fueron mejorando hasta ser hoy una práctica médica corriente, aunque todavía muy costosa y que se utiliza también en el caso de envenenamiento por tóxicos o drogas.

Una membrana de hemodiálisis debe permitir un transporte rápido y selectivo de la urea. Además debe ser hemocompatible, es decir, no provocar la alteración de la sangre. La membrana más eficaz es un film de celulosa regenerada artificialmente llamado *cuprofán* que se forma por coagulación de un colodión de celulosa disuelto en licor de Schweizer, (fig. 22).

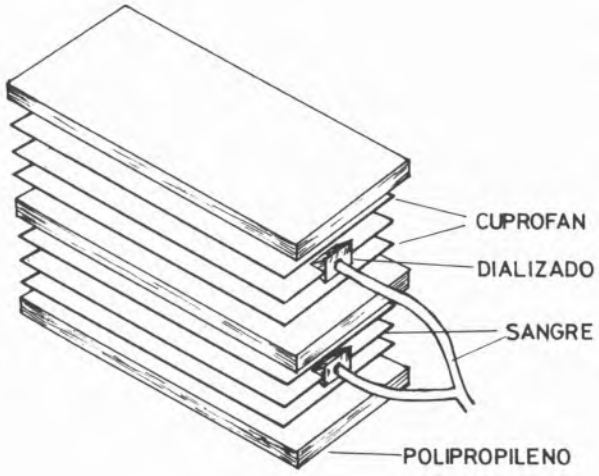

Fig. 22
El principio del riñón artificial es la diálisis extracorpórea entre la sangre y una solución de composición química definida por intermedio de una membrana semipermeable de cuprofán

FUERZA IMPULSORA: DIFERENCIA DE POTENCIAL ELECTRICO. ELECTRODIALISIS (fig. 23)

En la electrodiálisis se utilizan dos tipos distintos de membranas. Una célula de electrodiálisis consta de pares alternativos de membranas: una de cada par deja pasar sólo cationes; la otra sólo aniones. Cuando se aplica una f.e.m. a una de estas células formada por varios pares de membranas sumergidos en agua salina, los cationes (como el Na^+) pasan a través de las membranas permeables a los cationes, mientras que los aniones (como el Cl^-) se mueven en dirección opuesta y pasan a través de las membranas permeables a los aniones. Así entre pares alternativos de membranas el agua se limpia de sal; en los restantes recintos el agua es más salada. La electrodiálisis puede utilizarse tanto para desalinizar el agua del mar como para concentrar una salmuera.

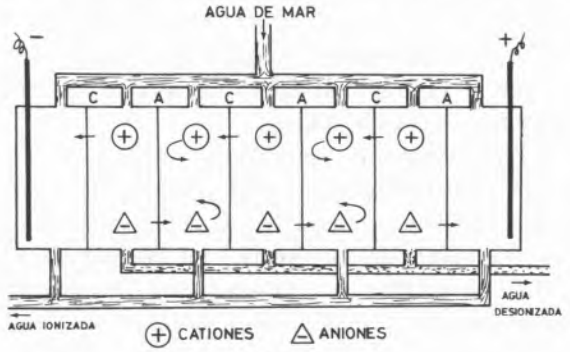

Fig. 23
Célula de electrodiálisis

Dispositivos análogos se han utilizado para efectuar reacciones de intercambio iónico o de doble descomposición salina. Un primer ejemplo es el endulzamiento de los jugos de fruta por extracción del ácido cítrico. Otra aplicación es la preparación de emulsiones fotográficas por inyección electrodialitica de AgBr en una capa de gelatina situada entre una membrana aniónica y una membrana catiónica.

5 — MEMBRANAS SEPARADORAS DE GASES

a) *PERMEACIÓN*

Para franquear la barrera que supone una membrana el gas debe disolverse en ella y difundirse de una cara a la otra. La velocidad de difusión depende de su naturaleza y de la del polímero que constituye la pared.

Se han realizado investigaciones sistemáticas para encontrar películas orgánicas muy selectivas, a base de poliéteres aromáticos y paredes de silicona que permiten ajustar la concentración de mezclas de O_2, N_2, CO_2 y H_2.

Aplicaciones: Regenerar el aire de un local público, hospitales, almacenes de frutas, etc. Recuperar el H_2 contenido en gases industriales. Esta permeación gaseosa viene limitada por el flujo insuficiente de las paredes actualmente disponibles y la imposibilidad de preparar películas muy delgadas.

Una aplicación reciente es "el pulmón de membrana" utilizado durante las operaciones de corazón extracorpóreas y en enfermos de insuficiencia respiratoria. La sangre es oxigenada y desprovista de CO_2 haciéndole circular entre dos membranas microporosas de silicona a través de las cuales el oxígeno gaseoso circula en contracorriente, (fig. 24).

b) *PERVAPORACIÓN*

La pervaporación se distingue de la permeación por el hecho de que el fraccionamiento se verifica sobre vapores saturantes. La película se situa directamente en contacto con una mezcla líquida. El flujo de materia se asegura manteniendo la otra cara de la membrana bajo presión reducida o barriéndola con una corriente gaseosa inerte que arrastra el filtrado.

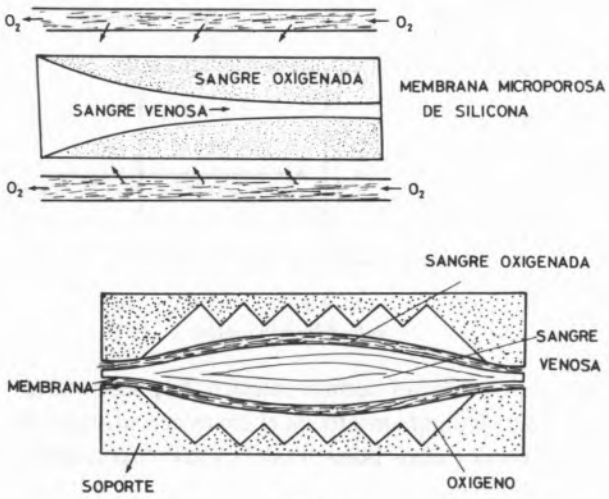

Fig. 24
Pulmón de membrana [(La Recherche, 41, 83, 1974)]

Aplicaciones: Fraccionamento de mezclas aceotrópicas de líquidos de bajo peso molecular que no pueden enriquecerse por destilación o por ósmosis inversa.

6 — TRANSPORTE ACTIVO

En este trabajo hemos limitado deliberadamente nuestra exposición a las membranas artificiales, es decir, barreras sintéticas más o menos selectivas en los flujos de materia. Este papel puramente pasivo les distingue fundamentalmente de las membranas biológicas. aquellas que limitan las células vivas, a través de las cuales se pueden observar transferencias incomparablemente más selectivas y que se realizan a veces en contra de los gradientes de concentración. La razón estaba en el hecho de que las membranas naturales poseen una estruc tura muy organizada en la que confluyen funciones y constituyentes que se acoplan al substrato transportado. Así se verifca en contragradiente la transferencia Na-K en los glóbulos rojos, lo que supondría un proceso termodinámicamente imposible si no fuera por la acción acoplada conjunta de la hidrólisis del ATP (bomba sodio-potasio) (fig. 25a). Recientemente se ha intentado reconstituir artificialmente en las membranas sintéticas este tipo de "transporte activo", utilizando para ello enzimas aisladas y purificadas que se fijan en capas de polímeros sintéticos hidrófilos. En la figura se representa la llamada *bomba de glucosa*, formada por una asociación de cuatro membranas sintéticas tratadas adecuadamente. Situada entre dos soluciones acuosas de glucosa este azúcar es arrastrado de izquierda a derecha independientemente de la mayor o menor concentración de las soluciones. El proceso depende de la propia asimetría del conjunto y como se indica en la fig. 25b de la acción de las enzimas y del ATP.

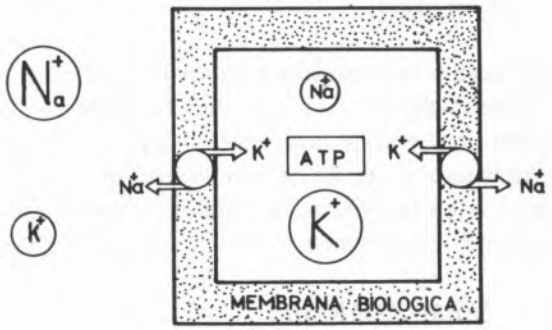

Fig. 25.a
Bomba Na-K. Gracias a la producción de ATP la membrana actua como una bomba en contra del gradiente (transporte activo)

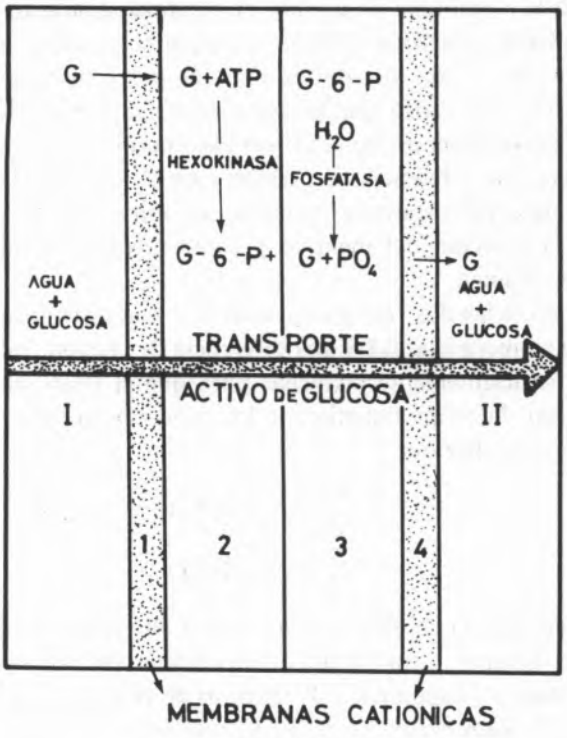

Fig. 25.b
Membrana artificial compuesta cuyo objeto es imitar la bomba de glucosa. [Reproducido de J. NEEL, La Recherche, *41, 42 (1974)]*

Esta información nos permite apreciar lo que puede esperarse a largo plazo de las membranas. Se trata,

en efecto de un dominio en evolución donde cada nueva realización sólo es posible al precio de un gran esfuerzo técnico.

6 — INVESTIGACIONES EN ESTE CAMPO REALIZADAS EN EL DEPARTAMENTO DE TERMOLOGIA DE LA UNIVERSIDAD COMPLUTENSE DE MADRID

Actualmente se realizan en nuestro Departamento de Termología de la Universidad Complutense de Madrid una serie de investigaciones de fenómenos de transporte a través de membranas que pueden agruparse en tres líneas de trabajo: termoósmosis, fenómenos electrocinéticos y permeación de gases.

6.1 — *TERMOOSMOSIS*

El fenómeno de la termoómosis consite en un flujo de líquido a través de una membrana debido a un gradiente de temperatura. En nuestros experimentos la membrana de acetato de celulosa separa dos cámaras simétricas donde se sitúan los fluidos a estudiar. Cada una de las cámaras posee un tubo capilar de vidrio que puede disponerse vertical u horizontalmente. En el primer caso permite estabelecer una diferencia de presión y en el segundo, la presión hidrostática es la misma en ambas cámaras y la posición del menisco permite medir el flujo de volumen.

Si entre las dos cámaras se establece una diferencia de temperatura, ΔT y una diferencia de presión Δp, lo suficientemente pequeñas para que el flujo sea lineal, la termodinámica de los procesos irreversibles nos dice que

$$J = \frac{S}{d}(A\Delta p + B\Delta T)$$

$$J_q \quad \frac{S}{d}(C\Delta p + D\Delta T)$$

en donde J es el flujo en moles de fluido por unidad de tiempo a través de la membrana de sección eficaz S y espesor d y J_q el flujo de calor a través de la membrana; A y B = C son los coeficientes fenomenológicos llamados "permeabilidad hidráulica" y "permeabilidad termoosmótica" respectivamente; D es la conductancia térmica. Estos coeficientes dependen de la naturaleza de la membrana y del fluido, así como de la temperatura y de la presión del sistema, (fig. 26).

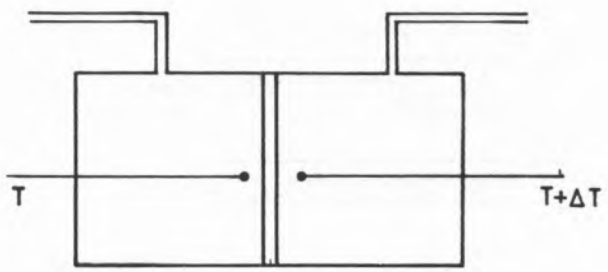

Fig. 26
Célula de termoosmosis

La permeabilidad termoosmótica B puede calcularse del siguiente modo. Si el Δp es cero durante la experiencia (tubos horizontales) y ΔT es constante, resulta

$$J = \frac{S}{d} B\Delta t$$

Para la medida de J se observa con un catetómetro el desplazamiento del menisco en los tubos de vidrio. Si $x = x(t)$ es la función que describe el desplazamiento del menisco en función del tiempo en los tubos de vidrio, el flujo a través de la membrana en moles por segundo será

$$J = \frac{dn}{dt} = \frac{1}{M}\frac{dm}{dt} = \frac{\varrho}{M}\frac{dV}{dt} = \frac{a\varrho}{M}\frac{dx}{dt}$$

en donde a = sección del tubo, ϱ = densidad del fluido y M = peso molecular del fluido. Por tanto,

$$\frac{dx}{dt} = \frac{JM}{a\varrho} = \frac{SB\Delta T\, M}{a\varrho d} = b$$

siendo **b** una constante. Por tanto

$$x = x_o + bt$$

y representando **x** en función de **t** resulta una línea recta cuya pendiente es b y a partir de la cual se puede determinar el *coeficiente de permeabilidad termoosmótica*, B.(*)

Otra serie de experiencias consiste en mantener ΔT = constante y estudiar la variación de Δp con el tiempo, hasta que el flujo termoosmótico se anule, (fig. 27). Como

$$-\frac{\Delta p}{\Delta T} = \frac{B}{A} - \frac{d}{q}\frac{J}{A\Delta T}$$

(*) J. MENGUAL, J. AGUILAR, C. FERNÁNDEZ-PINEDA, *Jour. of Membrane Science*, **4**, 209 (1978).

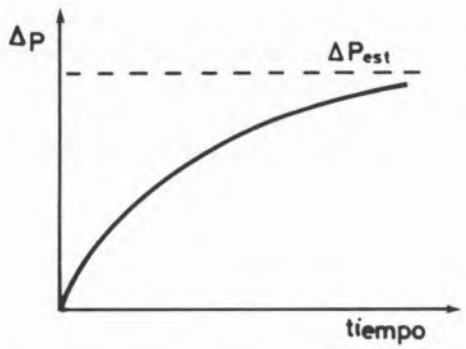

Fig. 27
Variación de Δp con el tiempo

resulta en régimen estacionario, J = 0 y por tanto:

$$\left(\frac{\Delta p}{\Delta T}\right)_{J=0} = \frac{\Delta p_{est}}{\Delta T} = -\frac{B}{A}$$

Conocido B, la medida de $\Delta p_{est}/\Delta T$ nos permite determinar la permeabilidad hidráulica A.
De igual modo puede deducirse el calor de transporte Q* a partir de la expresión

$$Q^* = \left(\frac{J_q}{J}\right)_{\Delta T=0} = \frac{C}{A}$$

6.2 — *FENOMENOS ELECTROCINETICOS*

Los fenómenos electrocinéticos se ponen de manifiesto utilizando una célula formada por dos recintos, cada uno de los cuales contiene una disolución electrolítica de igual concentración y separados por una membrana de cambio iónico con los dispositivos necesarios para producir diferencias de presión y de potencial eléctrico.
Si sobre una de las disoluciones a un lado de la membrana se aplica un exceso de presión respecto al otro recinto, el líquido contenido en los poros es forzado a atravesar la membrana. Como este líquido transporta una carga eléctrica neta, su desplazamiento da lugar a una diferencia de potencial eléctrico llamado potencial de flujo ("streaming potential").
Este potencial de flujo produce dos efectos: (1) actúa sobre el líquido inmerso en los poros de la membrana contrarrestando parcialmente el efecto de la presión y reduciendo el flujo; (2) acelera los iones del mismo signo que las cargas fijas de la membrana y frena los de sentido contrario de manera que ambos, a pesar de su diferente concentración, transfieren cantidades equivalentes de carga eléctrica.
El potencial de flujo puede ser anulado utilizando electrodos reversibles situados a ambos lados de la membrana. La carga neta transportada como consecuencia del mayor fluido de contraiones produce una corriente eléctrica llamada corriente de flujo ("streaming current").
El paso de corriente eléctrica en una célula de este tipo origina no sólo el paso de iones específicos a través de la membrana, sino también el transporte del líquido existente en sus poros. Este transporte de disolvente que acompaña al paso de iones se caracteriza por medio del parámetro t_w o número de moles transferidos por el paso de un faraday y el fenómeno se denomina *electro-osmosis*.
Siguiendo esta técnica(*) hemos determinado la permeabilidad electroosmótica a través de distintas membranas de cambio iónico electronegativas utilizando disoluciones de KCl y NaCl en función de la densidad de corriente I y de la concentración exterior C_o. Los resultados obtenidos se utilizan para calcular la permeabilidad electroosmótica, W y para estudiar el comportamiento de I y C_o.
Igualmente se ha determinado el número de transporte catiónico t_w a través de membranas electronegativas en función del logaritmo de la concentración, observándose que a partir de concentraciones del orden de 0,05 N el número de transporte disminuye al aumentar la concentración, lo cual se atribuye a la pérdida de selectividad de la membrana al aumentar la concentración del electrolito.

6.3 — *PERMEABILIDAD ISOTERMA DE GASES*

La permeabilidad de gases a través de membranas puede estudiarse mediante tres técnicas isotérmicas diferentes (presión, volumen y concentración variable) y una no isotérmica (transpiración térmica). En nuestro Departamento hemos utilizado un disposi-

(*) C. RUIZ BAUZÁ, J. AGUILAR, *Anales de Física*, serie B, **77**, 1,31 (1981).

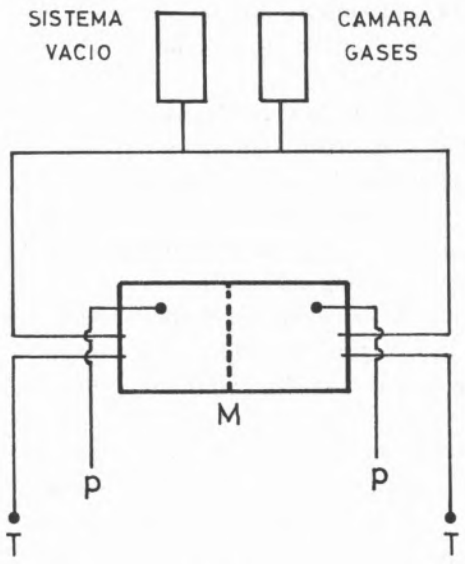

Fig. 28
Célula de separación de gases por membranas

tivo experimental que permite realizar medidas a presión variable y medidas de transpiración térmica(**).

El aparato (fig. 28) consiste en una célula de acero inoxidable dividida en dos cámaras cilíndricas por un soporte de polivinilo en el que se asienta la membrana. Una red de conducción comunica la célula con el sistema de vacío y con el depósito de gas.

Las medidas de presión se realizaron por medio de un manómetro diferencial de mercurio y las medidas de temperatura por medio de termopares de cobre-constantán.

la permeabilidad isoterma de un gas a través de la membrana se expresa mediante la ecuación fenomenológica

$$J_{iso} = -\frac{S}{kT} K \frac{\Delta p}{d}$$

donde J_{iso} es el flujo isotermo molecular por unidad de tiempo ocasionado por la diferencia de presión Δp entre las dos caras de la membrana de espesor **d** y área **S**; **k** es la constante de Boltzmann, **T** la temperatura y **K** el coeficiente de permeabilidad que depende de la naturaleza de la membrana y del gas, así como de la presión media a la que se realiza el experimento.

El coeficiente **K** se obtiene a partir de la variación temporal de Δp en el experimento isotermo que responde a la ecuación

$$\Delta p = \Delta p_o \, e^{-\frac{2Ks}{Vd}t}$$

en donde Δp_o es el valor inicial, **V** el volumen de la célula y **t** el tiempo.

El escenario actual en la tecnología de membranas es de gran agitación, análogo en muchos aspectos a la situación en el campo de los transistores hace unos años y análogo a la búsqueda actual de materiales fotovoltaicos de bajo precio para la conversión directa de energía solar en electricidad. Se conocen buenos convertidores como el silicio ultrapuro, pero son caros. Igualmente, todavía no tenemos buenas membranas que sean baratas. ¿Ocurrirá como en la técnica de los transistores y semi-conductores, cuya baja de precios revolucionó la electrónica? Sólo el tiempo lo dirá.

BIBLIOGRAFIA GENERAL

H. STRATHMANN, "Membrane separation processes", *Jour. of Memb. Science*, **9**, 121-189 (1981).

C. FERNÁNDEZ-PINEDA, J. AGUILAR, "La termodinámica irreversible y el transporte en membranas", *Las Ciencias*, **XL**, 4 (1975).

A. KATCHALSKY, "Non equilibrium thermodynamics", *Sc. et Tech.*, Oct. 1963, p. 43.

A. KATCHALSKY, "Living membranes", *Sc. et Tech.*, 52, Dic. 1967.

J. AGUILAR, C. RUIZ BAUZÁ, "Los fenómenos electrocinéticos a través de membranas", *Rev. de la Univ. Complutense*, 1981/2, p. 120.

(**) B. SEOANE RODRÍGUEZ, J. AGUILAR, C. FERNÁNDEZ-PINEDA, *Anales de Física*, B 77, 143 (1981).

H. J. M. HANLEY
Thermophysical Properties Division
National Engineering Laboratory
National Bureau of Standards
Boulder, Colorado 80303

PREDICTION OF TRANSPORT PROPERTIES: APPLICATION OF BASIC THEORY *

The transport prediction procedure of Ely and Hanley is discussed in this paper as an example of how theory can contribute to practical usable methods required by industry. The procedure is outlined and one particular failure of the original approach is isolated, i.e., that the procedure failed to predict correctly the viscosity of a mixture whose components differ substantially in size. A companion computer simulation molecular dynamic study is discussed, the results of which give insight into the problem of the real system. A correction based on the Enskog theory as introduced and suggested by Ely is proposed. The modified prediction procedure is shown to give excellent results.

This paper is an edited version of the lecture delivered at the Symposium on Transport Properties of Fluids, Lisbon (23-26 March 1982).

1 — INTRODUCTION

In this paper we discuss a procedure to predict the viscosity and thermal conductivity of pure fluids and mixtures. The results, some of which have been published previously [1-3], will be reviewed but our principal aim is to outline the procedure in a particular context; namely as an illustration of the role theory plays to develop a practical predictive method for thermophysical properties required by industry. From the larger viewpoint this is one example of the conflict between theory on the one hand and practical utility on the other.

On a positive note, there is no doubt that very real opportunities exist to combine basic science with realistic innovative engineering practice. Industry sets challenges which theory and experiment will have to meet and which sharpen the focus of current research. In turn, the results of a basic theoretical study, or from a controlled experiment, can suggest a possible industrial application.

As a slight digression, we remark that as much as 80% of the capital and annual operating costs in the major fluid industries — fuel, chemical and energy — come from separation and the processing of feedstocks. These industries are concerned with the conservation and productivity of their technology and with developing methods to handle new feedstocks. Moreover, the operating conditions will often be extreme: high temperatures, high pressures; the fluid could be near melting or freezing or a critical or consolute point, and so on. In short; theory is needed to understand fluid behavior; prediction prodecures are needed to estimate the thermophysical properties (and we emphasize prediction as opposed to correlation) because naturally one cannot have data for all possible systems of interest; and of course a data base has to be established.

A study of transport phenomena fits into the above scheme. We need a prediction procedure to estimate the viscosity and thermal conductivity of pure fluids and mixtures over a wide range of experimental conditions, and there are interesting and still unresolved problems associated with fluid nonequilibrium behavior in general. The problems range from the most fundamental such as questions on the definition of a system in nonequilibrium or on the form of the Hamiltonian, to the practical understanding and description of flow, multiphase flow, mixing and separation.

The approach we follow at the National Bureau of Standards is biased to the fact that common characteristics describe new feedstocks: most often they are defined mixtures whose species are substantially different (i.e., in size, polarity or chemical nature) or undefined mixtures such as coal liquid fractions, heavy oils or tars. Accordingly, experiments are made with a system which is simple yet represents a class which is relevant, *e.g.*, a mixture such as carbon dioxide and butane is relatively straightforward and accessible to a theoretical and experimental study, yet is a prototype of mixtures which are characterized by containing one species which is both small and of a different chemical nature than the others. Fig. 1 gives another example: it shows a

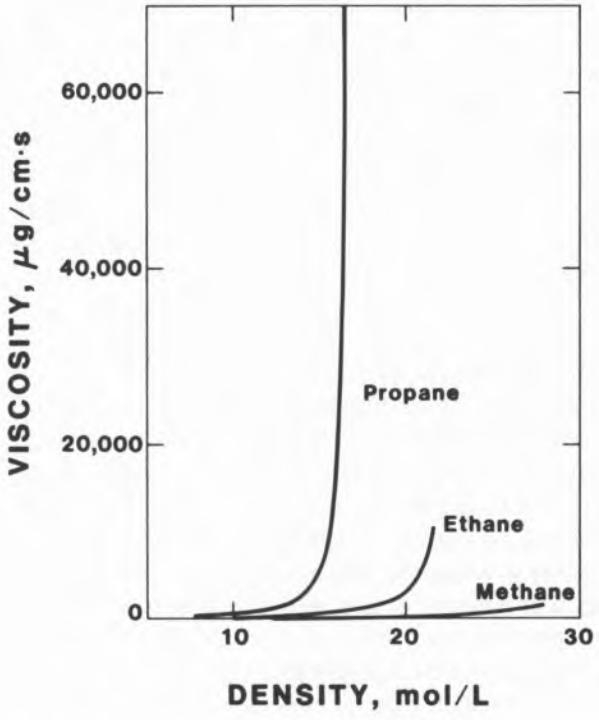

Fig. 1
Plot of the viscosity of methane, ethane and propane versus *density*

plot of the viscosity of methane, ethane and propane *versus* density. Note that the behavior of propane is quantitatively quite different from the other compounds. In fact the viscosity at high densities approaches that of a very heavy hydrocarbon such as C_{20}. The point to be made is that a theoretical and experimental investigation of propane — which is of interest in itself — will give an insight into the behavior of hydrocarbons such as C_{20} and can be undertaken with relatively simple theoretical and experimental tools.

No claim is made as to the originality of this plan, but the concept has perhaps not been followed as it might because of the gap between fluid theory and practice, and to a lack of high quality data. But one can argue that the situation has improved. The computer has had a tremendous impact; one can study a fluid via computer simulation, which allows theories to be tested unambigously and suggests lines for future research; and, of course, the computer has played a major role in data correlation, in numerical integration and differentation, and as general mathematical tool. On the experimental side, sophisticated electronics are common-place in measurement, control and data reduction. Laser light scattering, with neutron and X-ray scattering, have led to significant advances in our knowledge of fluid structure and in the measurement of fluid properties.

The organization of this paper is as follows. We outline the procedure which is based on the one-fluid conformal solution concept. A well-defined failure is commented on but we emphasize how a companion computer simulation study with a model mixture gives an insight for systematic improvement. A modification of the procedure is proposed. Finally, tables illustrating how the procedure predicts data are given and we emphasize that a computer package [TRAPP] is available.

2 — ONE-FLUID MODEL

The basis of this report is the technique proposed recently by ELY and HANLEY [1-3] and follows the earlier work of HANLEY [4] and MO and GUBBINS [5] which introduced the one-fluid equilibrium extended corresponding states arguments of LELAND [6] and others to transport phenomena. The basic idea is straightforward, that the configurational properties of a mixture can be equated to those of a hypothetical pure fluid. The properties of this hypothetical pure fluid are then evaluated via corresponding states with respect to a given reference fluid.

Since the expressions have been presented and discussed in detail in references [1-3], we only give an outline here. Also we will only discuss the viscosity (η) in any detail; similar equations can be written down for the thermal conductivity (λ).

Table 1

Summary of Viscosity and Thermal Conductivity Predictions for Pure Fluids Compared with Experiment (data sources in references [1-3] N = Number of points, AAD = Average absolute percent deviations, BIAS = Average percent deviation

Fluid type	Viscosity			Thermal conductivity		
	N	AAD	BIAS	N	AAD	BIAS
n-Paraffins	1301	4.89	− 0.48	721	4.44	0.03
i-Paraffins	155	21.17	−21.17	31	3.44	−1.16
Alkenes	58	11.29	7.85	251	5.77	−7.32
Cycloalkanes	89	40.56	−40.56	21	3.23	2.18
Alkylbenzenes	155	8.45	− 0.69	209	6.62	3.92
Carbon Dioxide	111	4.75	− 4.53	22	6.67	6.67
Overall	1869	8.42	− 4.10	1255	5.06	−0.67

Table 2

Summary of Calculated and Experimental Dense Fluid Binary Mixture Viscosities (see caption to Table 1)

Component 1	Component 2	N	AAD	BIAS
Methane	Propane	134	4.62	− 3.45
	n-Nonane	32	4.12	− 2.61
	n-Decane	71	5.35	− 1.54
2,3-Dimethylbutane	*n*-Hexane	2	5.31	− 5.31
	n-Octane	2	5.65	− 5.65
n-Hexane	*n*-Tetradecane	10	1.92	0.54
	n-Hexadecane	26	2.59	− 1.97
n-Heptane	*n*-Dodecane	3	3.44	3.44
	n-Tetradecane	3	1.82	1.51
	n-Hexadecane	3	2.52	− 1.32
	n-Octadecane	2	1.92	− 0.71
n-Octane	*n*-Decane	2	3.27	3.27
n-Tetradecane	*n*-Hexadecane	11	2.32	2.10
Benzene	*n*-Hexane	15	5.74	− 2.28
	n-Heptane	3	5.85	5.85
	2,2,4-Trimethylpentane	26	12.46	−12.46
	n-Decane	3	5.47	3.46
	n-Dodecane	3	6.47	6.47
	n-Tetradecane	3	3.63	2.55
	n-Hexadecane	3	3.76	1.46
	n-Octadecane	3	2.73	1.97
Toluene	*n*-Heptane	21	5.32	5.32
	n-Octane	20	9.50	9.50
	2,2,4-Trimethylpentane	28	6.62	− 4.37
	Overall	429	5.31	− 1.86

Consider the viscosity of a mixture η_{mix} at a density, ϱ, temperature, T, and composition $\{x_\alpha\}$ where x_α is the mole fraction of species α with $\alpha = 1,2....n$ for an n-component mixture. We assume $\eta_{mix}(\varrho,T,\{x_\alpha\}) \equiv \eta_x(\varrho,T)$ where η_x is the viscosity of the hypothetical pure fluid characterized by mole fraction set x. If a reference fluid is denoted by subscript *o* we have

$$\eta_x(\varrho,T) = \eta_o(\varrho_o,T_o)\, F_\eta \qquad (1)$$

where

$$F_\eta = \left(\frac{M_x}{M_o}\right)^{1/2} f_{x,o}^{1/2}\, h_{x,o}^{-2/3} \qquad (2)$$

Table 3
Summary of Calculated Results for Binary Mixture Thermal Conductivity (see caption to Table 1)

Component 1	Component 2	N	AAD	BIAS
Methane	*n*-butane	15	12.20	12.09
2,3-dimethylbutane	2,2,4-trimethylpentane	6	4.70	4.70
n-hexane	*n*-octane	14	6.17	− 6.17
n-heptane	*n*-octane	6	2.01	− 2.01
	2,2,4-trimethylpentane	6	1.96	1.81
	n-decane	6	8.99	− 8.99
	n-hexadecane	2	3.44	− 3.44
n-octane	2,2,4-trimethylpentane	9	4.97	− 4.97
	n-heptadecane	6	4.77	− 4.66
2,2,4-trimethylpentane	2,2,5-trimethylpentane	6	4.71	− 4.71
	n-tetradecane	6	5.06	− 5.06
1-hexene	*n*-heptane	279	8.11	− 8.09
	n-octane	279	8.84	− 8.83
Benzene	*n*-heptane	8	3.55	− 3.39
	Toluene	32	6.15	6.15
	Cyclohexane	4	4.42	4.42
Toluene	*n*-heptane	5	6.29	6.29
	2,2,4-trimethylpentane	6	10.78	10.78
	o-xylene	6	15.71	15.71
o-xylene	2,2,4-trimethylpentane	6	11.51	11.51
Cyclopentane	*n*-heptane	6	0.66	0.16
	Methylcyclohexane	6	5.20	5.20
Cyclohexane	Toluene	4	4.12	4.12
Methylcyclohexane	2,2,4-trimethylpentane	6	11.72	−11.72
	Overall	167	6.83	1.42

with M the molecular weight and T_o and ϱ_o defined by ratios

$$T_o = T/f_{x,o}\,; \quad \varrho_o = \varrho h_{x,o} \tag{3}$$

where $f_{x,o}$, $h_{x,o}$ are defined by the mixing rule expressions

$$f_{x,o} = h_{x,o}^{-1} \sum_{\alpha}\sum_{\beta} x_\alpha x_\beta f_{\alpha\beta,o} h_{\alpha\beta,o} \tag{4}$$

$$h_{x,o} = \sum_{\alpha}\sum_{\beta} x_\alpha x_\beta h_{\alpha\beta} \tag{5}$$

with

$$f_{\alpha\beta,o} = (f_{\alpha,o} f_{\beta,o})^{1/2}(1 - k_{\alpha\beta}) \tag{6}$$

$$h_{\alpha\beta,o} = \frac{1}{8}\left(h_{\alpha,o}^{1/3} + h_{\beta,o}^{1/3}\right)^3 (1 - \ell_{\alpha\beta}) \tag{7}$$

in which $k_{\alpha\beta}$ and $\ell_{\alpha\beta}$ are the usual correction binary interaction coefficients. The mass mixing rule is discussed in reference [10] and can be written as

$$h_{x,o}^{4/3} \sqrt{f_{x,o} M_x} = \sum_{\alpha}\sum_{\beta} x_\alpha x_\beta h_{\alpha\beta,o}^{4/3} \sqrt{f_{\alpha\beta,o} M_{\alpha\beta}}$$

where $M_{\alpha\beta} = 2M_\alpha M_\beta/(M_\alpha + M_\beta)$.
Finally we have

$$f_{\alpha,o} = (T_\alpha^c/T_o^c)\,\theta(T^*, V^*, \omega) \tag{8}$$

$$h_{\alpha,o} = (V_\alpha^c/V_o^c)\,\Phi(T^*, V^*, \omega) \tag{9}$$

where superscript *c* refers to the critical point value and θ and ϕ are shape factors which are functions of the Pitzer acentric factor ω and of reduced (asterisks) temperature and volume (or density, $V = 1/\varrho$). We refer to reference [1] for their functional form.

The key point of the extended corresponding states approach is that the format of classical corresponding states is followed. Should the solution be conformal [i.e., that all intermolecular interactions follow the same force law and $\omega_\alpha = \omega_o$ (and strictly that $\omega_o = 0$) and that the critical compressibility

factor becomes a universal constant) the ratios (5) and are simply the ratios of the critical constants and equations (4) and (5) are the "Van der Walls one" mixing rules.

Summary of the calculation procedure: A summary of the calculation procedure to evaluate the viscosity from equation (1) is as follows. We have a single phase mixture (or a pure) at a given temperature, pressure and mole fraction. Required as input parameters are the critical temperature, critical pressure, critical volume, acentric factor and molecular weight of each mixture component. We are given an equation of state and functional form for the viscosity of the reference substance. Note the method is thus predictive in that transport data for the mixture *or* its components are not needed. We also do not require the mixture to be in any particular phase or limit the number of components.

The first step is to evaluate the density. To do this the equivalent pressure (p_o) of the reference substance is evaluated via the ratio $p_o = p_x\ h_{x,o}/f_{x,o}$. Initially the shape factors of equations (8) and (9) are set to unity. Given $p_o = p(\varrho_o, T_o)$, the density ϱ_o follows and hence ϱ_x is obtained from equation (3). Repeated iterations give a final density $f_{x,o}$ and $h_{x,o}$ and T_o and ϱ_o. Hence the viscosity follows from equation (1).

Methane is used as the reference fluid in our work: the equation of state is the BENEDICT-WEBB-RUBIN of reference [7] and the viscosity and thermal conductivity equations are based on the correlation of reference [8]. Further details are given in reference [1].

3 — COMPUTER SIMULATIONS OF FLUIDS UNDER SHEAR: EVALUATION OF THE PROCEDURE

The transport procedure is generally very successful for nonpolar fluids and mixtures and some deviation tables will be given in section 5. There are some failures which were anticipated, *e.g.*, for polar molecules and molecules with pronounced structure such as very branched hydrocarbons. However, others occurred whose origin was not so obvious. In particular, the method did not predict too well the viscosity of mixtures whose species differ substantially in size and/or mass. The methane/decane mixture is an example. Fig. 2 shows the percent deviations for three mixtures and there is clearly

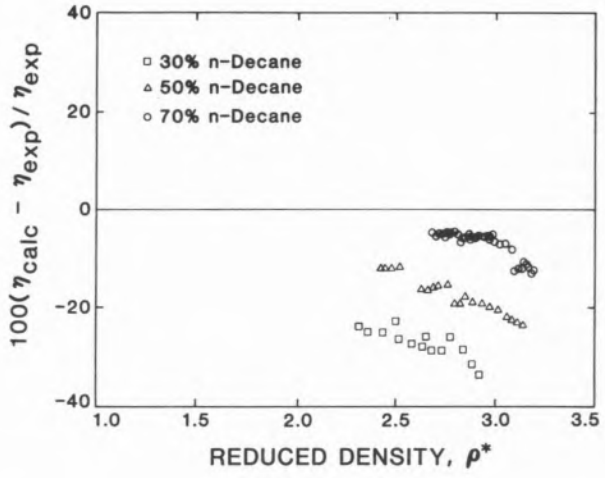

Fig. 2
Deviations between results calculated from equation (1) and experiment for methane/decane mixtures. Data sources listed in reference [13]

a systematic discrepancy at high densities. We stress, however, that this mixture is quite unusual as seen by fig. 3 which gives a plot of the viscosity

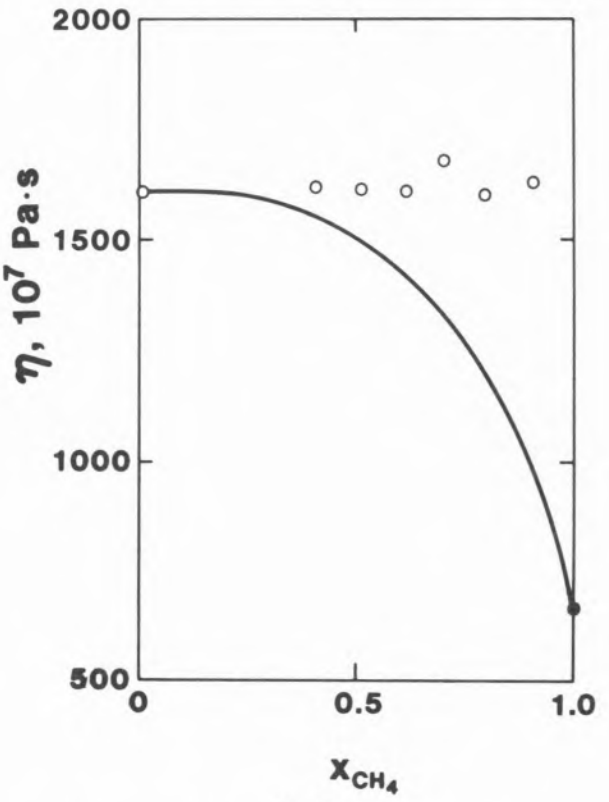

Fig. 3
Plot of the viscosity of a methane/decane mixture at 440 K at a constant density of 2.5 ϱ_c. The points are data, the curve is calculated using equation (1)

at the sample temperature of 440 K *versus* methane mole fraction at a *constant density* of about 2 1/2 times critical. The points are data, the curve is the prediction procedure. Note that the mixture viscosity is constant until $x(CH_4)$ is about 0.9.

Results such as those of fig. 2 suggested that a systematic evaluation of transport properties in mixtures in general, and of the assumptions of our predictive method in particular would be productive. It turned out that this goal dovetailed with an investigation of the nonequilibrium behavior of fluids using the computer simulation tecnique of nonequilibrium molecular dynamics carried out by EVANS [9], EVANS and HANLEY [10-11] and by HESS and HANLEY [12].

We will outline the simulation method but refer to reference [11] for details. A model system — that is, a system whose particles have a known size, shape and force law — is examined in equilibrium by conventional molecular dynamics. The system is then subjected to an external shear force by constraining the periodic boundaries. Results from this technique are very rich. Of interest here, we can evaluate the pressure tensor and the radial distribution function $g(\underset{\sim}{r})$ Under shear this latter quantity reflects directly the distortion of the microstructure of the system and can be written in the form

$$g(\underset{\sim}{r}) = g^s(r) + \Sigma\, v_k\, f_k(\underset{\sim}{r}) \qquad (10)$$

where g^s is the scalar contribution and v_k are expansion coefficients coupled with functions of $\underset{\sim}{r}$, the vector separation between molecular pairs. The scalar g^s would be the equilibrium radial distribution in equilibrium (g^s_o), the first coefficient v_1 is related to the potential contribution to the shear viscosity and the higher order coefficients are associated with other transport coefficients representing differences in the normal pressure.

The expansion (10) is powerful in that it depicts the microscopic distortion of the structure of a fluid in nonequilibrium and is especially useful in a study of mixtures because one can identify the contributions of a mixture species in the mixture. For the viscosity, for example, we have

$$\eta_{mix} = \Sigma\, x_i x_j\, \eta(ij) \qquad (11)$$

where

$$\eta(ij) = \frac{2}{15}\pi\varrho^2 \int v_1(ij)\, \phi'(ij) r^3\, dr \qquad (12)$$

with $v_1(ij)$ the coefficient from equation (10) and $\phi'(ij)$ the derivative of the pair potential for the i-j pair. Note that $\eta(ii)$ is *not* the viscosity of a pure but of species i in the presence of species j.

Simulation of a mixture of soft spheres: In reference [11] we decided to approximate a real binary equimolar mixture of decane and methane by a model mixture of soft spheres of different size and mass. No apologies were made for the obvious gross simplification because it turned out that the behavior of the model seems to represent the real liquid very closely.

The model mixture was characterized by soft spheres with the potentials

$$\phi_{11} = d/r^{12}\,,\ \phi_{12} = d/r^{12}\,,\ \phi_{22} = 1296\, d/r^{12} \qquad (13)$$

with species 1 representing the smaller lighter methane and species 2 representing decane. The factor 1296 arises from the ratio V^c(decane)/V^c(methane ≈ 6. Species 2 was given a mass ten times that of species 1. It should be stressed that equation (13) indicates that classical two parameter corresponding states is obeyed for all potential interactions.

The mixture was studied at a reduced state point (density) of $\varrho = 0.2667$: this state point corresponds to a pure fluid at a reduced equivalent density of 0.6, which is about three-quarters of the melting density, for an equivalent pure liquid.

We show two results here: (1) the variation of the distribution functions g^s_o and ν_1: (2) an evaluation of the local or ambient mole fractions x_{ij} as a function of partical separation r where $x_1 = x_2 = 0.5$ in the limit of $r \to \infty$:

$$x_{ij} = n_{ij}/(n_{ij} + n_{jj}) \qquad (14)$$

where n_{ij} is the number of particles of species j around a central particle i, all for a given r.

(1) *Variation of the distribution Functions.* Fig. 4 displays g^s_o and v_1 for a pure fluid at $\varrho = 0.6$ *versus* reduced r[r/d(ij), equation (13)] while fig. 5 shows g and v, scaled approximately, for the i-j contributions of the mixture at an equivalent state point. The basic assumption of

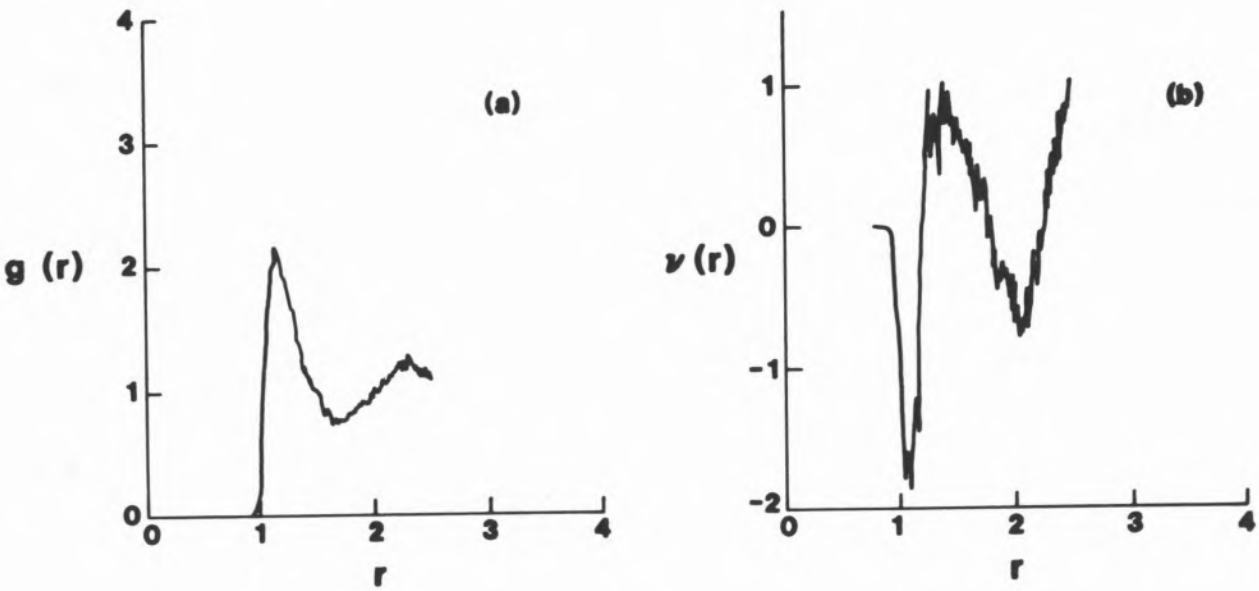

Fig. 4
Plots of $g^s_o(r)$ and v(r) for a pure soft sphere liquid at $\varrho = 0.6$

a conformal one fluid model is that the g(ij) and v(ij) scale with one another and with a pure. Thus all plots of g should show the same structure, as should the plots of v. This is not the case for this mixture in which it is seen from the figures that the larger species 2 dominates the g^s_o (and also v although it not quite so obvious).

Using these model results as a guide to the behavior of the real fluid, one would thus expect that our transport procedure will fail if the species of a real mixture are substantially different in size and/or mass, as is the case of methane/decane.

(2) *Local or Ambient Mole Fraction.* An alternative way to analyse the variation of g(r) is to consider the local mole fraction of equation (14) since

$$n_{ij}(R) = 4\pi \frac{\varrho}{2} \int_o^R r^2 g_{ij}(r)\, dr \qquad (15)$$

Hence given $g_{ij}(r)$, as in fig. 5, we calculate x_{ij} from equation (14), using (15). The results for x_{11} and x_{22} are shown in fig. 6. Although $x_1 = x_2 = 0.5$ overall, the results indicate that $x_{22} \approx 0.85$ and $x_{11} \approx 0.35$ for $r \lesssim 2.0$.

Since, moreover, the macroscopic properties of a system are largely controlled by intermolecular forces over short r only, effectively we do not have an equimolar mixture at all; rather the mixture is behaving approximately as pure species 2. This line of reasoning gives a facile answer to the apparently anomalous plot of fig. 3 for the real system. Even though the mole fraction of methane varies, the local or effective mole fraction of decane is close to one until x(methane)$\approx$0.9.

4 — SYSTEMATIC CORRECTION TO THE PROCEDURE: ELY's APPLICATION OF THE ENSKOG THEORY

In this next section we follow the philosophy of the introduction and suggest a correction to the transport procedure based on theory. The flavor is as follows: the computer simulations suggest that size and mass differences are of paramount importance to the properties of a mixture. but such differences are essentially structure or ordering effects and it is known that the structure of a fluid is not too dependent on the details of the pair potentials of the molecules. Consequently, one would hope that a correction to the transport procedure could be based on as simple a model as possible but yet apply to the real system. This idea was suggested by HANLEY in 1976 [4] and considerably expanded and reformulated by ELY recently [13]. The correction introduces the hard sphere ENSKOG model [14] which, although not exact, is a well known systematic transport theory whose assumptions can be justified quantitatively.

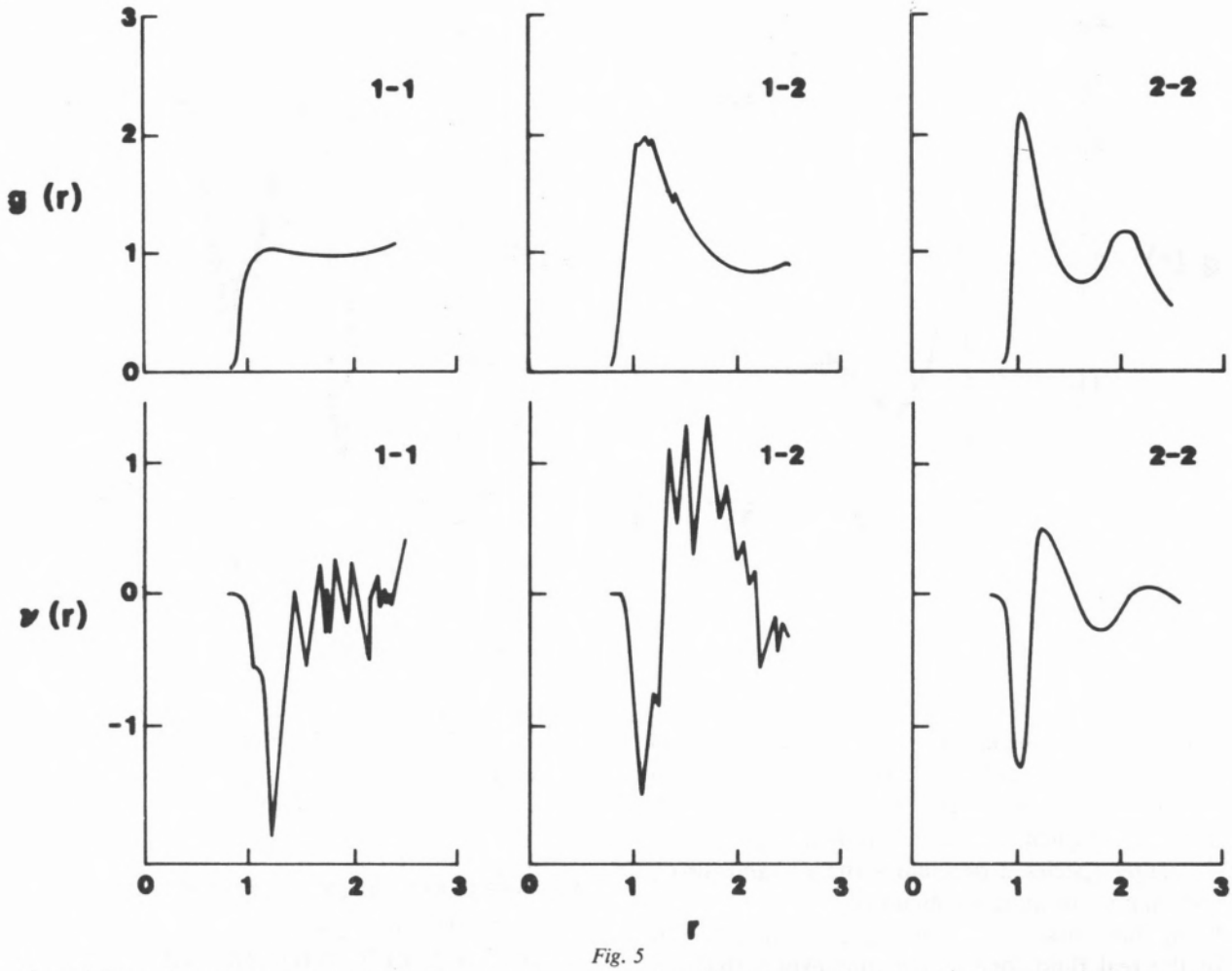

Fig. 5

Plots of $g_o^s(r)$ and v(r) for a mixture of soft spheres for which one species (2) is approximately twice as large and ten times as heavy as species 1. The state point for the mixture is equivalent to a pure at $\varrho = 0.6$. Note (a) differences between the plots of fig. 4 and 5 and, (b) that the curves for the i-j interactions do not scale

Let us write

$$\eta^E_{mix}(\{\varrho\sigma_\alpha^3\}, \{x_\alpha\}, \{m_\alpha\}) = \eta^E_x(\varrho\sigma_\alpha^3, m_x) + \Delta\eta^E \quad (16)$$

where η^E_{mix} is the exact Enskog viscosity of a mixture of hard spheres each of diameter σ_α and mass m_α for a given density and mole fraction set. The properties of this mixture can be evaluated, but we will not write down the expressions [13,15]. The hypothetical pure η^E_x can also be evaluated given the standard Enskog equation

$$\eta^E = \eta^{HS}(o) b\varrho \left[\frac{1}{b\varrho\chi} + 0.8 + 0.761\, b\varrho\chi\right] \quad (17)$$

where

$$\frac{p}{\varrho kT} = 1 + b\varrho\chi \quad (18)$$

where $b = 2\pi\sigma_\alpha^3/3$ and $\chi = 1 + 0.625 b\varrho + \ldots$. and $\eta^E(o)$ is the dilute gas hard sphere viscosity. We chose mixing a rule for σ_α:

$$\sigma_x^3 = \sum_\alpha \sum_\beta x_\alpha x_\beta \sigma_{\alpha\beta}^3 \quad (19)$$

with

$$\sigma_{\alpha\beta} = \frac{1}{2}[\sigma_\alpha + \sigma_\beta] \quad (20)$$

where σ_α is to be evaluated via equation (18) of reference [13]. The mass mixing rule is

$$\sigma_x^4 \sqrt{m_x} = \sum_\alpha \sum_\beta x_\alpha x_\beta \sigma_{\alpha\beta}^4 \sqrt{m_{\alpha\beta}} \quad (21)$$

where $m_{\alpha\beta} = 2m_\alpha m_\beta/(m_\alpha + m_\beta)$ as before.
We thus can obtain $\Delta\eta^E$ as a function of density and mole fraction for given ratios of $\sigma_\alpha/\sigma_\beta$ and

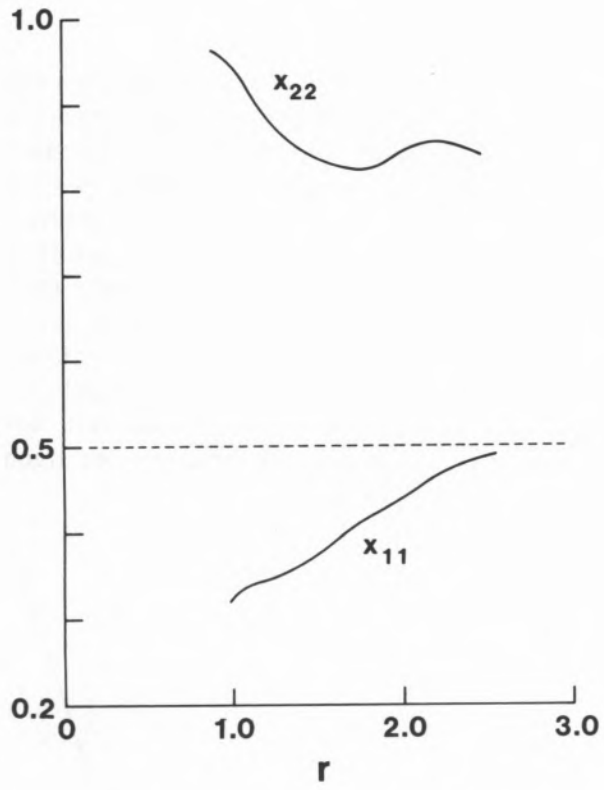

Fig. 6

Plot of the local mole fractions x_{22} and x_{11} defined by equation (14) using the g_o^s values of fig. 5 for the soft sphere mixture. Although the mixture is equimolar, i.e., $x_{22} \to x_2 \to 0.5$ and $x_{11} \to x_1 \to 0.5$ for $r \to \infty$, it behaves as a mixture in which $x \approx 0.9$

m_α/m_β. *And, as remarked, we then assume that* $\Delta\eta^E$ *is independent of the nature of the mixture, so the original equation (1) becomes*

$$\eta_{mix} = \eta_o(\varrho_o, T_o)\, F_\eta + \Delta\eta^E \qquad (22)$$

Equation (22) is now the basic equation for the viscosity procedure and as a first test we predict the viscosity of the methane/decane mixture shown before in fig. 3. The new result using equation (22) is presented as fig. 7 and one sees the substantial improvement.

5 — RESULTS

Detailed results are presented in references [1-3] and in reference [13]. Here we give three tables which summarize them. The computer program which generates the data is known as TRAPP and is available from the Gas Processors Association, 1812 First Place, Tulsa, Oklahoma 74103, USA.

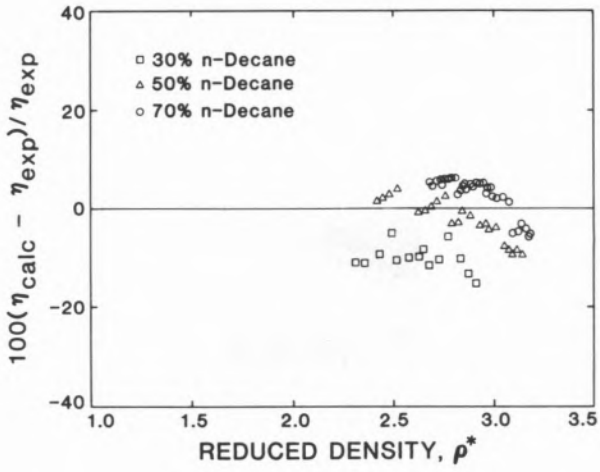

Fig. 7

Deviations between the methane/decane data and the revised equation (22): compare with fig. 2

ACKNOWLEDGEMENTS

We are grateful for discussions with Dr. Ely who provided much material prior to publication. the work was supported by the U.S. Department of Energy, Office of Basic Energy Sciences, Contract No. DE-A101-76PRO6010 with computer money supplied by the Gas Research Institute.

REFERENCES

[1] J.F. Ely, H.J.M. Hanley, *Ind. Eng. Chem. Fund.* **20**, 323 (1981).
[2] J.F. Ely, H.J.M. Hanley, *Nat. Bur. Stand.* (U.S.), Technical Note, No. 1039 (1981).
[3] J.F. ELY, H.J.M. Hanley, *Ind. Eng. Chem. Fund.* (in press). [Added in proof: **22**, 90 (1983)].
[4] H.J.M. Hanley, *Cryogenics* **16**, 643 (1976).
[5] K.C. Mo, K.E. Gubbins, *Mol. Phys.* **31**, 825 (1976).
[6] J.W. Leach, P.S. Chappelear, T.W. Leland, *A.I.Ch.E. J.* **14**, 568 (1968).
[7] R.D. McCarty, *Cryogenics* **14**, 276 (1974).
[8] H.J.M. Hanley, R.D. McCarty, W.M. Haynes, *J. Phys. Chem. Ref. Data* **3**, 979 (1974).
[9] D.J. Evans, *J. Stat. Phys.* **20**, 547 (1979).
[10] D.J. Evans, H.J.M. Hanley, *Phys. Rev.* **20A**, 1648 (1979).
[11] H.J.M. Hanley, D.J. Evans, *Int. J. Thermophysics* **2**, 1 (1981).
[12] S. Hess, H.J.M. Hanley, *Phys. Rev.* **25A**, 1801 (1982).
[13] J.F. Ely, *J. Res. Nat. Bur. Stand.* (U.S.), **86**, 597 (1981).
[14] H.J.M.Hanley, R.D. McCarty, E.G.D. Cohen, *Physica* **60**, 322 (1972).
[15] M.K.Tham, K.E. Gubbins, *J. Chem. Phys.* **55**, 268 (1971).

KEY WORDS:

Conformal solution theory; corresponding states; data prediction; Enskog theory; mixtures; non-equilibrium; viscosity.

ELECTRONIC CONFIGURATIONS *vs* ORBITAL ENERGIES

JOSÉ J.C. TEIXEIRA-DIAS
The University Chemical Department
3000 COIMBRA — PORTUGAL

INTRODUCTION

Comparision of electronic configurations of ground state atoms with orbital energies reveals interesting features as the atomic number varies, for the transition elements. In fact, it is not possible, in some cases, to correctly predict the electronic configuration of an atom by simply filling its manifold of orbitals, ordered by their increasing energies (aufbau principle), with the use of the Pauli exclusion principle. For instance, the ground state electronic configuration of scandium is neither $[Ar]3d^3$ nor $[Ar]3d^24s^1$ but $[Ar]3d^14s^2$, despite the fact that $\epsilon_{3d} < \epsilon_{4s}$ (fig. 1), where [Ar] represents the argon

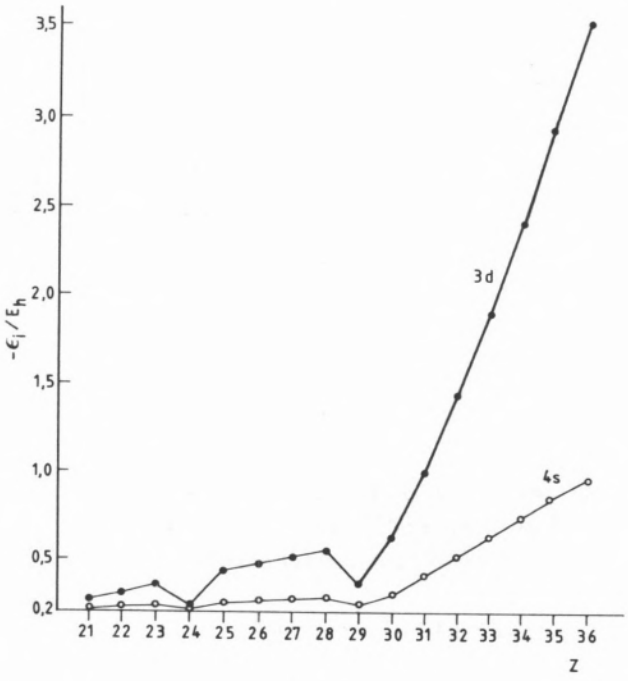

Fig. 1
3d and 4s orbital energies for the third row elements of the periodic table [1] ($E_h = 4.3598 \times 10^{-18}$ J, Hartree energy)

core and ϵ stands for an orbital energy. For yttrium, the ground state electronic configuration is $[Kr]4d^15s^2$ although $\epsilon_{4d} < \epsilon_{5s}$ (fig. 2).

Being a one-electron function useful for constructing many-electron wavefunctions and interpreting the periodic properties of elements, an atomic orbital has a rigorous and clear-cut definition in the context of self-consistent field methods. Besides being the most rigorously defined of all types of orbitals, the self-consistent field orbital is the

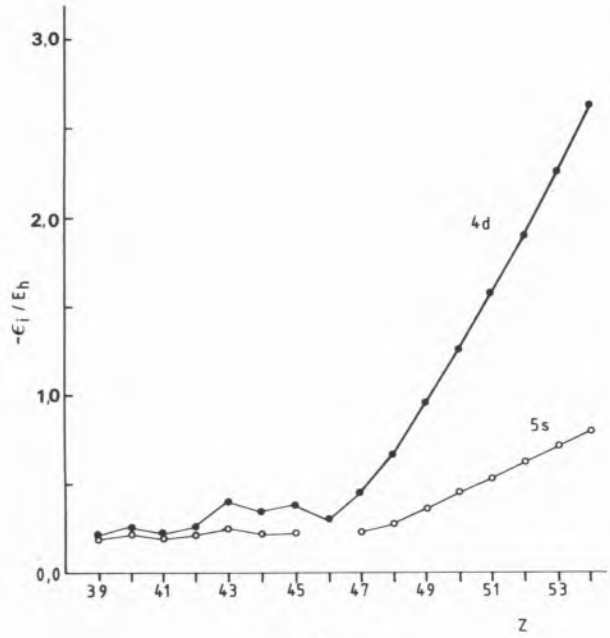

Fig. 2
4d and 5s orbital energies for the fourth row elements of the periodic table [1]. For Z = 46 the 5s orbital occupancy is zero, in the ground state. Therefore, ϵ_{5s} is not indicated

one whose energy is most closely related to experimental photoelectronic energies through Koopmans' approximation.

Within the Hartree-Fock self-consistent method, the total electronic energy of a many-electron atom is not simply the sum over the electrons of orbital energies. Under the non-relativistic hamiltonian approximation, the total electronic energy of an atom whose wavefunction is approximated by a Slater determinant is given by

$$E = \sum_{i=1}^{n} \epsilon_i - G \qquad (1)$$

where n is the number of occupied spin-orbitals and G is the electronic repulsion energy expressed in terms of Coulomb and exchange integrals. In this general from, (1) applies also to non-closed subshells.

Accurate Hartree-Fock wavefunctions [1, 2] enable us to interpret the electronic configurations of atoms and to understand the periodic properties of the elements [3]. Herewith we present Hartree-Fock results for a few electronic configurations of a scandium atom and its monopositive ion as well as for a neutral yttrium atom. The objective nature of these results speaks for itself, exempting us from wandering among less well founded predictions as it has been previously done quite so often. These values not only reveal important trends for the orbital and repulsion energies but also clarify the interpretation of ground state electronic configurations in terms of the atomic orbital concept [4, 5] on a well founded and objective basis. For the motivation of this article the reader is referred to [4].

Before starting with the analysis of Hartree-Fock results for ground state atoms, it is necessary to remark on an important, albeit frequently forgotten, point. Comparision of orbital energies should be limited to configurations where the compared orbitals are simultaneously occupied. In fact, while an occupied spin-orbital refers to the field of the nucleus and the n-1 other electrons, an unoccupied spin-orbital should be considered instead as the solution of the Hartree-Fock equations for an unexistent ghostlike charge acted upon by all the other n electrons in the atom.

2 — HARTREE-FOCK RESULTS ON SCANDIUM AND YTTRIUM ATOMS

Tables 1 and 2 show Roothaan-Hartree-Fock results for a few electronic configurations of a scandium neutral atom (Table 1) and its monopositive ion (Table 2).

The first interesting conclusion worth extracting from these tables is that small variations in the total electronic energy result from a critical balance of two large and approximately equal numbers: the variation in the sum over all orbital energies, $\Sigma\epsilon_i$, and in the electronic repulsion energy, G. Under these conditions, it may be difficult or even impossible to single out a particular and specific effect for the interpretation of any observed energy trend.

A second and equally important point is the appreciable variations exhibited by the 3d and 4s orbital energies upon alteration of the electronic configuration of the valence electrons (when an electron changes from 3d to 4s), in spite of a fixed atomic number. This is a relevant point not so much mentioned before as general attention is paid instead to the variation of orbital energies as functions of atomic number for ground state atoms.

In order to analyse the energy terms involved in a particular scheme of partioning the atom in different groups of electrons, like core and valence elec-

Table 1
Roothaan-Hartree-Fock energies for two electronic configurations of scandium [2] $E_h = 4.3598 \times 10^{-18}$ J (Hartree energy)

Electronic Configuration	ϵ_{3d}/E_h	ϵ_{4s}/E_h	$\Sigma\epsilon_i/E_h$	G/E_h	E/E_h
$[Ar]3d^24s^1$ (I)	−0.21529	−0.19537	−476.46291	283.23569	−759.69860
$[Ar]3d^14s^2$ (II)	−0.34357	−0.21014	−479.31765	280.41787	−759.73552
Δ(I-II)	0.12828	0.01477	2.85474	2.81782	0.03692

Table 2
Roothaan-Hartree-Fock energies for different electronic configurations of Sc^+ [2]

Electronic Configuration	ϵ_{3d}/E_h	ϵ_{4s}/E_h	$\Sigma\epsilon_i/E_h$	G/E_h	E/E_h
$[Ar]3d^2$ (I)	−0.45481	—	−480.71988	278.78986	−759.50974
$[Ar]4s^2$ (II)	—	−0.48719	−488.29584	271.16613	−759.46197
$[Ar]3d^14s^1$ (III)	−0.59990	−0.44926	−484.14304	275.39597	−759.53901
Δ (I-III)	0.14509	—	3.42316	3.39389	0.02927
Δ (II-III)	—	−0.03793	−4.15280	−4.22984	0.07704

trons, one should not forget that a particular sum of Hartree-Fock orbital energies over some or all of the occupied orbitals includes the electronic repulsion interactions twice, therefore requiring subtraction of the corresponding repulsion energy according to an equation like (1). However, the repulsion energy G cannot be rigorously partitioned in several terms, unlike any sum of orbital energies which are one-electron quantities. While we are aware of this fact it is nevertheless worth mentioning the appreciable variations observed in the sum of extracore orbital energies as they are of the order of magnitude of ϵ_{4s} or ϵ_{3d}.

On the other hand, the sum of core orbital energies $(\Sigma\epsilon_i)_{core}$, easily computed from the tables by subracting from $\Sigma\epsilon_i$ the sum of the valence electron energies, exhibit variations of the same order of magnitude as $\Sigma\epsilon_i$ (see Table 1 and 2). This legitimately suggests that the corresponding intracore repulsion energies should also balance variations in $(\Sigma\epsilon_i)_{core}$, therefore further stressing the importance of the variations in the valence electron energies, at least in relative terms. Now, as the orderings of $\Sigma\epsilon_i$ values for the various configurations of Sc and Sc^+ are due to core orbital contraction when an electron changes from 3d to 4s (see fig. 3), the same effect should also cause an increase in the intracore repulsion energies.

Another interesting observation, although purely factual and made in passing, can also be taken from the Sc^+ results shown in Table 2: the smallest values quoted for $\Sigma\epsilon_i$ and G do not correspond to the ground state configuration ($[Ar]3d^14s^1$), not even to the configuration with the largest number of 3d electrons, but to $[Ar]4s^2$.

By analysing Table 3 for two electron configurations of the yttrium atom, the reader can easily recognize several trends which are similar to those observed in the case of Sc and Sc^+ atoms, therefore exempting us from specific comments on that case.

The preceding results enable us to answer an usual and pratical question on the transition elements electronic configurations which we particularize for the scandium atom: why does this atom "prefer" the ground state configuration $[Ar]3d^14s^2$ to $[Ar]3d^24s^1$, despite the fact that $\epsilon_{3d} < \epsilon_{4s}$?

A possible answer, based on a simplistic and somewhat imprecise idea, attributes the stability of $[Ar]3d^14s^2$ relative to $[Ar]3d^24s^1$ to a large 4s-[Ar] repulsion, hypothetically considered to be greater than the corresponding 3d-[Ar] interaction. Then, the argument continues, the difference between $\Sigma\epsilon_i$

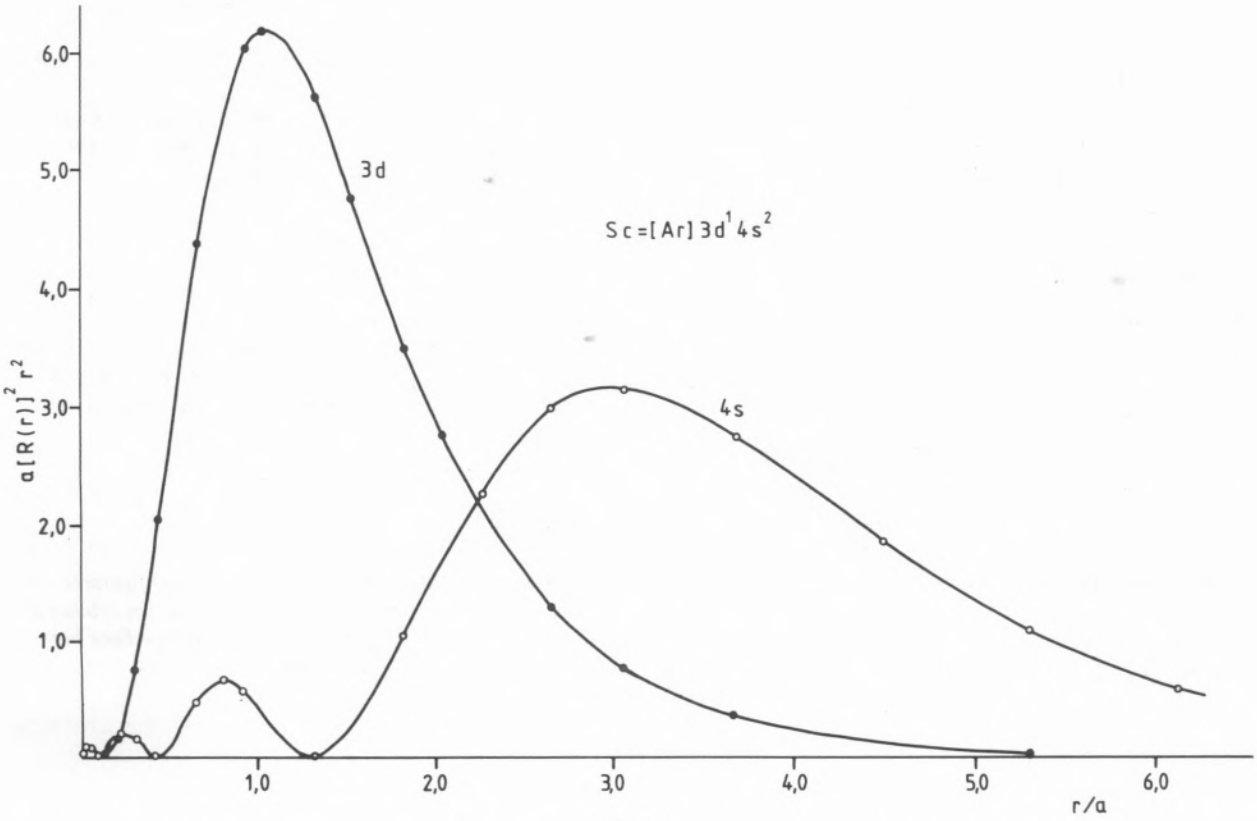

Fig. 3

Radial distribution functions for the 3d and 4s electrons of scandium [1] ($a_o = 5.2918 \times 10^{-11}$m, Bohr radius)

and G in (1) turns out to be smaller in the configuration with the largest possible number of 4s electrons which is 2, because of a larger G value.

Now, the results of Tables 1 and 2 show that both the premise — sum of orbital energies over all occupied spin-orbitals, $\Sigma\epsilon_i$, (wrongly) considered to be insensitive to the configuration of the outer electrons — and the conclusion — 4s-[Ar] repulsion assumed to be greater than 3d-[Ar] interaction — lack a well founded basis, at least within the Hartree-Fock methods which undoubtly provide the best definition of the atomic orbital concept. In fact, quite on the contrary, the 3d-[Ar] repulsion energy should be greater than that for 4s-[Ar] interaction, as it is qualitatively suggested by the observed increase of the G values as the number of 3d electrons increases in the electronic configurations considered (Tables 1 and 2). Furthermore, by plotting the radial distribution of 3d and 4s electrons in a scandium atom in its ground state electronic configuration, one can conclude that the existence of radial nodes in a 4s orbital is not enough to assume a 4s-[Ar] repulsion greater than the 3d-[Ar] interaction (see fig. 3).

Table 3

Roothaan-Hartree-Fock energies for two electronic configurations of yttrium [2]

Electronic Configuration	ϵ_{4d}/E	ϵ_{5s}/E_h	$\Sigma\epsilon_i$/E_h	G/E_h	E/E_h
[Kr]4d²5s¹ (I)	−0.19375	−0.19233	−2050.01337	1281.64163	−3331.6550
[Kr]4d¹5s2 (II)	−0.24987	−0.19578	−2053.51973	1278.15147	−3331.6712
Δ (I-II)	0.05612	0.00345	3.50636	3.49016	0.0162

3 — CONCLUSION

The self-consistent field orbital is a one-electron function rather useful for constructing many-electron wavefunctions and interpreting the periodic properties of elements. Accurate Hartree-Fock results for atoms yield a correct and well founded basis for interpreting ground state electronic configurations in terms of the orbital concept. By taking the scandium and yttrium atoms as examples of the above mentioned considerations, this article provides objective answers to several previously and yet unanswered questions raised on the relative stability of different electronic configurations interpreted in terms of orbital energies.

Received 28.February.1983

LITERATURE CITED

[1] F. HERMAN, S. SKILLMAN, "Atomic Structure Calculations", Prentice-Hall, Inc., Englewood Cliffs, N.J., 1963.

[2] E. CLEMENTI, C. ROETTI, *At. Data Nucl. Data Tables*, **14**, 177 (1974).

[3] J.J.C. TEIXEIRA DIAS, *Química Quântica*, Fundação Calouste Gulbenkian, Lisboa, 1982.

[4] F.L. PILAR, *J. Chem. Educ.*, **55**, 2 (1978). T.S. CARLTON, *ibid.*, **56**, 767 (1979). F.L. PILAR, *ibid.*, **56**, 767 (1979).

[5] R.E. PRESS, *Educ. Chem.*, **6**, 10 (1969).

ABSTRACT

A controversial point on the interpretation of electronic configurations of atoms in relation with orbital energies is reanalysed in the light of previously published accurate Hartree-Fock results.

RESUMO

A controvérsia suscitada na interpretação das configurações electrónicas de átomos em relação com as energias das orbitais atómicas é reanalisada à luz de resultados de Hartree-Fock bastante precisos e previamente publicados.

M. ROMAN*
A. FERNANDEZ-GUTIERREZ
M. C. MAHEDERO
A. MUÑOZ DE LA PEÑA
Departamento de Química Analítica
Facultad de Ciencias de Badajoz
Universidad de Extremadura
Badajoz. España

ALIZARINCOMPLEXONA COMO REACTIVO DE In(III). DETERMINACION ESPECTROFOTOMETRICA DE CANTIDADES TRAZA DE In(III)

Se ha realizado el estudio espectrofotométrico del complejo alizarincomplexona-In(III) en disolución acuosa, determinándose sus condiciones óptimas de reacción, la estequiometría del mismo (2:1, reactivo:In(III), y el valor de su constante de estabilidad (log K = 11,8). Se propone un nuevo método de determinación de trazas de In(III) para concentraciones comprendidas entre 1 y 9 ppm. El error relativo y las interferencias del método han sido establecidos.

(*) Dirección actual: Departamento de Química General. Facultad de Ciencias. Universidad de Granada. Granada.

INTRODUCCION

Es conocido que la alizarincomplexona (1,2-dihidroxiantraquinona-3-metilamino-N,N-diacético), es usada como indicador metalocrómico en la valoración complexométrica de In(III) [1]; sin embargo no hemos encontrado datos en la bibliografía que indiquen que haya sido estudiado el complejo alizarincomplexona-In(III). En este trabajo se realiza dicho estudio, habiéndose determinado la influencia que ejercen diversos factores sobre la formación del complejo, así como su estequiometría y su constante de estabilidad, lo cual nos ha permitido proponer un nuevo método de determinación espectrofotométrica de In(III) que es de rápida y fácil aplicación. Siendo la alizarincomplexona un reactivo ampliamente difundido en los laboratorios, al haber sido propuesto para la determinación fotométrica de los iones F^- [2], Zn(II) [3], Cd(II) [4], Mn(II) [5], Ca(II) [6], Ge(IV) [7], Al(III) [8], U(VI) [9], Ni(II) [10] y Mo(VI) [11], y como indicador metalocrómico en valoraciones complexométricas, pensamos que es interesante disponer de un método de determinación de In(III) utilizando este reactivo.

MATERIAL Y MÉTODOS

REACTIVOS

Todos los reactivos usados fueron de calidad analítica. Alizarincomplexona: Solución 2×10^{-3} M preparada por pesada de 0,77066 gr del reactivo Merck, que se disolvieron en 50 ml de NaOH 2 N. Se fijó el pH a continuación en 5-6 por adición de ClH y se completó con agua destilada hasta 1 litro. Disoluciones de In(III). Se prepararon a partir de $(NO_3)_3In.5H_2O$ Merck por dilución en agua destilada; su exacta concentración fue determinada a pH 9,12 con EDTA y NeT como indicador.

APARATOS

Espectrofotómetro Beckman 25, provisto de registrador gráfico y cubetas de vidrio de 1,0 cm; en el cálculo de la constante de estabilidad se utilizaron cubetas de 1,0 a 5,0 cm de paso de luz.

PROCEDIMIENTO RECOMENDADO PARA LA DETERMINACIÓN DE TRAZAS DE In(III)

Se introduce en un matraz aforado de 25 ml la muestra problema con una cantidad de In(III) tal que la disolución final contenga entre 25 y 225 γ. Se le agregan 4 ml de reactivo 10^{-3} M, 5 ml de goma arábiga al 1% y 10 ml de tampón AcH/AcNa de pH 4,3. Se mide la absorbancia de la disolución a una longitud de onda de 520 nm, frente a blanco reactivo. La cantidad de In(III) en la muestra se determina a partir de una recta de calibrado preparada bajo idénticas condiciones.

RESULTADOS Y DISCUSIÓN

ESTUDIO ESPECTROFOTOMÉTRICO DEL COMPLEJO ALIZARINCOMPLEXONA-In(III)

Determinación de las condiciones óptimas de reacción

Experiencias previas pusieron de manifiesto que el complejo formado entre la alizarincomplexona y el In(III) en medio acético, presentaba una cierta inestabilidad que se traducía en la aparición de un precipitado con el tiempo, al igual que les ocurre a otros complejos de este reactivo. Esto nos obligó a plantear experiencias de las que pudimos deducir la obligatoriedad del uso de estabilizadores. Se ensayaron alcohol polivinílico, gelatina y goma arábiga, siendo ésta última la que dió mejores resultados.

La concentración óptima de goma arábica elegida fue de 2 g/l (5 ml al 1% en un volumen final de 25 ml), siendo estable la absorbancia del complejo más de 8 horas en estas condiciones.

El estudio de la influencia del pH sobre los espectros de absorción de complejo y reactivo, nos puso de manifiesto la existencia del complejo entre pH 2 y pH 7, siendo óptima su formación en el intervalo de pH comprendido entre 3 y 5, en el que complejo y reactivo presentan máxima absorción a 510 nm y 430 nm, respectivamente. En la fig. 1 representamos las diferencias de absorbancia entre ambos en función del pH a 520 nm (longitud de onda donde estas son máximas).

Como valor óptimo de pH se eligió el de 4,3 (10 ml de tampón AcH/AcNa en un volumen final de 25 ml). Los espectros de absorción de complejo y reactivo y las diferencias entre ambos para este valor de pH se representan en la fig. 2.

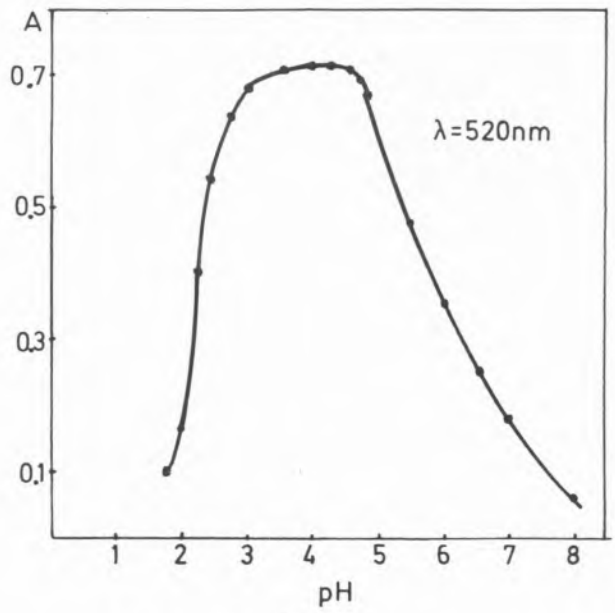

Fig. 1
Influencia del pH en la formación del complejo.
$[In(III)] = 8\times10^{-5}$ M, $[R] = 1{,}6\times10^{-4}$ M

En la fig. 3 mostramos la influencia de la concentración de reactivo, manteniendo fija una concentración 6×10^{-5} M de In(III). En ella se observa un aumento lineal de la absorbancia del complejo hasta una concentración 10^{-4} M; manteniéndose constante para concentraciones superiores. A partir del estudio efectuado, elegimos como óptima una concentración $1{,}6\times10^{-4}$ (4 ml de reactivo 10^{-3} M en un volumen final de 25 ml).

El orden de adición de los reactivos no afecta a la formación del complejo.

Naturaleza del complejo

Hemos obtenido un valor de 11.200 $l.mol^{-1}.cm^{-1}$ para el coeficiente de extinción molar a 520 nm de longitud de onda.

La estequiometría del complejo se ha determinado aplicando los métodos clásicos de Job (fig. 4), de Yoe-Jones y de Harvey-Manning, resultando ser 2:1, reactivo:catión.

Para la determinación de la constante de estabilidad del complejo en estudio, y dado que estamos ante un complejo fuerte, se aplicó el método de GONZÁLEZ, ARREBOLA y ROMÁN [3]. En la fig. 5 se representa βA frente a $(\beta A)^{1/3}/(b_o/\beta)^{2/3}$, obser-

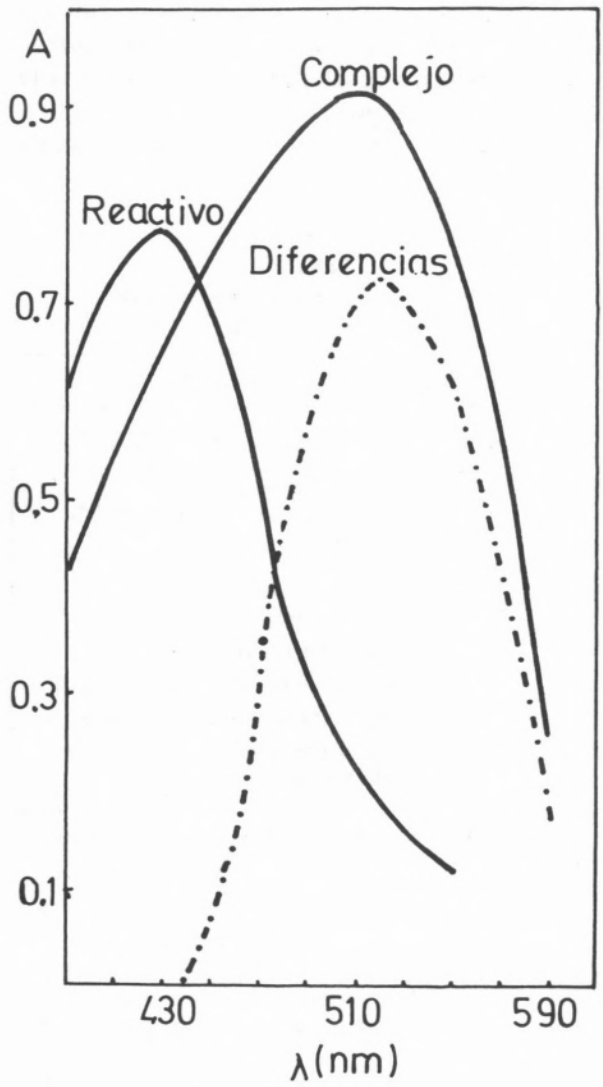

Fig. 2
Espectros de absorción de complejo, reactivo y diferencias entre ambos, pH = 4,3

vándose una línea recta, com era de esperar para un complejo de estequiometria 2:1, reactivo:In(III). La pendiente de la recta se calculó gráficamente, obteniendose un valor de 21.100. Aplicando la expresión $\text{pendiente} = (\frac{4K}{A_{o(b_o)^2}})^{1/3}$, se calculó la constante de estabilidad, resultando un valor de 11,8 para el log K.

Determinación espectrofotométrica de In(III)

En las condiciones elegidas como idóneas, existe un adecuado cumplimiento de la ley de Lambert--Beer en el intervalo de concentraciones compren-

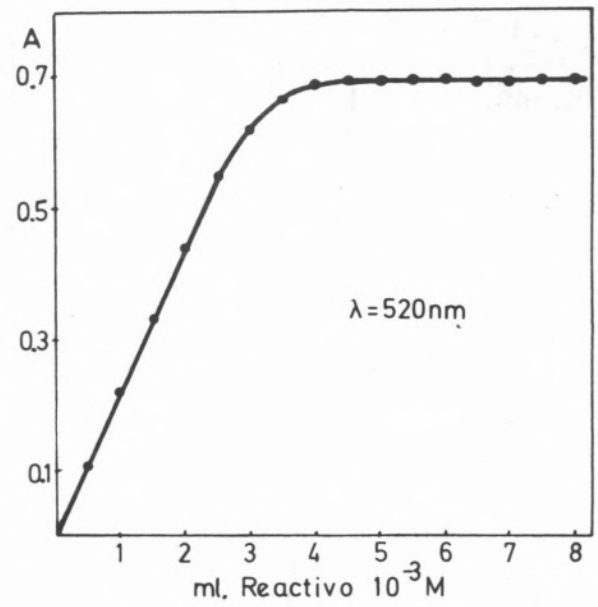

Fig. 3
Influencia de la concentración de reactivo, [In(III)] = 6 × 10⁻⁵ M

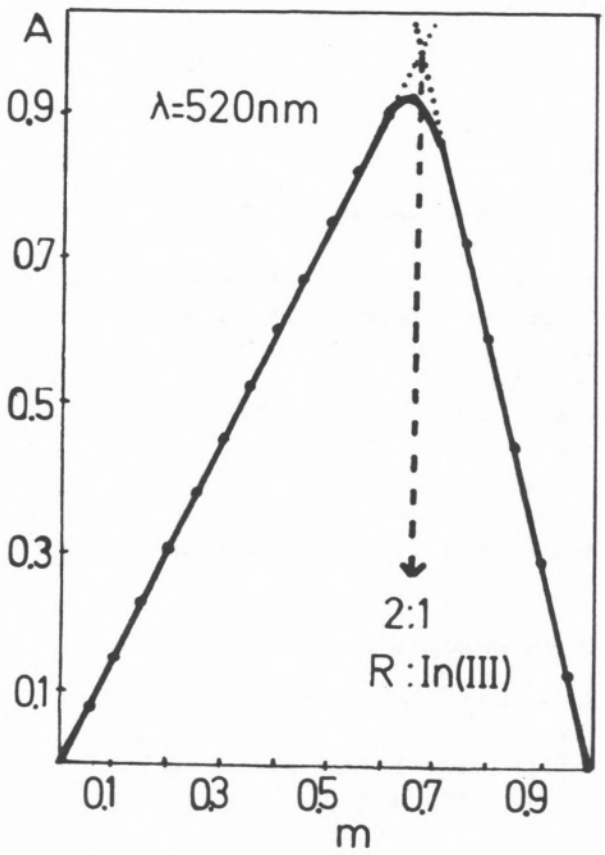

Fig. 4
Método de Job, m = [R]/[R] + [In(III)], [R] + [In(III)] = = 2,4 × 10⁻⁴ M

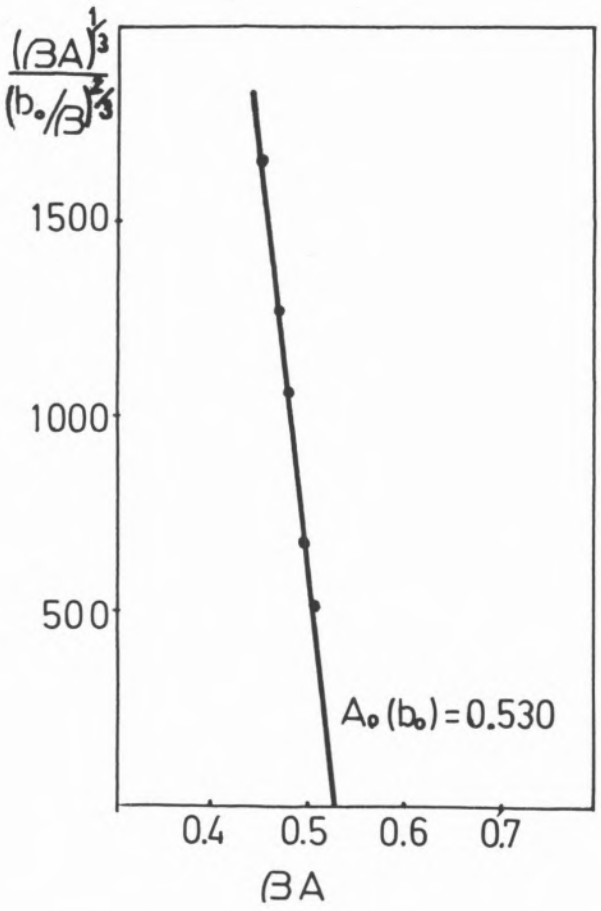

Fig. 5
Método de González, Arrebola y Román, $b_0 = 4 \times 10^{-5}$ M

dido entre 1 y 9 ppm de In(III). El estudio realizado nos permite proponer un nuevo método de determinación espectrofotométrica de In(III), siendo la zona de mínimo error del mismo, la comprendida entre 1,80 y 8,00 ppm según el gráfico de Ringbom.
Aplicando el cálculo estadístico de errores a los resultados obtenidos, encontramos una desviación standart de ±0,042 y un error relativo sobre el valor medio de 0,74%, para un nivel de confianza del 95%.

Interferencias de iones extraños

Se estudió el efecto de algunos iones extraños en la determinación de 5 ppm de In(III) según el método propuesto. El valor límite de la concentración del ión extraño fue el que causó un error no mayor de un 2,5% en la absorbancia. Los cationes fueron añadidos en forma de cloruros, nitratos o sulfatos hasta un máximo de 100 ppm; los aniones fueron añadidos en forma de sales sódicas o potásicas hasta un máximo de 1000 ppm.

En la Tabla 1 se encuentran reunidos los resultados obtenidos.*

Tabla 1
Efecto de iones extraños en la determinación de 5 ppm de In(III)

Tolerancia (ppm)	Ión añadido
1000	$S_2O_3^{2-}$, Cl^-, Br^-, I^-, tartratos, NO_3^-, SO_4^{2-}, NO_2^-, SCN^-
100	Alcalinos, Alcalinoterreos, Au(III)*, Tl(I), F^-
50	Hg(II)
25	Mn(II), Pt(IV)
10	Hg(I), Ag(I), Cr(III), PO_4^{3-},
5	Cr(VI), Rh(III), U(VI), Ge(IV), Cd(II)*
<2,5	Zn(II), Fe(III), Fe(II), Co(II), Ni(II), Pd(II), Cu(II), Al(III), Pb(II), EDTA, Mo(VI), Be(II)

* Se añaden 1000 ppm de $S_2O_3^{2-}$ como agente enmascarante.

BIBLIOGRAFIA

[1] R. Belcher, M.A. Leonard, T.S.West, *J. Chem. Soc.*, 2390 (1958).
[2] R. Belcher, M.A. Leonard,T.S. West,, *J. Chem. Soc.*, 3577 (1959).
[3] F.burriel, A. Cabrera, C. Fuentes, *Inform. Quim. Anal.*, **19**, 165 (1965).
[4] F. Capitán, M. Román, A. Fernández-gutiérrez, *Bol. Soc. Chil. Quim.*, **17**, 29 (1971).
[5] F. Capitán, M. Román, A. Guiraum, *Quim. e Ind.*, **3**, 15 (1971).
[6] F. Capitán, A. Guiraum, J. Bullejos, *Afinidad*, **32**, 461 (1975).
]7] M. Román, A. Fernández-gutiérrez, *Quim. Anal.*, **29**, 281 (1975).
[8] F. Ingram, *Talanta*, **20**, 999 (1973).
[9] M.A. Leonard, F.I. Nagi, *Anal. Lett.*, **2**, 15 (1969).
[10] M.A.Leonard, F.I. Nagi, *Talanta*, **16**, 1104 (1969).
[11] M. Krizau, J. Nozaki, *Mikrochim. Acta*, 882 (1969).
[11] D.V. González, A. Arrebola, M. Román, *Talanta*, **26**, 215 (1979).

C. FERREIRA DE MIRANDA
M. MANUELA MOTA BATISTA
Departamento de Química
Universidade de Évora
ÉVORA
e
Centro de Electroquímica
e Cinética da Universidade de Lisboa (INIC)
Faculdade de Ciências
LISBOA

M. DE LOURDES PIMENTA DA SILVA
Departamento de Química
Universidade de Évora
ÉVORA

AVAILABILITY INDICES, PHYSICO-CHEMICAL ASPECTS
I — Available Molybdenum in some Alentejo Soils

Available molybdenum was determined in 7 soils of the Evora region using the Lowe and Massey and the Grigg extraction methods. Some likely pertinent soil parameters were also determined. A discussion of the correlation analysis of the data is presented and a tentative description of the experimental results in terms of a physico-chemical model is put forward. The precision of the analytical methods is evaluated and discussed.

INTRODUCTION

Since the creation of Agricultural Chemistry by Liebig in the eighteen forties, chemists and agronomists have attempted to define and to determine the availability of nutrients in soils by using analytical chemistry procedures. This is an ambitious task as it amounts to quantifying the driving force involved in the transfer of chemical species from a polyphased system (the soil) to another polyphased system (the plant) through an interphase where active transport may be operating. Furthermore, some feed-back may occur owing to the complexing action of the plant exudates, and prevailing conditions may be those of non-equilibrium. Availability indices are generally determined by extraction procedures and that makes the situation more difficult, from the conceptual point of view at least, because measurement alters the very variables which are supposed to be measured. Experience shows, however, that this is no sufficient reason for abandonning chemical availability indices but, certainly, there is a strong case for trying to understand the chemistry underlying their definitions.

The time scale of such chemistry may range from the century, for the weathering of the parent-rock materials, to that of some minutes for the kinetics of the extraction procedures used in measuring a particular availability index. Involved are: (i), a *non-mobile form* of the nutrient (consisting e.g. of minerals of the parent-rock materials, precipitates and oclusions) whose level changes slowly over the years or the centuries; (ii), a *mobile form* (comprising complexes, either labile or more or less inert, with colloidal organic matter, and adsorbates on clay minerals), whose level can change in a month-to-years time scale; and (iii), the *available form* whose level is quickly adjusted (say, at the hour-to-days time scale) to a steady state equilibrium, with the mobile form on the one hand, and the plant or other source of uptake, on the other hand. This is summarised in fig. 1 where the parallel between available and extractable forms of a micronutrient is also indicated. The proposed scheme is in agreement with the translocation process advanced by ZUNINO and MARTIN [1] but emphasis is given here to mobility rather than to possible mechanisms.

Knowledge of the mechanisms of the *mobile form* → *available form* conversion is fundamental, both from the standpoint of the agronomist

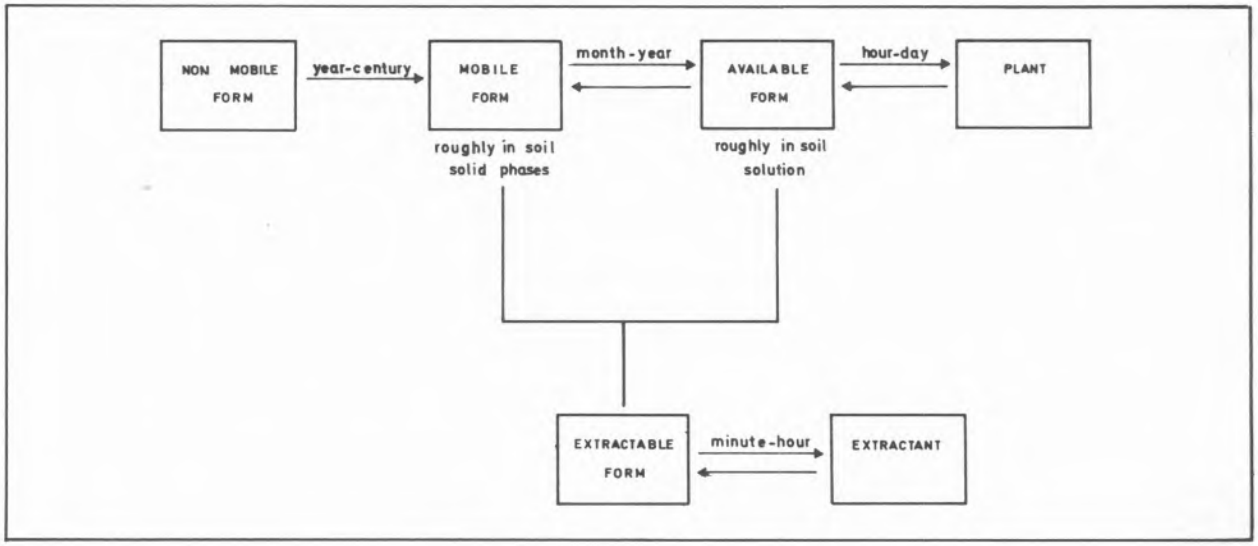

Fig. 1
A simple model for relating nutrient mobility and metrology

who may want to improve the level of available nutrients in a given soil, and from the standpoint of the chemist who seeks good chemical indices of availability. However, such mechanisms are difficult to investigate because, for the systems concerned, it is not possible to fix all variables but one in order to study its influence. Thus, statistical analysis of the data is often resorted to, generally using a linear model which may prove justified for interpolation purposes but less so for the elucidation of mechanisms.

It is important to realize that extraction procedures introduce a distribution equilibrium completely alien to the natural system, which is nevertheless supposed to simulate the distribution equilibrium between available nutrient and plant. Now, if one keeps in mind that transfer of a nutrient from soil to plant involves an acceptor, an interphase and a donnor, it is surprising that chemically defined availability indices work at all. Indeed, (i), extractant and plant are altogether different acceptors; (ii) the interphase is drastically modified when soil is put into contact with extractants; and (iii) soil donnor properties change as its composition is altered by the extraction procedure itself. Ideally, the transfer-to-plant ability of the available form species should be measured using a standard donnor, and the donnor capacity of the soil should be measured against a standard acceptor; and the chemical potential of the species should be evaluated without distubing it. As they stand, availability indices are crude estimations which have to be — and actually are — tested against the real behaviour of groups of plants and soils.

Molybdenum is one of the most important micronutrients, being a determining factor in the natural process of atmospheric nitrogen fixation by microorganisms as well as in nitrogen metabolism, where it plays a role comparable to that of the first transition elements iron, copper and manganese in the metabolism of oxygen. The literature on molybdenum in soils is very extensive and has been recently reviewed [2]. However, data concerning the mobility and the availability of molybdenum and the relevant controlling factors are fragmentary and often conflicting [2]. There is in this field a large scope for the chemist, both from the fundamental point of view and from that of potential applications.

In the present preliminary investigation, we report some results concerning availability indices for molybdenum deficient soils of the region of Evora. The analytical experience we gathered is used in discussing precision and sensitivity of methods, and the statistical analysis of data is tentatively and critically exploited as a tool for obtaing hints about possible physico-chemical interactions.

EXPERIMENTAL

Seven soils of the Evora region were studied. All were reputedly deficient in molybdenum and

though proceeding from neighbouring areas they corresponded to different geomorphological characteristics (Cf. Table 1).

Four *ca* 3 kg field samples of each soil were taken with the usual precautions, down to a depth of 15--20 cm. The samples were air dried, gently ground and screened to 2 mm, then finely ground and sieved to 0.2 mm [3]. The samples were kept in appropriate stoppered bottles. From each sample aliquots of adequate size were taken for the analyses. The following parameters were evaluated: humidity; total molybdenum content; available molybdenum; free iron; organic matter; pH; clay fraction; and qualitative mineral composition of the clay fraction.

Table 1
Nature of the soils investigated in this work

Soil number	Classification
1	Entisol. Typic xerofluvent
2	Entisol. Lithic xerofluvent
3	Alfisol. Typic haploxeralf
4	Entisol. Typic xerorthent (granite)
5	Alfisol. Lithic rhodoxeralf
6	Alfisol. Aquic haploxeralf
7	Entisol. Typic xerorthent (gneiss)

Humidity was determined by loss of weight of a 10 g sample at 105° C ±3° C until constant weight. Analytical results are reported on a dry weight basis. Total molybdenum determinations were carried out with 2 g soil samples which were melted with sodium carbonate (10 g), followed by the usual classical treatment [4]. Available molybdenum was determined by two methods: (i), the Lowe and Massey method [5] — continuous extraction by boiling water in a Soxhlet apparatus (soil, 50 g; water 250 ml; 16 hours): and (ii), the Grigg method [6] — extraction with an oxalate buffer solution of pH = 3.3 (soil, 40 g; 0.2M oxalic acid plus 0.1M ammonium oxalate, 250 ml; 16 hours with stirring). In all cases molybdenum was estimated spectrophotometrically by the thiocyanate-stannous chloride method which is the most widely used owing to its sensitivity and general freedom from interference [7]. Butyl acetate [8], amyl alcohol plus carbon tetrachloride (1:1) [9], and isopropyl ether [4] were tested as organic extractants for stability of colour and easy separation of phases; the later was found to be the most convenient.

Free iron was determined in the TAMM'S extract [10] (soil, 10 g; 0.2M oxalic acid plus 0.1M ammonium oxalate, 100 ml; 16 hours with stirring) by spectrophotometry of the 1,2-dihydroxybenzene 3,5--disulphonate (tiron) complex [11].

Organic matter was estimated volumetrically according to ANNE'S method [12].

The pH of soils was measured with the glass electrode in water (soil, 20 g; water 20 ml; 30 minutes stirring; 1 hour decantation) and in calcium chloride 0.01M medium (soil, 10 g; solution 20 ml; 30 minutes stirring, 30 minutes decantation) [13].

The clay fraction in the soils was determined as usual by the pipette sampling method [13]. The qualitative mineral composition of the clay fraction was established by x-ray diffraction.

RESULTS AND DISCUSSION

1 — *RESULTS AND PRECISION OF THE ANALYTICAL PROCEDURES*

The results of the evaluation of molybdenum levels as well as those of some potentially determining factors are presented in Table 2. Both total and available molybdenum levels are considerably lower than the normal values which are 1-2 ppm and 0.2-0.4 ppm respectively [14]. For a total molybdenum level of 0.5-0.8 ppm, the Lowe and Massey extraction method seems to be more discriminative than Grigg method for defining available levels, in agreement with LOWE and MASSEY [5]. Indeed, availability indices span a single to double interval the first case, whereas in the second one, values cluster within 20% (at most) around the average, fluctuations being thus rather small, though analytically significant.

Independently from difficulties associated with significant soil sampling and adequate soil extraction procedures, molybdenum determination in soil at the ppb-ppm level is a delicate analytical problem. Therefore, assessments of its precision are desirable. Variance in molybdenum determinations (in a given soil sample, by a given extraction procedure, and by a given colorimetric method) arises from

Table 2
Molybdenum levels and likely correlated parameters of soils of the Évora region

Soil	Total Mo (ppb)	Available Molybdenum (ppb) (Grigg)	(Lowe & Massey)	Free iron (ppm)	Organic matter (%)	pH water	pH $CaCl_2$	Clay fraction (%)	Clay minerals
1	698	55	14	1177	0.79	5.0	4.1	5.3	illite + kaolinite
2	510	55	15	2364	1.11	6.6	5.3	11.9	kaolinite
3	651	54	28	1566	1.52	6.6	5.4	16.1	kaolinite + montmorillonite
4	768	56	28	2113	0.88	6.7	5.5	13.0	kaolinite + montmorillonite
5	719	43	26	1443	3.25	7.1	6.3	13.6	illite + kaolinite
6	730	59	25	1644	1.80	7.6	7.0	11.3	illite + kaolinite
7	545	51	24	1667	1.65	8.3	7.6	19.4	illite + kaolinite

three sources: (i), the instrumental uncertainty of the absorbance reading; (ii), variance associated with the preparation of the colorimetric solution; and, (iii), variance due to the soil extraction procedure.

Uncertainty due to instrument reading is negligible, not more than 0.001 at any point in the absorbance scale. The standard deviation of an absorbance measurement is therefore essentially due to variance of colour development. A direct estimation based on replicate measurements with Mo standards — which were perfomed for establishing the colorimetric calibration curve — yielded 0.003; this value was corroborated by the external estimation, resulting from the fitting of the calibration curve. Molybdenum concentration c (ppm) in a soil sample of mass M(g) is given as a function of the absorbance measurement, A, by $c = 1.112 \times 10^4\ A/M$ where the factor 1.112×10^4 is derived from the calibration curve and the appropriate dilution factors. Therefore, the standard deviation of c arising from the colorimetry is $\sigma_c = 0.003 \times 1.112 \times 10^4 / M = 33.36/M$ (Table 3, column 3a).

On the other hand, for each type of determination (total Mo, Grigg available Mo and Lowe and Massey available Mo) we have 7 averages and variances, one foreach soil. CHOCHRAN test [15] showed that the variances were not significantly different from soil to soil, as it could be antecipated from the fact that the same analytical procedure was used for all soils. The combined estimation of variance comprising thus 28 results is presented for each type of determination on Table 3, column 3b.

Clearly, the variance of the molybdenum determinations is not mainly associated with the soil extraction method; colorimetry itself contributes to roughly 50% of the standard deviation. Precision of the determinations is 3-6% down to the 40 ppb level and 7-14% at the 15 ppb level. Detection limits are of the order of 50 ppb for total molybdenum and 5 ppb for available molybdenum determinations.

As to free iron, when 10 g samples are used, precision is 1-4% at the 1000-3000 ppm level. Variance is practically entirely due to the extraction procedure. The detection limit is 80 ppm.

Organic matter can be estimated at the 1-3% level in 1-2 g samples with a precision of 1-3%; the detection limit is 0.06%.

2 — *THE CORRELATION ANALYSIS OF THE DATA*

The correlation matrix for our data is presented in Table 4. Except for a significant positive correlation between pH in water and pH in 0.01M $CaCl_2$, which is trivial, and the correlation between pH and clay

Table 3
Precision of molybdenum, iron and organic matter determination

Determination	Weight of sample (g)	Standard deviation (ppb)	Concentration level (ppb)	error (%)	Detection limit (ppb)
MOLYBDENUM					
Total Mo	2	17[a] 30[b]	500 — 800	4 — 6	60
Available Mo (Grigg)	40	0.8 2	40 — 60	3 — 4	4
Available Mo (Lowe & Massey)	50	0.7 2	15 — 30	7 — 14	4
IRON					
Free Fe	10	0[a] 40 ppm[b]	1000 — 3000 ppm	1 — 4	80 ppm
ORGANIC MATTER					
Organic matter	1-2	0.03 %	1 — 3 %	1 — 3 %	0.06 %

(a) Standard deviation for colorimetry alone
(b) Standard deviation for the whole procedure, including extraction from soil

Table 4
Simple correlation coefficient between pairs of variables

	Mo_T	Mo_G	Mo_{LM}	MO	pH_1	pH_2	MA	Fe
Mo_T	1	0.050	0.450	0.146	—0.245	—0.171	—0.381	—0.377
Mo_G		1	—0.186	—0.787*	—0.162	—0.216	—0.323	0.296
Mo_{LM}			1	0.426	0.566	0.513	0.637	—0.008
MO				1	0.442	0.527	0.343	—0.309
pH_1					1	0.978***	0.813**	0.255
pH_2						1	0.724*	0.082
MA							1	0.248
Fe								1

* Significant at the 10% level
** Significant at the 5% level
*** Significant at the 1% level

fraction, MA (probably not pertinent in the present context), the only significant correlation is between Grigg available molybdenum (Mo_G) and organic matter. In particular, Lowe and Massey available molybdenum (Mo_{LM}) levels, which definitely vary from soil to soil, do not seem to be correlated with any of the factors we have considered.

Since the influence of each one of these might be obscured by the variations of the others, the partial correlation coefficients were evaluated according to

the general equation $r_{ij,\ldots,p} = -C_{ij}/C_{ii}\ C_{ij}$, where $[C_{ij}]$ is the inverse of the simple correlation matrix [16]. The results are presented in Tables 5 and 6. At this stage, only organic matter, pH in 0.01M $CaCl_2$, clay fraction and free iron were taken into account as potentially determining factors for Mo_G and Mo_{LM} levels. (The reasons for eliminating one of the pH indices are obvious, and those for not considering total molybdenum content will be apparent later). Again, only Grigg available molybdenum and organic matter are significantly correlated (at the 10% level).

These results call for some comments as the plots of Mo_G and Mo_{LM} against the potentially pertinent variables do not rule out some trends, though not linear, especially for Mo_{LM} (figs. 2 and 3).

Table 5
Third order partial correlation coefficients (excluded variables: Mo_T, Mo_{LM} and pH_1)

	Mo_G	MO	pH_2	MA	Fe
Mo_G	—	—0.826 *	0.605	—0.530	0.138
MO		—	0.685	—0.411	—0.118
pH_2			—	0.753	—0.044
MA				—	0.301
Fe					—

* Significant at the 10% level.

Table 6
Third order partial correlation coefficients (excluded variables: Mo_T, Mo_G and pH_1)

	Mo_{LM}	MO	pH_2	MA	Fe
Mo_{LM}	—	0.208	—0.024	0.483	—0.112
MO		—	0.407	—0.058	—0.379
pH_2			—	0.573	0.046
MA				—	0.291
Fe					—

It can be argued that, for our data, the number of fixed variables is high compared to the number of samples and in fact we even had to leave out some variables in order to dispose of at least 2 degrees of freedom for the significance tests concerning the partial correlation matrices. A more relevant point however is that calculation of correlation coefficients is based on a covariance/variance ratio definition. Now, this implies a linear model which may be inadequate. Indeed a linear model cannot be justified on mechanism grounds: even a single chemical reaction or ion exchange equilibrium would rather lead to linear log-log relationships between variables, and several coupled equilibria would

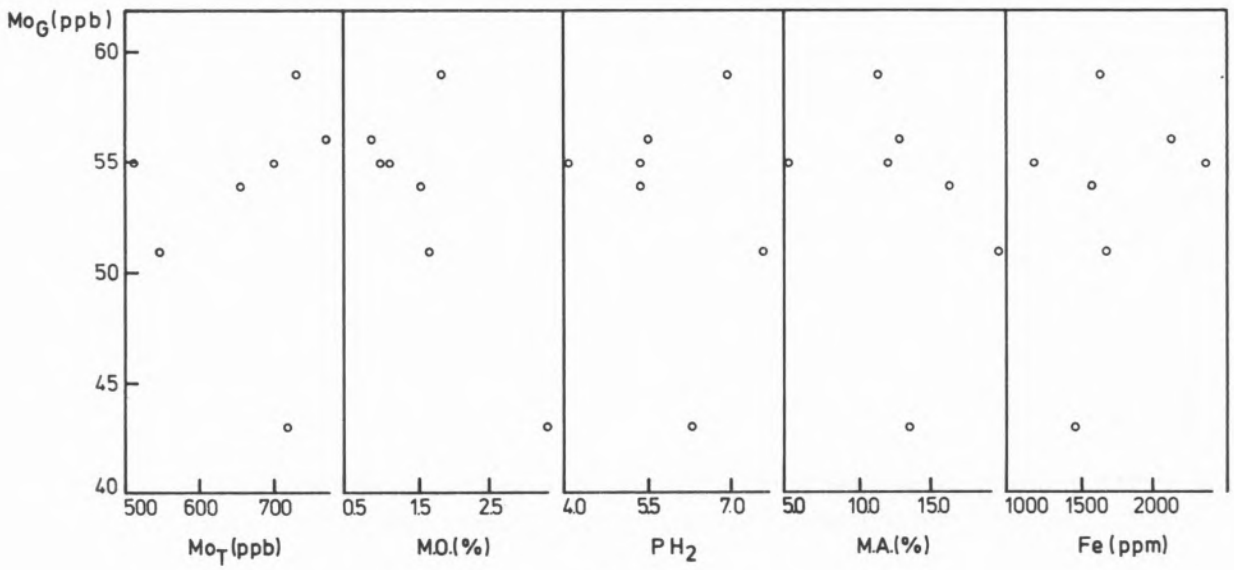

Fig. 2
Plots of Grigg's molybdenum against potentially pertinent variables

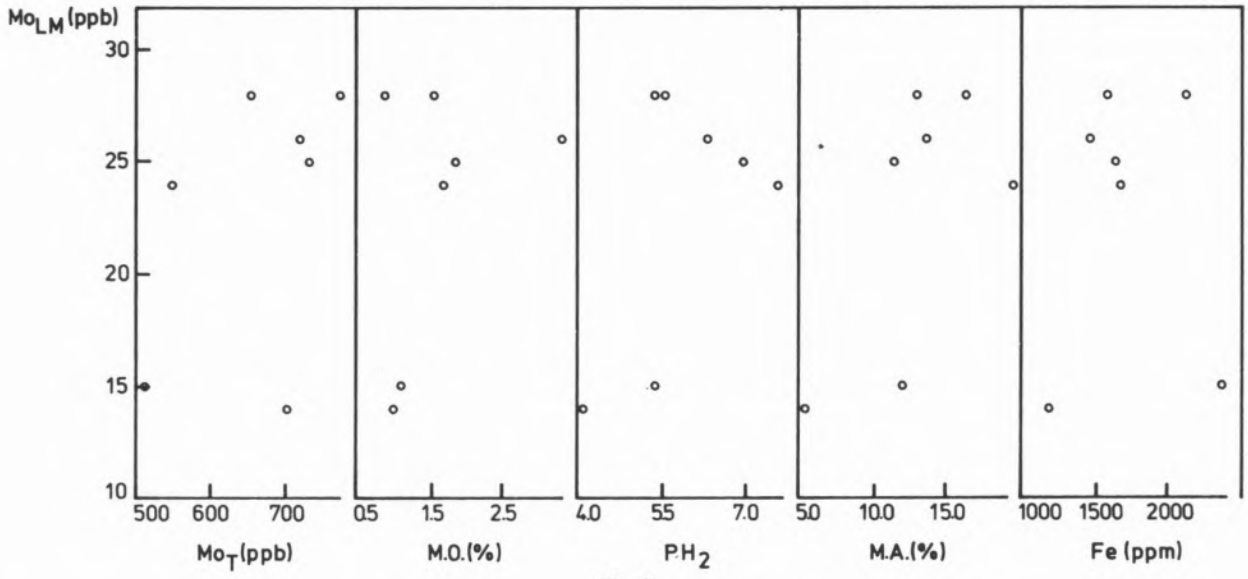

Fig. 3

Plots of Lowe and Massey's molybdenum against pertinent variables

result in more complicated relationships. It is not surprising therefore that we also failed to find significant linear simple and partial correlations between the logarithms of variables.

Single and multiple linear regressions are not reported here since the data interpolation aspects are not pertinent in the present context. On the contrary, principal component analysis may offer some interest and was therefore carried out [17], in spite of the limited number of OTU's, in order to assess their degree of similarity or otherwise (fig. 4):

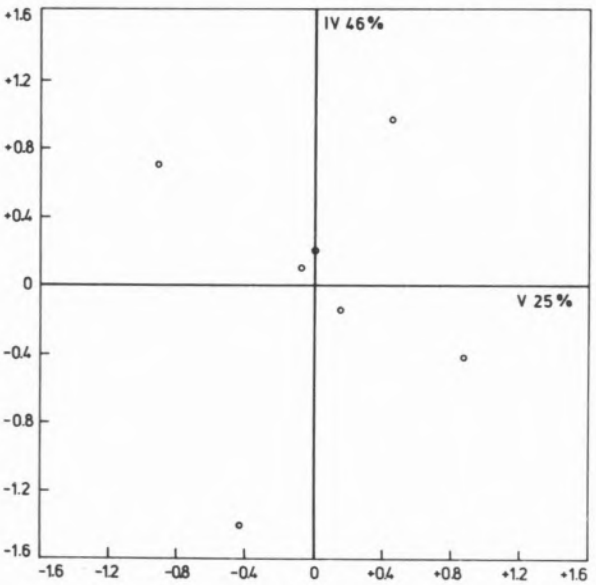

Fig. 4

Ordination plot from principal component analysis

points are fairly scattered in the plane of the principal components as we hoped, though three soils tend to form a cluster.

3 — *PHYSICO-CHEMICAL ASPECTS*

Within the framework we put forward in the introduction, our results for Grigg available molybdenum, Mo_G, are easily understood on the assumption that mobile molybdenum levels are about the same for all the soils we investigated and that Mo_G is nearly equal to the sum of mobile plus available molybdenum. (This is likely since oxalate ion is a fairly strong complexant for Mo (VI)). In this view, the negative correlation between Mo_G and organic matter then merely reflects the competition between insoluble organic matter and oxalate ion for Mo(VI). A predominant role is thus implicitly attributed to organic matter; this seems to be justified in the present case, considering the relatively low levels of clay fraction (5-20%) and its nature (little or no montmorillonite and low ferric oxide content, 0.2--0.3%). This is not in contradition with JONES [18] results for a krasnozem soil from Wollongbar (South Wales Australia) which indicated ferric oxide as the chief factor controlling molybdenum mobility: Wollongbar soil contains 72% clay fraction and 15% ferric oxide.

As to Lowe and Massey available molybdenum levels, Mo_{LM}, they correspond, in our view, to the partial dissociation of the complex Mo(VI)-soil

organic matter, the Mo(VI) concentrations in the extract being lower than in the case of a Grigg extract because the amount of competitive complexant in solution is now nearly zero. Actually, since some organic matter and other potentially complexing species may be solubilized by hot water, the final concentration of complexing agent in the solution is not only low but also ill-defined. This is a drawback of Lowe and Massey method (unbuffered extractant medium) and can explain the apparently advantageous descriminative character of the index. 0.01M $CaCl_2$ might prove a more rational non complexing extractant.

ACKNOWLEDGMENTS

The authors wish to thank Professor J. Lima de Faria of the "Laboratório de Técnicas Físico-Químicas aplicadas à Mineralogia e Petrologia" of the "Junta de Investigação Científica do Ultramar" for the x-ray diffraction analysis of the clay fractions and Mrs. Helena Mafalda Carolino of the Departamento de Fitotecnia of the Universidade de Évora for the determination of the clay fraction in the soils investigated.

REFERENCES

[1] H. Zunino, J.P. Martin, *Soil Sci.*, **123**, 65 (1977).
[2] M.M. Mota Batista, C. Ferreira de Miranda, "O Molibdénio nos solos", Monograph of the Instituto Macional de Investigação Científica, Lisbon (1981).
[3] "Methodes d'Analyse Physique et Chimique des Sols". Office de la Recherche Scientifique et Technique d'Outre-Mer, Bondy, France.
[4] E.R. Purvis, N.K. Peterson, *Soil Sci.*, **81**, 223 (1956).
[5] R.H. Löwe, H.F. Massey, *Soil Sci.*, **100**, 238 (1965).
[6] J.L. Grigg, *N.Z.J. Sci. Technol.*, **34**, 405 (1953).
[7] E.B. Sandell, "Colorimetric Determination of Traces of Metals". Interscience Publishers, New York, 644 (1959).
[8] J. Rodier, "L'Analyse de l'Eau", Dunod, Paris, 272 (1976).
[9] C.M. Johnson, T.H. Arkley, *Anal. Chem.*, **26**, 572 (1954).
[10] O. Tamm, *Meddn. St. Skosforsk Inst.*, **19**, 385 (1922).
[11] J.H. Yoe, A.R. Armstrong, *Anal. Chem.*, **19**, 100 (1947).
[12] P. Anne, *Ann. Agron.*, **5**, 161 (1945).
[13] C.A. Black, D.D. Evans, J.L. White, L.E. Ensminger (ed.) "Methods of Soil Analysis", American Society of Agronomy, Inc., Publisher, Madison, Wisconsin, USA, 552 (1965).
[14] B.T. Cheng, G.J. Ouellette, *Soil Fertil.*, **36**, 207 (1973).
[15] V.P. Spiridonov, A.A. Lopatkin, "Tratamiento Matematico de Dados Fisico-Químicos", Editorial Mir, Moscow, 100 (1973).
[16] K.W. Smillie, "An Introduction to Regression and Correlation", Ryerson Press, Toronto, Academic Press, London, 58 (1966).
[17] P.H. Sneath, R.R. Sokal, "Numerical Taxonomy", W.H. Freeman and Company, San Francisco, 245 (1973).
[18] L.P.H. Jones, *J. Soil Sci.*, **8**, 313 (1957).

RESUMO

Determinou-se o teor em molibdénio assimilável em sete solos da região de Évora pelos métodos de extracção de Lowe e Massey e Grigg. Alguns parâmetros susceptíveis de condicionar os níveis de molibdénio assimilável foram igualmente determinados. Apresenta-se uma discussão da análise de correlação dos resultados e sugere-se uma descrição destes em termos de um modelo físico-químico. Apresenta-se também uma avaliação da precisão dos métodos empregados.

M. JOAQUINA S. A. AMARAL TRIGO
M. ISABEL A. OLIVEIRA SANTOS
Centro de Investigação em Química da Universidade do Porto
Faculdade de Ciências
4000 PORTO
Portugal

A NEW METHOD FOR THE SYNTHESIS OF SYMMETRICALLY CYCLIC PEPTIDES OF L-CYSTINE[1]

A new approach to the synthesis of symmetrically protected cyclic peptides of L-*cystine, containing two disulphide bonds, by using derivatives of* L-*cystine and* L-*cysteine, simultaneously, is described.*

The synthesis of peptides with disulphide bonds has been achieved through the preparation of peptides containing *S*-protected cysteine residues. The disulphide bonds can, then, be formed all in one step, simultaneously, or one by one, selectively, by oxidation of the corresponding cysteine residues. The development of methods for the direct conversion of protected thiol groups to disulphides by HISKEY and his co-workers [2] and the CIBA-GEIGY group [3,4] has greatly improved the synthesis of cystine-containing peptides.

In this work a new approach to the synthesis of symmetrically protected cyclic peptides of L-cystine, containing two disulphide bonds, by using derivatives of L-cystine and L-cysteine, simultaneously, is described. Thus, one of the disulphide bridges is introduced from the beginning of the synthesis by using a L-cystine derivative. The second is formed at the end of the synthesis by direct oxidative removal of the *S*-trityl protection of two L-cysteine residues, by the procedure of KAMBER and RITTEL [3], which involves treatment of the peptide with iodine in methanol.

The strategy of the synthesis is outlined in the following scheme:

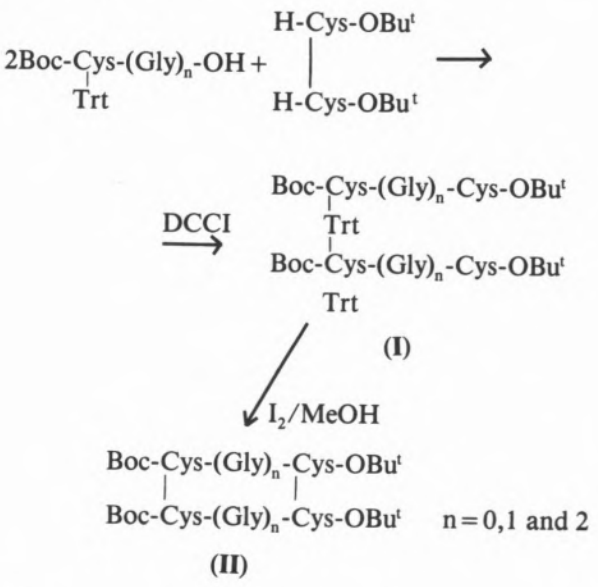

The protected peptides (**I**), containing L-cystine and L-cysteine were prepared by condensation of L-cystine bis-t-butyl ester with the compounds *N*-t-butyloxycarbonyl-*S*-trityl-L-cysteine, *N*-t-butyloxycarbonyl-*S*-trityl-L-cysteinylglycine and *N*-t-butyloxycarbonyl-*S*-trityl-L-cysteinylglycylglycine, using the *N,N'*-dicyclohexylcarbodi-imide method.

(1) A communication on this work was presented at the 16th European Peptide Symposium, Helsingor, Denmark, 1980, reference [1].

The cyclic protected peptides (**II**), *S,S-S',S'*-bis (*N*-t-butyloxycarbonyl-L-hemicystinyl-L-hemicystine t-butyl ester), *S,S-S',S'*-bis (*N*-t-butyloxycarbonyl-L-hemicystinylglycyl-L-hemicystine-t--butyl ester) and *S,S-S',S'*-bis (*N*-t-butyloxycarbonyl-L-hemicystinylglycylglycyl-L-hemicystine t-butyl ester), were obtained by direct oxidative removal of the *S*-trityl group from the corresponding petides (**I**). The reactions proceeded in good yields to give crystalline products. The peptides with n = 0 and 2 were purified by column chromatography (silica gel) and that with n = 1 by crystallization from methanol. The molecular masses of the pure cyclic peptides were determined by mass spectrometry.

EXPERIMENTAL

The purity of all compounds was confirmed by t.l.c. on Kieselgel 60 F_{254}, usually in the four systems chloroform-methanol (9:1), benzene-chloroform--ethanol (12:12:1), acetic acid-chloroform (1:9), and ethyl acetate-methanol (40:1). The compounds were revealed by the $(NH_4)_2SO_4$-H_2SO_4 method [5]. Evaporations and concentrations were all carried out under reduced pressure with a rotary evaporator. Extracts were dried over magnesium sulphate. Light petroleum was the fraction b.p. 40-60°C. When purification was achieved by column chromatography, silica gel (<0.08 mm) from Merck was used. Optical rotations were measured with a Bellingham and Stanley Pepol 66 polarimeter. N.m.r. spectra were recorded by Dr. J.A.B. Baptista at 33°C with a Perkin-Elmer R32 90 MHz spectrometer. The microanalyses were carried out by Dr. Ilse Beetz (Kronach, Germany).

N-*t-Butyloxycarbonyl*-S-*trityl*-L-*cysteinylglycyl-glycine.*

N-t-Butyloxycarbonyl-*S*-trityl-L-cysteine *N*-hidroxysuccinimidyl ester [6] was coupled with glycylglycine hydrochloride [7], yielding the peptide (62%), m.p. 104°C (softening from 82°C), $[\alpha]_D^{20} + 19.1°$ (c 1.00 in MeOH) (Found: C, 64.8; H, 6.3; N, 7.2; S, 5.1. $C_{31}H_{35}N_3O_{16}S$ requires C, 64.6; H, 6.1; N, 7.3; S, 5.5%).

N-N'-*Bis (*N-*t-butyloxycarbonyl*-S-*trityl*-L-*cysteinyl)*-L-*cystine bis*-t-*butyl ester.*

To a solution of *N*-t-butyloxycarbonyl-*S*-trityl-L--cysteine [8,9] (1.42 g, 0.0031 mol) in dichloromethane (4 ml), cooled to —10°C and stirred, was added *N,N'*-dicyclohexylcarbodi-imide (0,63 g, 0.0031 mol). A solution of L-cystine bis-t-butyl ester) [10] (0,53 g, 0.0015 mol), recently prepared, in dicholoromethane (3 ml) was added. The mixture was kept at —10°C for 2 h and at room temperature for 4 days. The precipitated *N,N'*-dicyclohexylurea was filtered off and the filtrate was washed (saturated aqueous sodium chloride, aqueous 5% citric acid, aqueous M-sodium hydrogen carbonate, and saturated aqueous sodium chloride), dried and evaporated. The residue was dissolved in acetone and kept at 0°C for 24 h. The solution was filtered and evaporated and the residue triturated with light petroleum, giving a solid. Two recrystallisations from diethyl ether gave the pure *peptide* (0.84 g, 50%), m.p. 114°C (softening from 99°C), $[[\alpha]_D^{20} — 3.4°$ (c 0.5 in MeOH), τ($CDCl_3$), 2.40-3.00 (30 H, complex, Ph), 3.00-3.18 (2 H, d, NH), 4.70-5.00 (2 H, d, NH), 5.27-5.60 (2 H, complex, CH), 5.94-6.28 (2 H, complex, CH), 6.80-7.10 (4 H, d, CH_2), 7.22-7.50 (4 H, d, CH_2), 8.40-8.73 (36 H, s, Bu^t) (Found: C, 66.0; H, 6.5; N, 4.5; S, 11.2. $C_{68}H_{82}N_4O_{10}S_4$ requires C, 65.7; H, 6.6; N, 4.5; S, 10.8%).

N,N'-*Bis (*N-*t-butyloxycarbonyl*-S-*trityl*-L-*cysteinylglycyl)*-L-*cystine bis-t-butyl ester.*

N-t-Butyloxycarbonyl-S-trityl-L-cysteinylglycine [6] was coupled with L-cystine bis-t-butyl ester [10] by the *N,N'*-dicyclohexylcarbodi-imide method, as described above. The crude compound after trituration with light petroleum and diethyl ether, was recrystallised from ethyl acetate, giving the *peptide* (40%), m.p. 155°C (softening from 112°C), $[\alpha]_D^{22} + 25.7°$ (c. 1.00 in $CHCl_3$), τ ($CDCl_3$) 2.43-3.00 (34 H, complex, Ph and NH), 4.72-5.02 (2 H, d, NH), 5.12-5.50 (2 H, complex, CH), 5.90--6.30 (6 H, complex, CH and CH_2), 6.90-7.15 (4 H, d, CH_2S), 7.20-7.50 (4 H, d, CH_2S), 8.40-8.68 (36 H, 2 s, Bu^t) (Found: C, 62.4; H, 6.5; N, 6.2; S, 9.8. $C_{72}H_{88}N_6O_{12}S_4$ requires C, 62.6; H, 6.5; N, 6.2; S, 9.4%).

N,N'-*Bis (*N-*t-butyloxycarbonyl*-S-*trityl*-L-*cysteinylglycylglycyl*-L-*cystine bis-t-butyl ester*

N-t-Butyloxycarbonyl-*S*-trityl-L-cysteinylglycylglycine was coupled with L-cystine bis-t-butyl ester [10] by the *N,N'*-dicyclohexyl-

carbodi-imide method, keeping the temperature at — 15°C for 10 days. The crude solid isolated from the reaction was applied to a column of silica gel. Gradient elution with chloroform to cloroform-ethanol (9:1), yielded a chromatographically homogeneous *peptide* (55%), which after crystallisation from acetone had m.p. 122--124°C (softening from 104°C), $[\alpha]_D^{25} + 18.0°$ (c 0.90 in $CHCl_3$), τ($CDCl_3$) 2.20-3.20 (36 H, complex, Ph and NH), 4.68-4.96 (2 H, d, NH), 5.20-5.56 (2 H, complex, CH), 5.82-6.50 (10 H, complex, CH and CH_2), 6.80-7.10 (4 H, d, CH_2S), 7.23-7.53 (4 H, d, CH_2S), 8.30-8.83 (36 H, 2 s, Bu^t) (Found: C, 61.4; H, 6.3; N, 7.8; S, 8.4. $C_{76}H_{94}N_8O_{14}S_4$ requires C, 61.0; H, 6.4; N, 7.6; S, 8.7%).

S,S-S',S'-*Bis (*N-*t-butyloxycarbonyl*-L-*hemicystinyl*-L-*hemicystine t-butyl ester).*

To a solution of *N,N'-bis-(N*-t-butyloxycarbonyl-*S*-trityl-L-cysteinyl)-L-cystine bis-t-butyl ester (0.747 g, 0.0006 mol) in methanol (300 ml), was added a solution of iodine (0.735 g, 0.003 mol) in methanol (75 ml), dropwise and with stirring. The reaction mixture was, then, kept with stirring for a further 30 min. After cooling to 0°C, aqueous M-sodium thiosulphate was added until a colourless solution was obtained. Evaporation of the solvent to about a volume of 30 ml, followed by the addition of water (200 ml) yielded a white solid. This was filtered off, washed throughly with water, and dried. The purification of the compound was achieved by column chromatography (silica gel), using chloroform as eluent, followed by two recrystallisations from chloroform-ethyl acetate. The pure *peptide* was obtained in 56% yield, m.p. 198-199°C, $[\alpha]_D^{25} + 102.4°$ (c 0.50 in $CHCl_3$), τ($CDCl_3$) 2.42--2.67 (2 H, d, NH), 3.72-4.00 (2 H, d, NH), 5.07--5.47 (4 H, complex, CH), 6.00-6.45 (4 H, 2 d, CH_2S), 6.76-7.02 (4 H, complex, CH_2S), 8.30-8.62 (36 H, s, Bu^t) (Found: C, 47.4; H, 6.9; N, 7.6; S, 16.4; $C_{30}H_{52}N_4O_{10}S_4$ requires C, 47.6; H, 6.9; N, 7.4; S, 16.9%), molecular-mass (EI-MS): m/e = 757 (calc. 757).

S,S'-S',S'-*Bis (*N-*t-butyloxycarbonyl*-L-*hemicystinylglycyl*-L-*hemicystine t-butyl ester).*

The same procedure was applied to *N,N'*-bis--(*N*-t-butyloxicarbonyl-*S*-trityl- L-cysteinylglycyl)--*L*-cystine bis-t-butyl ester. The isolated crude material on crystallisation from methanol and trituration with ethanol and diethyl ether gave the *cyclic peptide,* chromatographically homogeneous, in 53% yield, m.p. 200-202°C (decomp.), τ [$(CD_3)_2SO$] 1.60-2.00 (4 H, d, NH), 2.80-3.20 (2 H, d, NH), 5.30-5.83 (4 H, complex, CH), (6.10-6.35 (4 H, d, CH_2), 6.85-7.15 (8 H, d, CH_2S), 8.30-8.90 (36 H, s, Bu^t) (Found: C, 46.9; H, 6.7; N, 9.6; S, 14.3. $C_{34}H_{58}N_6O_{12}S_4$ requires C, 46.9; H, 6.7; N, 9.6; S, 14.7%), molecular-mass (FD-MS): m/e = 871 (calc. 871).

S,S-S',S'-*Bis (*N-*t-butyloxycarbonyl*-L-*hemicystinylglycylglycyl*-L-*hemicystine t-butyl ester).*

Identical procedure was applied to *N,N'*-bis (*N*-t--butyloxycarbonyl-*S*-trityl-L-cysteinylglycylglycyl)--L-cystine bis-t-butyl ester. The compound was purified by column chromatography (silica gel), using chloroform-ethanol (19:1) as eluent and chrystallisation from methanol. The *cyclic peptide,* chromatographically homogeneous was obtained in 73% yield, m.p. 164°C (softening from 154°C), τ (CD_3OD) 5.30-5.60 (8 H, complex, NH), 5.86--6.26 (12 H, complex, CH and CH_2), 6.88-7.16 (8 H, complex, CH_2S), 8.40-8.76 (36 H, s, Bu^t) (Found: C, 44.8; H, 6.6; N, 11.4; S, 12.0. $C_{38}H_{64}N_8O_{14}S_4$, $2H_2O$ requires C, 44.6; H, 6.7; N, 11.0; S, 12.5%), molecular-mass (FD-MS): m/e = 985 (calc. 985).

Received 15.November.1982

ACKNOWLEDGEMENTS

We thank the Instituto Nacional de Investigação Científica, Portugal, for financial support. We also wish to thank Dr. J. H. Jones, the Dyson Perrins Laboratory, Oxford, and Mr. J. C. Promé, CNRS, Toulouse, for the mass spectra of the cyclic peptides.

REFERENCES

[1] M.J.S.A. AMARAL TRIGO, M.I.A. OLIVEIRA SANTOS, «Peptides 1980», ed. K. Brunfeldt, Scriptor, Copenhagen, 1981, p. 139.

[2] R.G. HISKEY, A. WITTINGHOFER, A.N. GOUD, R.R. VUNNAM, «Peptides: Chemistry, Structure and Biology», Proceedings of the Fourth American Peptide Symposium, 1975, eds. R. Walter and J. Meienhofer, Ann Arbor Science Publ. Inc., Ann Arbor, 1975, p. 487.

[3] B. KAMBER, W. RITTEL, *Helv. Chim. Acta,* **51,** 2061 (1968).

[4] B. KAMBER, A. HARTMANN, A. JÖHL, F. MÄRKI, B. RINIKER, W. RITTEL, P. SIEBER, «Peptides: Chemistry, Structure and Biology», Proceedings of the Fourth American Peptide Symposium, 1975, eds. R. Walter and J. Meienhofer, Ann Arbor Science Publ., Inc., Ann Arbor, 1975, p. 477.

[5] T. ZIMIŃSKI, E. BOROWSKI, *J. Chromatog.*, **23**, 480 (1966).

[6] R.G. HISKEY, L.M. BEACHAM III, V.G. MATL, J.N. SMITH, E.B. WILLIAMS Jr., A.M. THOMAS, E. T. WOLTERS, *J. Org. Chem.*, **36**, 488 (1971).

[7] H.F. SCHOTT, J.B. LARKIN, L.B. RUCKLAND, M.S. DUNN, *J. Org. Chem.*, **12**, 490 (1947).

[8] L. ZERVAS, I. PHOTAKI, A. COSMATOS, D. BOROVAS, *J. Amer. Chem. Soc.*, **87**, 4922 (1965).

[9] R.G. HISKEY,, L.M. BEACHAM, V.G. MATL, *J. Org. Chem.*, **37**, 2472 (1972).

[10] M.J.S.A. AMARAL, M.A. MACEDO, M.I.A. OLIVEIRA, *J. Chem. Soc. Perkin I*, 205 (1977).

RESUMO

Novo método de síntese de peptídeos cíclicos simétricos de L-cistina

Neste trabalho descreve-se um novo método de síntese de péptidos cíclicos simétricos, protegidos, de L-*cistina, contendo duas ligações dissulfureto, usando derivados de* L-*cistina e* L-*cisteína, simultaneamente.*

A. M. AMORIM DA COSTA
Departamento de Química
Universidade de Coimbra
3000 COIMBRA
Portugal

RAMAN LONGITUDINAL ACOUSTIC MODE IN *N*-DODECYL COMPOUNDS

ABSTRACT

Raman spectroscopic measurements on different n-*dodecyl compounds show that the frequency and bandwidth differences in the fundamental longitudinal acoustical mode are most likely associated with variations in end group effects and physical state which greatly affect the effective chain length mainly due to chain folding.*

1 — INTRODUCTION

The observation and characterization of a longitudinal acoustic mode (LAM) in *n*-alkanes is well established [1-7]. The earliest observation of such a Raman active fundamental mode, whose frequency is inversely proportional to the planar zig-zag chain length was made by MIZUSHIMA and SHIMANOUCHI [1]. A more detailed study was subsequently done by SCHAUFELE and SHIMANOUCHI [2] who observed higher orders of the LAM and showed that their frequencies were in a good agreement with calculated dispersion curves for an infinite planar zig-zag chain. Further studies have defined the frequencies and the detailed form of such modes and the effect of crystal and chain branching upon the LAM frequencies [4-7].

Following SCHAUFELE and SHIMANOUCHI studies, the frequency/chain length relationship found for *n*-alkanes has been widely used to deduce the length of the all-*trans* chain segments in polyethylene single crystals and to determine the paraffinic chain lengths and conformations in phospholipids and other hydrocarbon compounds [12,17-18]. Actually, it was found by FAIMAN *et al.* [17] that the relation between alkyl-chain length and accordion-mode vibration in saturated hydrocarbon chain anionic K,Na and Ca soaps of chain length C_{10}-C_{28} is more complex than for the corresponding alkyl chain in *n*-alkanes. They found that the divergence from the chain length/ /frequency relation increases as the temperature decreases for crystalline materials and also that it increases with increasing atomic weight of the cation. When the longitudinal acoustical modes of each soap are compared with their corresponding *n*-alkane chain-length using a frequency/chain length curve taken from Schaufele's polynomial expression, it appears that in the crystalline state the degree of chain bending increases with increasing size of cation.

The Raman spectra of the K and Na oleates show weak accordion modes at frequencies corresponding to chain lengths equivalent to nine carbon atoms [17]. Paralell studies of various synthetic phospholipids in the powder form show that the degree of chain extension in the case of lipids appears to be still more complex than in the case of soaps [17]. Not surprisingly, it has been observed [8-9] that the frequencies of the normal carbon saturated fatty acids in the acoustical region are slightly lower than

those for the same *n*-carbon alkanes. The same was reported recently for long chain *n*-primary amines [10].

Such a divergence from the Schaufele's chain length/longitudinal acoustical mode frequency relationship can either be due to disordered chains or to chain bending as an effect of interchain interactions, terminal chain groups and conformational or mass effects.

However, no systematic experimental investigations of interchain, mass, conformation and terminal group effects on the frequencies of longitudinal acoustical modes have been reported. The present work is a study of possible 'irregularities in the hydrocarbon chains' of some *n*-dodecyl compounds by looking at the effects of different terminal chain groups on the longitudinal acoustical mode Raman frequencies and band profiles.

2 — EXPERIMENTAL

Raman spectra were obtained with 514.5 nm excitation from a Spectra-Physics 164 argon ion laser. The scattered light from the sample was focused onto the entrance slit of a Varian Cary 82 Raman Spectrophotometer operating with a spectral slitwidth of 3-4 cm^{-1} (constant over displacement 0-3500 cm^{-1}). The signal from the photon counting system was displayed on a strip chart recorder.

The *n*-dodecane, lauric acid, *n*-dodecanol, *n*-dodecanthiol, sodium lauryl sulphate and dodecylamine used in this study were of purum grade and have been purified either by distillation or by recrystallization from acetone. Dodecylamine hydrochloride and zinc laurate were prepared, respectively, by reacting a known quantity of dodecylamine with hydrochloride solution and lauric acid with zinc nitrate in solution. The salts were purified by recrystallization from acetone. Mixtures of dodecylamine with water were prepared by measured amounts of amine and double distilled water in sealed glass cells which were allowed phase equilibria during two days in a temperature bath of about 90°C.

The solid samples were contained in 1 mm melting point cappilaries; solution samples were contained into 10×10×50 mm glass cells.

The accuracy in reported frequencies is estimated to be ±2 cm^{-1}.

Recordings above room temperature were achieved by a temperature bath design based on an insulated aluminium jacket fitted with an ITT Vulcan heater in the solid block. A temperature accuracy better than ±2°C was obtained for these recordings.

In the evaluation of peak intensities, Raman band heights were measured as the spectral heights above a background drawn as a straight line between minima in the spectra which is the combination of broad band luminescence with the Raman spectrum of the sample. The experimental error in these intensity measurements could be of the order of 10%.

In the bandshape analysis, the effect of spectrometer slit was taken into consideration. For the samples studied here, a 3-4 cm^{-1} slitwidth results in negligible band shape error, as it has been inferred by estimating its effect on the halfwidth of the band. Even so, some increased accuracy has been tried through deconvolution using a triangular slit function, following DIJKMAN and co-workers procedure [11].

3 — THEORY

The longitudinal acoustical modes represent the symmetric longitudinal accordion-like motion of an extended zig-zag carbon chain:

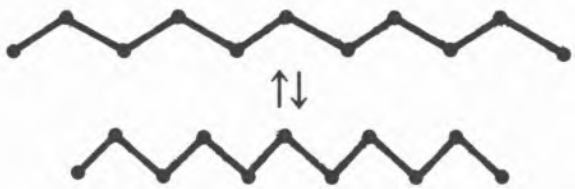

The Raman number shifts of these vibrations are approximately linear in (m/n) where m is the order of the vibration and n is the number of carbon atoms in the chain.

Considering the actual planar zig-zag geometry and methyl end groups, SCHAUFELE *et. al.* [2-3] have shown that the frequencies of the accordion modes for finite polymethylene chains could be fitted to a polynomial in (m/n) of the form:

$$\upsilon = A_1 + A_2(m/n) + A_3(m/n)^2 + \ldots + A_7(m/n)^6$$

where υ is the longitudinal acoustical mode frequencies and A_1-A_7 are parameters which can be determined from a least-squares treatment of the experimental frequencies.

In general, for a free end chain with n atoms per translational repeat unit and M repeat units, there are 3Mn vibrations, including six zero-frequency vibrations. These vibrations are distributed in 3n frequency branches at M phase angles [8]:

$$\phi_k = \frac{k\,\pi}{M} \quad \text{with } k = 0,1,2,\ldots M\text{-}1$$

For an infinite chain it can be shown that only those vibrations which remain invariant under any primitive translation along the chain axis will be active either in the infra-red or Raman. These vibrations correspond to those with $k = 0$, i.e., those with identical nuclear displacements. The frequency of the $k = 1$ mode (or any $k = 0$ mode) will be a function of the chain length, L [8].

The fundamental longitudinal acoustical vibration ($m = 1$, LAM-1) is the most intense of the series observed for a particular chain length, with the intensities of the overtones approximately proportional to (1/m). Only overtones corresponding to odd values of m are observed in the Raman spectra, as to a first approximation, since even values of m correspond to vibrations that give no change in the molecular polarizability [9].

The relationship between the LAM frequency (in cm^{-1}) and the length L of the straight-chain segment consisting of identical CH_2 groups unperturbed by intermolecular effects is [3,7]:

$$\upsilon\,(\text{LAM-k}) = \frac{k}{2cL}\left(\frac{E}{\varrho}\right)^{1/2}$$

where E is Young's elastic modulus, ϱ is the density, c is the speed of light, L refers to the equilibrium distance between chain units. As mentioned above, the observed values of $\upsilon_{(\text{LAM-1})}$ were found to be linearly related to 1/L for the all-trans *n*-paraffins. The way in which the all-*trans* chain in terminated does, however, play a role in variations of the chain mode frequencies. It has been shown [8] that while the selection rules for free ethylene chains are $\phi_k = k\,\frac{\pi}{M}$ with $k = 0,1,2,3,\ldots M\text{-}1$, a polyethylene chain with both ends fixed has allowed frequencies $\phi_j = j\,\frac{\pi}{M+1}$ with $j = 1,2,3,\ldots M$ on the same dispersion curve. If a particular k mode is allowed in the Raman for a free polyethylene chain, then the $j+1$ vibration is allowed for the fixed end chain.

The fundamental longitudinal acoustical mode frequencies of normal carbon saturated fatty acids [8] and long chain *n*-alkylamines [10] are slightly lower than those for the same *n*-carbon chainlength corresponding to a decrease in phase angle from a lighter end to a heavier end polyethylene chain.

Variations in the halfwidth of LAM-1 are an indicative of the uniformity of the chain length. An increase in linewidth usually indicates a decrease in periodic order of the chain core [12]. However, quantitative determinations of the shape of the distribution have not yet been reported partly because it is difficult to measure accurately the Raman spectra in the low frequency region. In addition to the problem of reducing background scattering, the effect of finite spectrometer slitwidth and the natural width of the LAM-1 Raman band are factors that must be considered.

4 — RESULTS AND DISCUSSION

The frequencies and fullwidths at halfheight corrected for the instrumental widths of the fundamental longitudinal acoustical mode for the systems studied are listed in Table 1. This Table includes also the nominal Raman length which is the length of an all-*trans* *n*-paraffin having the same LAM-1 frequency as that of a given sample under study. This length has been calculated using SCHAUFELE'S data [3] on variation of primary longitudinal mode frequencies for polymethylene solids and liquids with the number of chain units.

Assuming that each sample can be thought of as ressembling a stack of coupled lamellae vibrating in phase, it has been observed [13] that the nominal Raman length is always larger by 10 to 20% than the average lamellar thickness, being, however, equal to the segment length between folds. Thus, the different nominal Raman lengths of the dodecyl compounds under study must be related with differences in structure of the chain fold due to pecularities in its morphological structure as an effect of end group substitution.

It is known [14] that in the LAM-1 vibration the largest contribution to the vibrational energy occurs at the ends of the chain, since the nodal carbon is at the chain center. Bulky end groups would lower the LAM-1 frequency. LIPPERT and PETICOLAS [8] have made an attempt to fit the LAM frequencies of some fatty acids using a fixed end calculation.

Table 1
Fundamental longitudinal acoustical mode frequencies, bandwidths and nominal Raman chain lengths

System	Physical state	m.p. (K)	Frequency (cm^{-1})	Width (cm^{-1})	Nom. Length (CH_2 units)
n-dodecane	Liquid (295 K)	263	239	36±2.5	11
n-dodecanol	Liquid (295 K)	299	235	45±2.5	12
n-dodecanethiol	Liquid (295 K)	264	226	45±2.5	12
Sodium lauryl sulphate	Solid (295 K)	—	225	26±2.5	10
Lauric acid	Solid (295 K)	317	207	12±1.5	11
Zinc laurate	Solid (295 K)	401	189	—	13
n-dodecylamine	Solid (295 K)	301	184	8±1.5	13
n-dodecylamine hydrochloride	Solid (295 K)	371	183	8±1.5	13
25% dodecylamine in water	a) Solid solution				
	295 K	—	185	16±1.5	
	320 K	—	185	36±2.5	
	b) Isotropic solution (335 K)		190	—	

But, such a calculation predicts higher LAM frequencies than the LAM frequencies of *n*-alkanes, contrary to what is observed. To explain the experimental lowering of the LAM-1 frequencies one must admit that the functional end group has mobility. With a mobile polar group as the chain end it is necessary to know how its size could affect the degree of all-*trans* chain configuration which depends not only on chain length but also on the size of such a polar group.

Two different structural models of chain fold have been frequently invoked, the so-called 'tight chain folds' in which the chain is supposed to be folded in a short, tight hair pin turn, and the 'loose loops' model which assumes the chain to meander along an irregular path of considerable length before reentering the stack lamellae. In any case, the coupling between consecutive lamellae will be significant only when chains become numerous. Here weak interlamellar forces will result in a characteristic upward shift of the frequencies of the longitudinal acoustic modes, which is independent of the chain length. They are van der Waal's forces, not only operative at the chain ends but also, although reduced in strength, on neighbouring layers. The penetration depth of these interlamellar forces is unknown; however, the effect of the resulting constraints will lead to a retarding force upon (or barrier to) molecular motion. For a flexible molecule, such an effect will integrate conformational changes and molecular distortions.

On this basis, is seems possible to advance some conclusions on the possible morphology of chains for the studied *n*-dodecyl compounds:

As compared with the all-*trans* crystalline *n*-dodecane which has a LAM-1 frequency of 194 cm^{-1} [15], a higher LAM-1 frequency occurs for the liquids *n*-dodecane, *n*-dodecanol and *n*-dodecanethiol and for the solids sodium lauryl sulfate and lauric acid. The distortion of the chain in the three referred liquids, where micellar aggregation occurs, due to an intermolecular effect which leads to a chain alignment in a parallel ordering with a decrease in the fraction of the chain having a *trans* geometry, resulting in two conformational distributions and chain shortening, explains the observe increase in the fundamental longitudinal acoustic mode frequency. In solid sodium lauryl sulfate and lauric acid it appears that the heavy groups SO_4^{2-} and COOH respectively, and the dimerization which will exist in the case of the acid, act like an anchor fixing the chain end and even leading to possible tight chain folding.

— Zinc laurate, *n*-dodecylamine and *n*-dodecylamine hydrochloride in the solid state have a LAM-1 frequency lower than the all-*trans* crystalline *n*-dodecane LAM-1 frequency. The bulky end groups of these compounds instead of anchoring the chain

seem to have a great amount of mobility. And this mobility is expected to lower the LAM-1 frequency as it has been mentioned above.

— As it has been observed previously [13], within the experimental error, no change of the LAM-1 frequency is expected with change of temperature. The LAM-1 frequency change we had observed for the 25% dodecylamine in water on raising the temperature from 320 K to 335 K should be interpreted not as a temperature effect upon the frequency of the longitudinal acoustic mode but rather as a temperature effect upon the composition of the system: a solid solution of dodecylamine plus dodecylamine monohydrate at 295 K; solid solution of dodecylamine plus dodecylamine tetrahydrate at 320 K; and dodecylamine-water isotropic solution at 335 K [16].

— The progressive broadening of the primary longitudinal acoustic band with increasing frequency undoubtedly results from an increasing number of gauche rotations. As has been already mentioned, from the all-*trans* crystalline solid to the amorphous or to the liquid, the *trans* geometry effectively vanishes resulting in two conformational distributions, one relatively narrow and the other quite broad. The observed increase in the LAM-1 linewidth indicates a decrease in the periodic order of the crystalline core.

— The chain length of large molecules has been related with some of their thermodynamic properties, namely, the melting temperature, the osmotic pressure, the surface tension, the volume and entropy changes, etc. [19]. From a statistical point of view, the melting may be considered as the introduction of new equilibrium positions into the solid. For large molecules long enough to act in segments, the entropy of fusion will be that of the disorder and rotation of segments, and the heat of fusion will be that for the deforming of bonds required to introduce the new equilibrium positions for segments. Thus, the melting point will be determined mainly by the properties of the segments.

In this way, there is a limiting melting point for all series of long chain hydrocarbon compounds, a temperature about 395 K. For even paraffins, odd paraffins, olefins and alcohols, it has been observed [19], there is an amounting of *ca.* 20° per each CH_2 group increase of the chain length. Therefore, the estimated ratio melting temperature (K)/20 will give the effective chain length in CH_2 groups. Applying this criterium to the compounds under study, the following effective chain lengths for the solids, are obtained:

n-dodecane	13 CH_2 groups	Zinc laurate	20 CH_2groups
n-dodecanol	15 » »	*n*-dodecylamine	15 » »
n-dodecanethiol	13 » »	*n*-dodecylamine	
Lauric acid	16 » »	hydrochloride	18 » »

These results show that for all these compounds the effective chain length obtained by the melting temperature method is longer than the nominal Raman chain length based upon the fundamental longitudinal acoustical mode frequencies. Nevertheless, such a method clearly shows the effect of strong chain interaction in dodecanol, lauric acid, dodecylamine, dodecylamine hydrochloride and zinc laurate. They are compounds where further than the 'normal' van der Waals forces responsible for chain association, hydrogen bonding and strong ionic interactions are possible and expected. Considering the nominal Raman length as the effect of the hydrocarbon interactions added to the 'normal' van der Waals forces due to the chain end groups, one could conclude that the functional group introduces additional mass which leads to folding of the chain. The effects of that folding result in an acoustical mode frequency which generally overestimates the actual length as compared with all-*trans* crystalline homolg *n*-alkanes.

Received 26.November.1982

ACKNOWLEDGEMENTS

The financial support from JNICT and the work facilities in the Department of Chemistry of the University of Coimbra are greatly acknowledged.

REFERENCES

[1] S.I. Mizushima, T. Shimanouchi, *J. Am. Chem. Soc.*, **71**, 1320 (1949).
[2] R.F. Schaufele, T. Shimanouchi, *J. Chem. Phys.*, **47**, 3605 (1967).
[3] R.F. Schaufele, *J. Chem. Phys.*, **49**, 4168 (1968).
[4] M. Tasumi, S. Krimm, *J. Chem. Phys.*, **46**, 755 (1967).
[5] T. Shimanouchi, M. Tasumi, *Ind. J. Pure Appl. Phys.*, **9**, 958 (1971).
[6] J.F. Rabolt, B. Fanconi, *Macromolecules*, **11**, 740 (1948).
[7] R.G. Snyder, S. J. Krause, J.R. Scherer, *J. Polym. Sci: Polym Phys. Ed.*, **16**, 1593 (1978).
[8] J.L. Lippert, W.L. Peticolas, *Biochim. Biophys. Acta*, **282**, 8 (1972).

[9] C.H. WARREN, D.L. HOOPER, *Can. J. Chem.*, **51**, 3901 (1973).
[10] A.M. AMORIM DA COSTA, C.F.G. GERALDES,, J.J.C. TEIXEIRA-DIAS, *J. Raman Spectrosc.*, **13**, 56 (1982).
[11] F.G. DIJKMAN, J.H. VAN DER MASS, *Appl. Spectrocosp.*, **30**, 545 (1976).
[12] J.L. KOENIG, D.L. TABB, *J. Macromol. Sci. Phys.*, **B9**, 141 (1974).
[13] H.G. OLF, A. PETERLIN, W.L. PETICOLAS, *J. Polym. Sci: Polym. Phys. Ed.*, **12**, 359 (1974).
[14] B. FANCONI, J. CRISSMAN, *J. Polym. Sci: Polym. Lett. Ed.*, **13**, 421 (1975).
[15] S.I. MIZUSHIMA, T. SIMANOUTI, *J. Am. Chem. Soc.*, **71**, 1320 (1949).
[16] A.W. RALSTON, C.W. HOERR, E.J. HOFFMAN, *J. Am. Chem. Soc.*, **64**, 1516 (1942).
[17] R. FAIMAN, G. VERGOTEN, Y. MOSCHETTO, D.A. LONG, Proc. 5th International Conference on Raman Spectroscopy, Freiburg, Germany, September, 1976, pp. 544-5.
[18] G. VERGOTEN, G. FLEURY, Y. MOSCHETTO, in «Advances in Infrared and Raman Spectroscopy» (Ed. R.J.H. Clark and R.E. Hester, Heyden and Sons Ltd., 1978), vol. 4, pp. 195-269.
[19] R.E. POWELL, C.R. CLARK, H. EYRING, *J. Chem. Phys.*, **9**, 268 (1941).

RESUMO

Modo longitudinal acústico do espectro de Raman em compostos de *n*-dodecilo

Por análise da frequência e largura das bandas devidas ao primeiro modo longitudinal acústico do espectro de Raman, procura racionalizar-se o efeito de diferentes grupos terminais sobre o comprimento efectivco da cadeia hidrocarbonada de alguns compostos de n-*dodecilo.*